Estimation of Strong Ground Motions from Hypothetical Earthquakes on the Cascadia Subduction Zone, Pacific Northwest

THOMAS H. HEATON[1] and STEPHEN H. HARTZELL[1]

Abstract—Strong ground motions are estimated for the Pacific Northwest assuming that large shallow earthquakes, similar to those experienced in southern Chile, southwestern Japan, and Colombia, may also occur on the Cascadia subduction zone. Fifty-six strong motion recordings for twenty-five subduction earthquakes of $M_s \geq 7.0$ are used to estimate the response spectra that may result from earthquakes $M_w < 8\frac{1}{4}$. Large variations in observed ground motion levels are noted for a given site distance and earthquake magnitude. When compared with motions that have been observed in the western United States, large subduction zone earthquakes produce relatively large ground motions at surprisingly large distances. An earthquake similar to the 22 May 1960 Chilean earthquake (M_w 9.5) is the largest event that is considered to be plausible for the Cascadia subduction zone. This event has a moment which is two orders of magnitude larger than the largest earthquake for which we have strong motion records. The empirical Green's function technique is used to synthesize strong ground motions for such giant earthquakes. Observed teleseismic P-waveforms from giant earthquakes are also modeled using the empirical Green's function technique in order to constrain model parameters. The teleseismic modeling in the period range of 1.0 to 50 sec strongly suggests that fewer Green's functions should be randomly summed than is required to match the long-period moments of giant earthquakes. It appears that a large portion of the moment associated with giant earthquakes occurs at very long periods that are outside the frequency band of interest for strong ground motions. Nevertheless, the occurrence of a giant earthquake in the Pacific Northwest may produce quite strong shaking over a very large region.

Key words: Earthquake, strong motion, subduction, Cascadia, Washington, Oregon.

Introduction

This is the last in a sequence of papers that lead to estimates of the type of ground motions that might be caused by earthquakes on the Cascadia subduction zone. HEATON and KANAMORI (1984) compared physical characteristics of many world-wide subduction zones and concluded that the Cascadia subduction zone is similar to other subduction zones with strong seismic coupling. HEATON and HARTZELL (1986) extended those studies and concluded that the Cascadia subduction zone is most similar to the subduction zones of southern Chile, southwestern Japan, and Colombia; each of which have experienced sequences of very large

---

[1]U.S. Geological Survey, 525 S. Wilson Ave., Pasadena, CA 91106, U.S.A.

shallow subduction earthquakes. HEATON and HARTZELL (1986) also presented several hypothetical earthquake sequences that may be plausible for the Cascadia subduction zone. HARTZELL and HEATON (1985) compared the nature of the time history of energy release for large subduction earthquakes by studying broad-band teleseismic P-wavetrains from sixty of the largest events in the last fifty years. This survey gave insight to the variation in source parameters and shorter-period radiated energy (2 to 50 sec) for earthquakes from different subduction zones. More informed judgements could then be made concerning the use of available strong motion data from world-wide subduction zones to predict the ground motion at a specific site. In this paper, we present estimates for the strong ground motions that might be expected if large subduction earthquakes do occur on the Cascadia subduction zone.

We assume that gap-filling earthquake sequences that are similar to those already observed in southern Chile, southwestern Japan, and Colombia may also occur in the northwestern United States. The largest earthquakes in these sequences range in size from M_w 8 to M_w $9\frac{1}{2}$. Strong ground motion records are available for shallow subduction earthquakes as large as M_w 8.2, but strong ground motions have not yet been recorded for larger events. In this study, we assume that ground motions from M_w 8 earthquakes on the Cascadia subduction zone are not systematically different from the motions that have been recorded during M_w 8 earthquakes on other subduction zones. Although the comparison of teleseismic P-waves from large shallow subduction earthquakes on differing subduction zones (HARTZELL and HEATON, 1985) indicates that there is a great variability between earthquakes in the time histories of energy release, no obvious systematic pattern could be recognized that would suggest inherent differences in the nature of energy release from earthquakes at subduction zones that are similar to the Cascadia subduction zone. For hypothetical earthquakes of M_w less than $8\frac{1}{4}$, our approach is to simply collect and categorize existing ground motion records according to earthquake size and site distance. We then create a suite of ground motions that have been recorded under conditions similar to those existing at a site for which ground motion estimates are desired. Motions within the suite are scaled to account for variations in earthquake size and site distance. This procedure is similar to that described by GUZMAN and JENNINGS (1976) and also HEATON et al. (1986).

As discussed by HEATON and HARTZELL (1986), there are several similarities between the Cascadia and southern Chile subduction zones. The 1960 Chilean earthquake (M_w 9.5) is thought to be the largest earthquake of this century (KANAMORI, 1977); it is also the largest event which we consider to be feasible in the northwestern United States. Estimation of strong ground motions for the 1960 earthquake is necessarily problematic since its seismic moment is approximately one hundred times that of the largest earthquake for which strong ground motions have been recorded. In order to obtain some estimate of the nature of shaking from such giant earthquakes, we employ the empirical Green's function technique

(HARTZELL, 1978, 1985; KANAMORI, 1979; IRIKURA, 1983; HOUSTON and KANAMORI, 1986). That is, we model a giant earthquake as a summation of smaller earthquakes for which we have ground motion records. Unfortunately, there are many poorly justified assumptions that are required in the application of this technique. We use teleseismic P-wave recordings, of both the earthquakes that we wish to model and the earthquakes for which we have strong motion recordings, to help constrain model assumptions.

Strong Motion Estimates for Earthquakes of $M_w < 8\frac{1}{4}$

Fifty-six recordings of strong ground motion from twenty-five shallow subduction earthquakes of $M_w \geq 7.0$ were collected for this study. Figures A1–A20 in Appendix A show the locations of recording sites relative to aftershock zones, the time histories of one component of horizontal ground acceleration and velocity for each recording, and the time histories of the mainshock moment release as inferred from teleseismic body waves by HARTZELL and HEATON (1985). These figures only briefly summarize this important data set; more detailed descriptions of the nature of each earthquake and the geologic setting of each recording site would undoubtedly allow us to rank the significance of individual records in our study of the Pacific Northwest.

There are several notable features in the figures in Appendix A. In most cases, the recordings sites are at vast distances from the earthquakes when compared with the strong motions data set recorded in the western United States. For instance, we do not know of any western U.S. records having site distances of over 150 km and peak accelerations of over 0.05G. However, this situation is fairly common in the figures in Appendix A. HEATON et al. (1986) conclude that the distribution of peak values of ground motion observed in Japan is quite different from that observed in the western U.S. Although the very largest ground motions have been observed at relatively close distances in the western U.S., impressively large motions have been recorded at distances of 100 km and more in Japan. HEATON et al. (1986) conclude that a major reason for this difference is simply due to differences in station distributions and earthquake sizes. That is, there have been many near-source recordings of moderate-sized U.S. earthquakes, but earthquakes of $M > 7$ have been rare. In contrast, there are numerous recordings of large Japanese earthquakes, but very near-source records are rare.

Every record in Appendix A is plotted on a common time scale which is quite compact so that these long-duration records fit within the confines of the figures. Although these ground motion records may, at first, appear to be very high frequency, a closer inspection shows that many of the ground accelerations records are dominated by frequencies of less than several hertz.

Comparison of the strong ground motions with the teleseismic time functions of

HARTZELL and HEATON (1985) gives somewhat inconsistent results. In some cases, there is fairly good correspondence between envelopes of the strong motion recordings and the envelope of the teleseismic time function. For example, the 1968 Hyuganada earthquake and the 1978 Miyagi-Oki earthquake both have relatively simple and short duration accelerograms and teleseismic time functions. Furthermore, the 1968 Tokachi-Oki earthquake, the 1979 St. Elias earthquake, and the 1983 Akita-Oki earthquake all have more complex teleseismic time functions whose envelopes are comparable to the envelopes of their strong motion recordings. These examples indicate that teleseismic records can be used to infer the overall duration and complexity of large earthquakes. Unfortunately, there are also examples where there is clearly no correlation between the teleseismic time function and the recorded strong ground motion; the 1968 Iwate-Oki earthquake, the 1973 Nemuro-Oki earthquake, and the 1966 Peruvian earthquake all have teleseismic time functions that are considerably longer than the observed strong ground motions. Without more detailed study of these earthquakes and local site effects, we can only speculate on the causes of the discrepancies between the strong motion records and the teleseismic time functions. HARTZELL and HEATON (1985) show that their time functions are very complex when they are derived from stations that are near theoretical body wave nodes. Problems of this type are undoubtedly present in some of the teleseismic time functions shown in Appendix A. However, despite the poor comparison of the teleseismic time function and the strong ground motion for the 1973 Nemuro-Oki earthquake, the teleseismic time function of HARTZELL and HEATON (1985) compares well with the teleseismic time function that KIKUCHI and FUKAO (1987) derived for this earthquake using an entirely independent set of teleseismic P-waveforms. We believe that these comparisons demonstrate that the teleseismic time functions provide useful estimates of the source duration and complexity as observed in the near-source region. However, there are also inconsistencies in these comparisons and one should be careful not to overinterpret the teleseismic time functions of HARTZELL and HEATON (1986).

In Figure 1, we show the response spectra of all of the horizontal components of ground motion for the records presented in Appendix A. The spectra are grouped according to earthquake size and the distance of the recording sites from the earthquakes. Of course, earthquakes are described by a complex 3-dimensional rupture surface and the definition of distance is necessarily ambiguous. For simplicity, we use the epicentral distance. However, because of the large fault dimensions of the 1968 Tokachi-Oki earthquake, we choose to measure distance from a point that is more central to the rupture surface than the epicenter is. This point is shown in Appendix A.

One of the most striking features of Figure 1 is the large degree of scatter in the spectra for ground motions observed at similar distances and from similar sized earthquakes. This scatter is quite troublesome when one is confronted with the problem of estimating the ground motions that a particular site may experience.
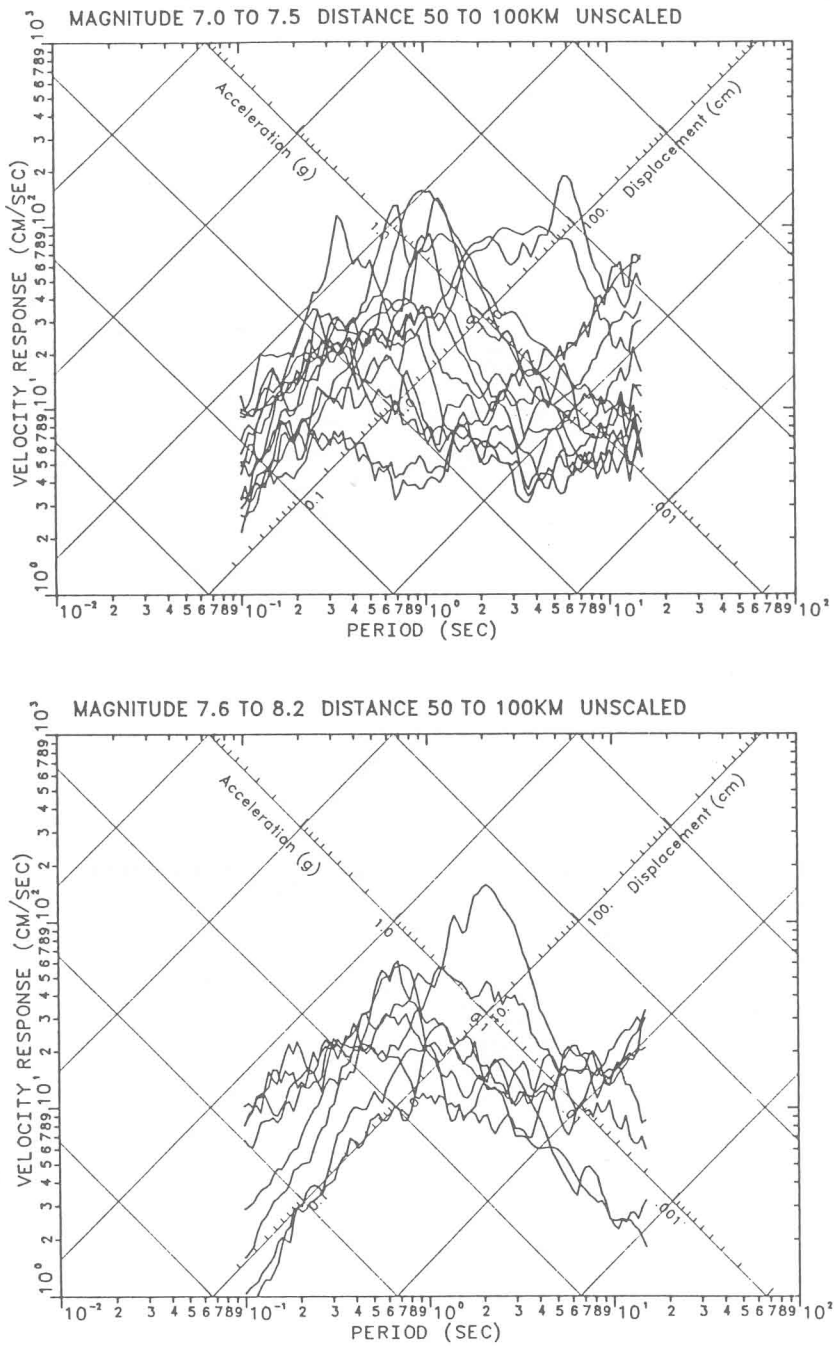
Fig. 1(a).

Figure 1

Pseudo-velocity response spectra (5% damped) of horizontal components of ground motion from large shallow subduction earthquakes. Time histories of one of the components are shown in Appendix A. The spectra from earthquakes of $7.0 \leq M_w \leq 7.5$ are shown above and spectra from earthquakes of $7.6 \leq M_w \leq 8.2$ are shown below. The spectra are further segregated by site distance: a) 50 to 100 km, b) 101 to 140 km, c) 151 to 200 km, d) 201 to 250 km, and e) 251 to 300 km.
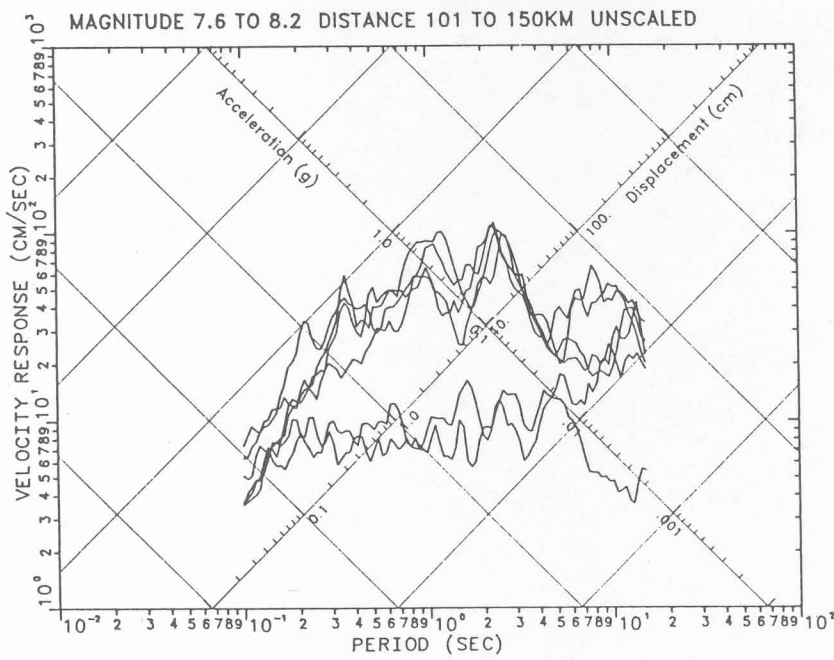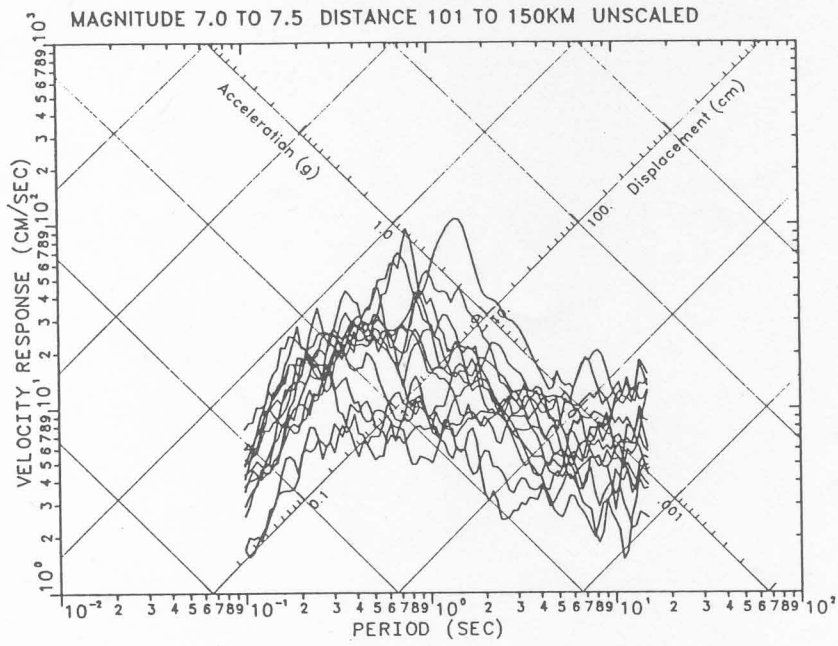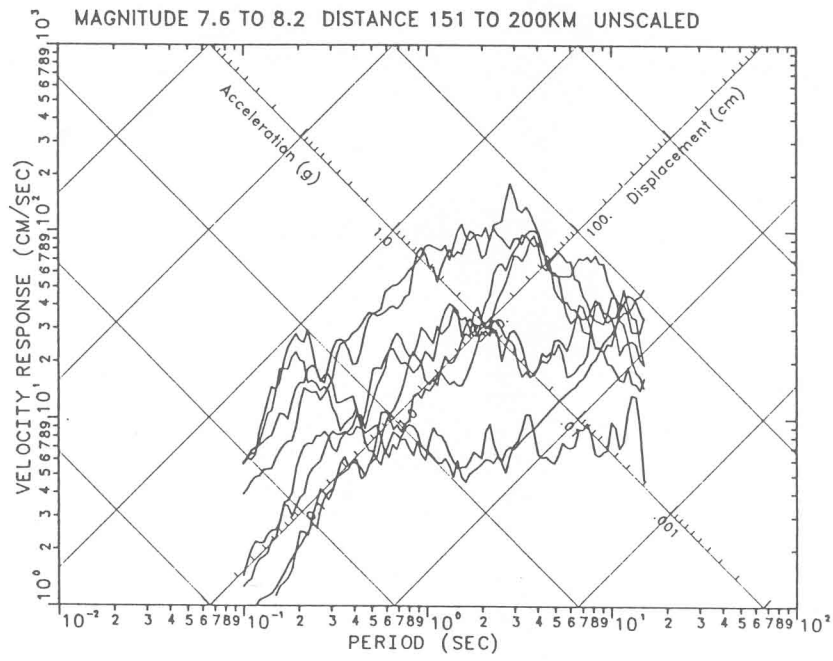
MAGNITUDE 7.0 TO 7.5 DISTANCE 101 TO 150KM UNSCALED

MAGNITUDE 7.6 TO 8.2 DISTANCE 101 TO 150KM UNSCALED

Fig. 1(b).

MAGNITUDE 7.0 TO 7.5 DISTANCE 151 TO 200KM UNSCALED

MAGNITUDE 7.6 TO 8.2 DISTANCE 151 TO 200KM UNSCALED

Fig. 1(c).

MAGNITUDE 7.0 TO 7.5 DISTANCE 201 TO 250KM UNSCALED

MAGNITUDE 7.6 TO 8.2 DISTANCE 201 TO 250KM UNSCALED

Fig. 1(d).

MAGNITUDE 7.0 TO 7.5 DISTANCE 251 TO 300 KM UNSCALED
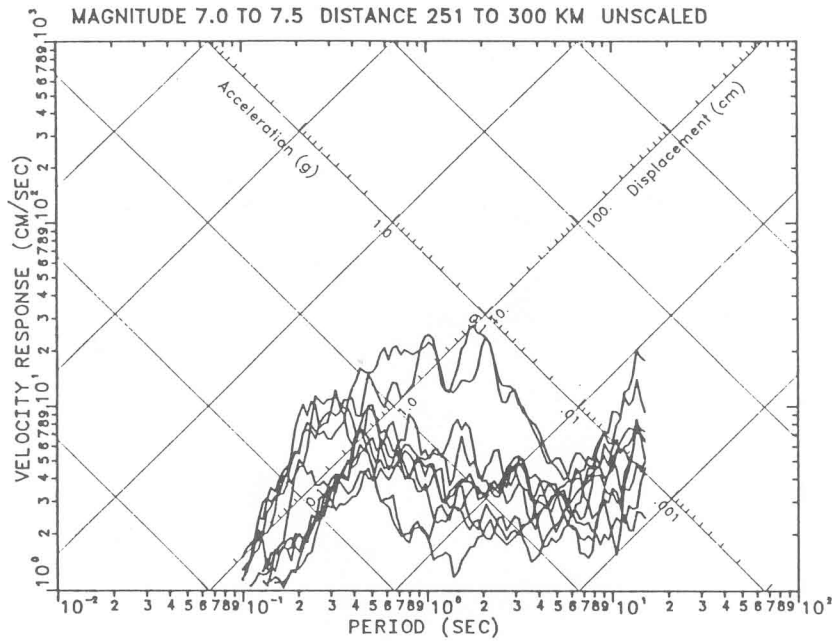
MAGNITUDE 7.6 TO 8.2 DISTANCE 251 TO 300 KM UNSCALED

Fig. i(e).

Even if the earthquake magnitude and distance is known (and it usually is not), the resulting ground motions are uncertain by more than a factor of ten. In many respects, the uncertainties arising from this scatter are larger than those in estimating the earthquake magnitude or distance. This problem is not restricted to this data set; strong ground motions recorded in the western United States are plagued by scatter of similar magnitude (HEATON et al., 1986).

Is there some other way to regroup these records so that more certain estimates of ground motion can be obtained at a particular site? TRIFUNAC (1976) and JOYNER and BOORE (1982) present convincing evidence that lower frequency (less than 2 Hz) ground motions are systematically larger, by about a factor of two, at soil sites than at rock sites for ground motions recorded in the western United States. Higher frequency ground motions, however, show no significant correlation with site conditions. KAWASHIMA et al. (1984) report similar conclusions for ground motions from earthquakes of less than M 7 in Japan. They also report that soft soil sites experience low-frequency (less than 1 Hz) ground motions of about four times that of rock sites. LIU and HEATON (1984) suggest that the larger ground motions observed at soft sites result from the excitation of surface waves within basins on which soft sites usually sit.

In Figure 2, we compare response spectra that are obtained from a variety of earthquakes that are recorded at the same site. It is clear that the characteristics of the motion observed at a particular site are very similar from one earthquake to another and can dominate the source effects. Although site effects can sometimes be anticipated using simple models of plane body waves in horizontally layered media, there are undoubtedly important effects from complex three-dimensional geologic structures such as basins (LIU and HEATON, 1984). One promising technique for recognizing the effect of the recording site on strong gound motions is to record and analyze the weak motions from smaller earthquakes. Similar transmission effects should be seen in both strong and weak ground motions.
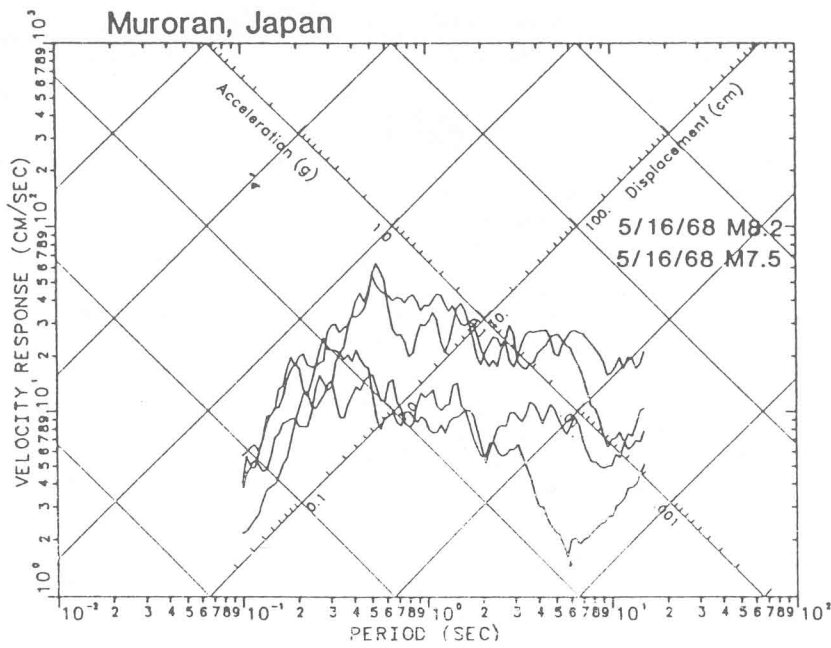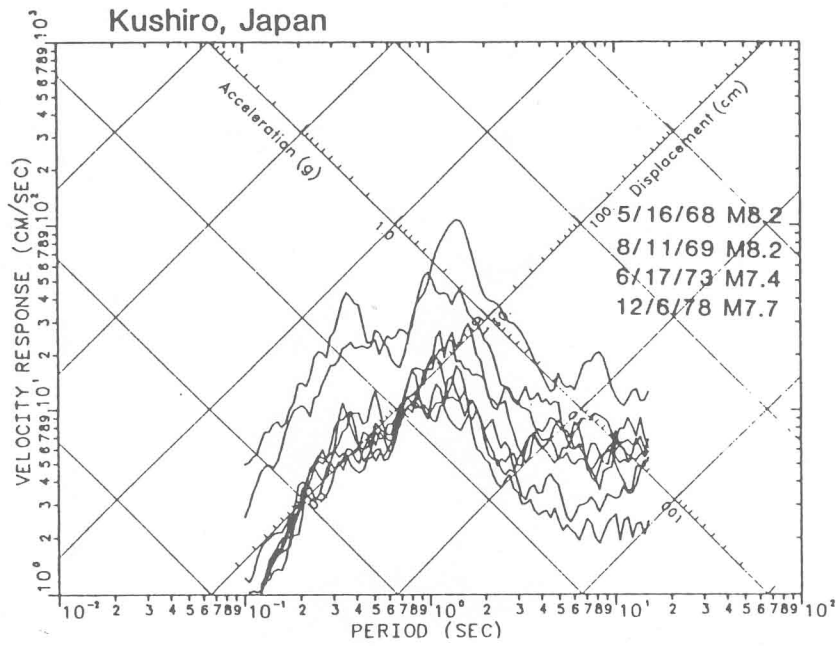
Of course, the details of the earthquake rupture process also affect the characteristics of strong ground motion. Directivity, fault finiteness, and slip distribution must control the overall characteristics of strong ground motion. Although significant peaks in response spectra are probably caused by reverberations within some geometrically regular velocity structure, the partition of energy in different frequency bands may be strongly affected by the nature of the rupture process. CROUSE et al. (1988) investigate response spectra from shallow earthquakes in seven different subduction zones and they conclude that, for the most part, systematic differences are not seen from one zone to another. However, they do present evidence that motions recorded in Peru/northern Chile and New Britain/ Bougainville regions were significantly smaller than other zones in the period range from 1 to 3 seconds. Although source characteristics may be important, they are very difficult to anticipate for design purposes. Transmission effects are also clearly important and may be quite complex. However, to some degree

they can be anticipated through the study of weak ground motions from smaller earthquakes.

In Figure 3, we compare the smoothed response spectra that are the averages of the spectra in each of the distance and magnitude ranges presented in Figure 1. The average spectra were obtained by taking the average of the logarithmic values. Tables 1 and 2 give spectral velocities and standard deviations for these averaged spectra at selected periods. Although the large scatter in the data makes even these smoothed, average spectra appear to be somewhat chaotic functions of distance and magnitude, some general trends can be seen. At periods of less than 0.3 seconds, spectral velocities from magnitude 7.6 to 8.2 earthquakes are not significantly greater than those from magnitude 7.0 to 7.5 earthquakes. However, at periods greater than 1.0 seconds, the larger earthquakes are clearly associated with larger spectral velocities. Curiously, spectral velocities in the closest distance range, 50 to 100 km, do not seem significantly larger than those at distances from 101 to 150 km. However, the scatter in this data set is so large, that this observation may not be significant.

KAWASHIMA et al. (1984) and CROUSE et al. (1988) have both applied multiple regression analyses to response spectra from earthquakes at convergent plate boundaries (principally from Japan). In addition to considering ground motions from the large earthquakes included in this study, they also considered ground motions from earthquakes as small as M 5.0. Since their regression analyses presume that the motions can be characterized by smooth monotonic functions of distance and magnitude, the estimation of ground motions using their formulae does not lead to such apparent paradoxes as having the motions increase with distance as they sometimes do in Figure 3. Of course, a price is paid for this aesthetically pleasing smoothness. Ground motion predictions, particularly for magnitudes and distances near the end members of the data set, depend upon the specific functional forms chosen and upon data taken at other magnitudes and distances.

A comparison of ground motions predicted by the formulae of KAWASHIMA et al. (1984) and CROUSE et al. (1988) with the logarithmic averages of the data in this report is found in Tables 1 and 2. Ground motion predictions for shallow crustal earthquakes in the western United States are also given for comparison (JOYNER and BOORE, 1981; JOYNER and BOORE, 1982). In Figure 4, we compare the predicted ground motions of KAWASHIMA et al. (1984) with those for the western United States for earthquakes of M_w 7.9. The ground motions predicted for subduction earthquakes are dramatically larger than those for the western United States, at least at distances greater than 50 km. Unfortunately, the western United States curves are uncertain since there have been no strong motion recordings from earthquakes of this size in the western United States and these curves are extrapolations outside of the data. Curiously, peak ground accelerations and velocities for earthquakes of magnitude less than 7 are not dramatically different for Japanese
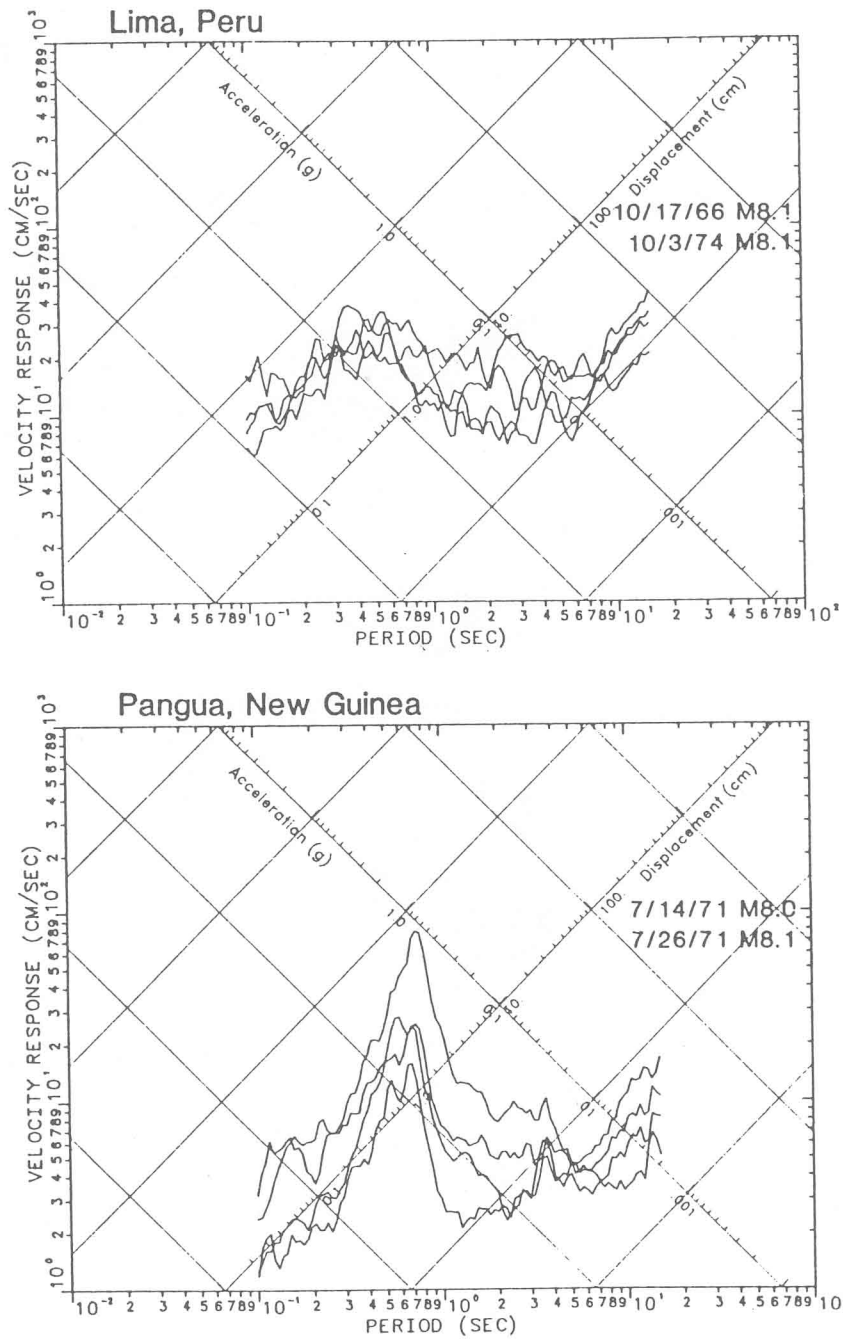
Kushiro, Japan

5/16/68 M8.2
8/11/69 M8.2
6/17/73 M7.4
12/6/78 M7.7

Muroran, Japan

5/16/68 M8.2
5/16/68 M7.5

Figure 2
Pseudo-velocity response spectra (5% damped) of horizontal components of ground motion grouped by
recording site.

Table 1

Magnitude 7.0 to 7.5.

	Observed, This Study									
	50–100 km		101–150 km		151–200 km		201–250 km		251–300 km	
$\ddot{U}_{max}$ (cm/sec^2)	230.	$\binom{392.}{135.}$	161.	$\binom{247.}{105.}$	66.	$\binom{104.}{42.}$	43.	$\binom{91.}{20.}$	39.	$\binom{66.}{23.}$
$\dot{U}_{max}$ (cm/sec)	19.0	$\binom{44.0}{8.2}$	12.2	$\binom{21.6}{6.9}$	6.5	$\binom{10.9}{3.9}$	3.6	$\binom{5.8}{2.2}$	3.1	$\binom{5.3}{1.8}$
U_{max} (cm)	5.2	$\binom{13.1}{2.0}$	2.9	$\binom{5.2}{1.6}$	1.7	$\binom{2.5}{1.2}$	0.9	$\binom{1.7}{0.5}$	0.7	$\binom{1.3}{0.4}$
PSV (0.1) cm/sec	5.1	$\binom{8.6}{3.0}$	3.9	$\binom{6.0}{2.5}$	1.3	$\binom{2.1}{0.7}$	0.9	$\binom{2.0}{0.4}$	0.9	$\binom{1.3}{0.6}$
PSV (0.3) cm/sec	17.9	$\binom{32.7}{9.8}$	17.1	$\binom{26.5}{11.0}$	8.0	$\binom{12.7}{5.0}$	4.9	$\binom{8.7}{2.7}$	5.0	$\binom{8.3}{3.0}$
PSV (1.0) cm/sec	23.0	$\binom{72.1}{7.3}$	16.4	$\binom{35.7}{7.6}$	16.1	$\binom{27.4}{9.5}$	5.9	$\binom{10.8}{3.3}$	5.1	$\binom{11.9}{2.2}$
PSV (3.0) cm/sec	14.6	$\binom{35.6}{6.0}$	8.7	$\binom{15.3}{5.0}$	6.2	$\binom{8.4}{4.5}$	4.4	$\binom{7.6}{2.5}$	4.4	$\binom{8.1}{2.4}$
PSV (10.0) cm/sec	13.6	$\binom{30.0}{6.2}$	6.1	$\binom{10.2}{3.7}$	4.0	$\binom{5.3}{3.0}$	3.4	$\binom{6.2}{1.9}$	4.3	$\binom{6.8}{2.7}$

CROUSE, Depth = 30 km, M 7.25				
	75 km	125 km	175 km	225 km	275 km
PSV (0.1) cm/sec	2.4	1.6	1.3	1.0	0.9
PSV (0.3) cm/sec	11.7	7.7	5.6	4.4	3.5
PSV (1.0) cm/sec	18.9	12.6	9.3	7.3	6.0
PSV (3.0) cm/sec	11.5	7.6	5.6	4.4	3.6

KAWASHIMA, M 7.25				
$\ddot{U}_{max}$ (cm/sec^2)	149.2	92.8	66.0	50.6	40.7
$\dot{U}_{max}$ (cm/sec)	12.5	7.7	5.5	4.2	3.4
U_{max} (cm)	2.3	1.4	1.0	0.7	0.6
PSV (0.1) cm/sec	4.4	2.8	2.0	1.5	1.3
PSV (0.3) cm/sec	16.8	10.6	7.6	5.9	4.8
PSV (1.0) cm/sec	31.3	19.8	14.2	11.0	8.9
PSV (3.0) cm/sec	12.7	8.0	5.8	4.4	3.6

JOYNER and BOORE, M 7.25				
$\ddot{U}_{max}$ (cm/sec^2)	51.0	22.9	12.2	7.1	4.3
$\dot{U}_{max}$ (cm/sec)	9.5	4.2	2.2	1.3	0.78
U_{max} (cm)			0.1	0.03	0.01
PSV (0.1) cm/sec	1.1	0.3	0.1	0.2	0.09
PSV (0.3) cm/sec	4.4	1.4	0.5	0.7	0.4
PSV (1.0) cm/sec	10.4	3.8	1.6	5.8	4.7
PSV (3.0) cm/sec	17.5	10.5	7.4		

( ) = ± one standard deviation.

Table 2

Magnitude 7.6 to 8.2.

	Observed, This Study									
	50–100 km		101–150 km		151–200 km		201–250 km		251–300 km	
$\ddot{U}_{max}$ (cm/sec^2)	144.	$\binom{233.}{89.}$	199.	$\binom{289.}{137.}$	108.	$\binom{202.}{57.}$	104.	$\binom{262.}{41.}$	47.	$\binom{57.}{39.}$
$\dot{U}_{max}$ (cm/sec)	18.5	$\binom{28.3}{12.0}$	18.5	$\binom{42.8}{8.0}$	17.2	$\binom{36.8}{8.1}$	14.7	$\binom{28.3}{7.6}$	5.0	$\binom{5.7}{4.3}$
U_{max} (cm)	6.7	$\binom{10.2}{4.4}$	7.8	$\binom{18.0}{3.4}$	8.9	$\binom{24.1}{3.3}$	5.3	$\binom{13.1}{2.1}$	1.0	$\binom{1.4}{0.7}$
PSV (0.1 cm/sec	3.4	$\binom{8.8}{1.3}$	4.7	$\binom{6.3}{3.5}$	2.3	$\binom{5.4}{1.0}$	2.3	$\binom{7.3}{0.7}$	1.0	$\binom{1.2}{0.8}$
PSV (0.3) cm/sec	13.0	$\binom{23.9}{7.1}$	18.6	$\binom{33.0}{10.5}$	9.5	$\binom{17.3}{5.2}$	9.7	$\binom{24.3}{3.9}$	5.4	$\binom{6.9}{4.2}$
PSV (1.0) cm/sec	25.0	$\binom{38.2}{16.3}$	35.9	$\binom{95.4}{13.5}$	20.7	$\binom{48.9}{8.8}$	21.8	$\binom{50.4}{9.4}$	8.1	$\binom{15.5}{4.3}$
PSV (3.0) cm/sec	16.4	$\binom{38.0}{7.1}$	34.3	$\binom{77.8}{15.1}$	36.5	$\binom{109.7}{12.1}$	14.6	$\binom{25.6}{8.3}$	3.9	$\binom{4.8}{3.1}$
PSV (10.0) cm/sec	9.2	$\binom{20.7}{4.1}$	22.4	$\binom{48.4}{10.3}$	27.6	$\binom{44.9}{16.9}$	14.9	$\binom{33.5}{6.6}$	4.7	$\binom{6.8}{3.2}$

CROUSE, Depth = 30 km, *M* 7.9

	75 km	125 km	175 km	225 km	275 km
PSV (0.1) cm/sec	2.9	2.1	1.6	1.4	1.1
PSV (0.3) cm/sec	16.0	11.0	8.2	6.6	5.4
PSV (1.0) cm/sec	36.1	25.2	19.2	15.3	12.7
PSV (3.0) cm/sec	26.3	18.3	13.8	11.1	9.2

KAWASHIMA, *M* 7.9

	75 km	125 km	175 km	225 km	275 km
$\ddot{U}_{max}$ (cm/sec^2)	238.4	148.3	105.5	80.9	65.0
$\dot{U}_{max}$ (cm/sec)	23.7	14.7	10.5	8.0	6.4
U_{max} (cm)	5.4	3.3	2.3	1.8	1.4
PSV (0.1) cm/sec	6.6	4.2	3.0	2.3	1.9
PSV (0.3) cm/sec	28.1	17.8	12.8	9.9	8.0
PSV (1.0) cm/sec	71.2	45.0	32.4	25.0	20.2
PSV (3.0) cm/sec	30.5	19.3	13.9	10.7	8.7

JOYNER and BOORE, *M* 7.9

	75 km	125 km	175 km	225 km	275 km
$\ddot{U}_{max}$ (cm/sec^2)	74.0	33.2	17.7	10.3	6.3
$\dot{U}_{max}$ (cm/sec)	19.7	8.8	4.7	2.7	1.6
PSV (0.1) cm/sec	1.1	0.3	0.1	0.04	0.01
PSV (0.3) cm/sec	4.7	1.5	0.5	0.2	0.1
PSV (1.0) cm/sec	13.2	4.8	2.0	1.0	0.5
PSV (3.0) cm/sec	23.0	13.7	9.8	7.6	6.2

( ) = ± one standard deviation.
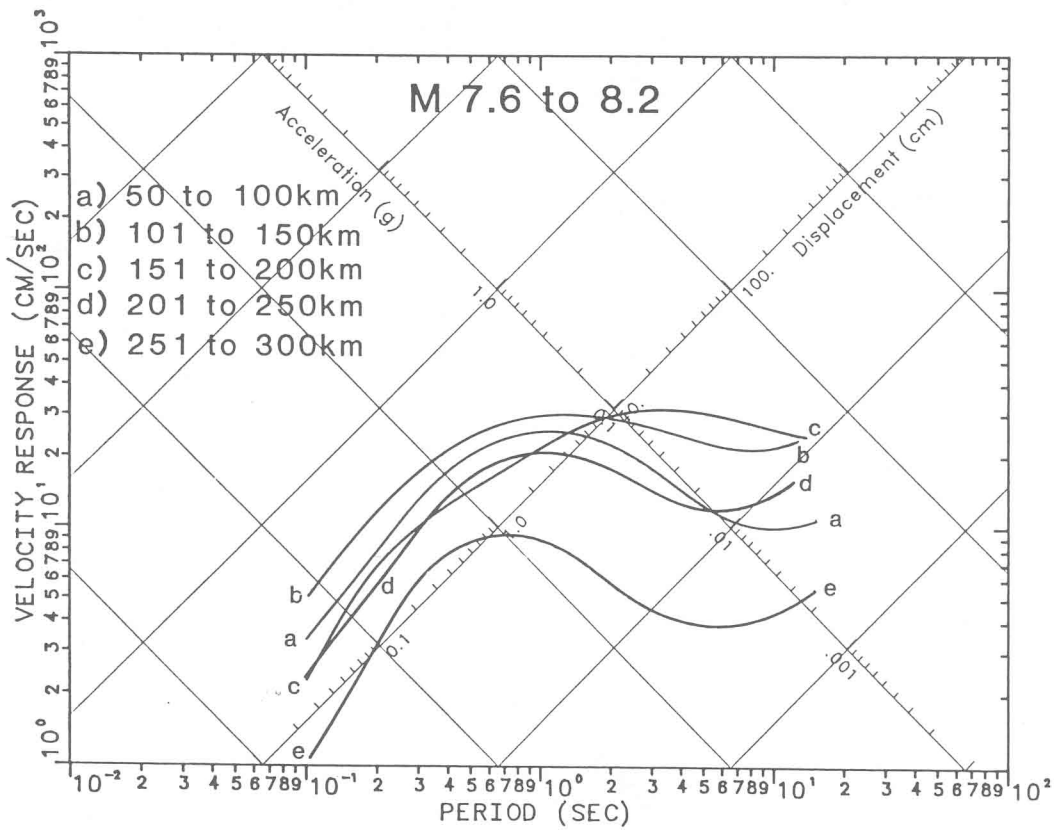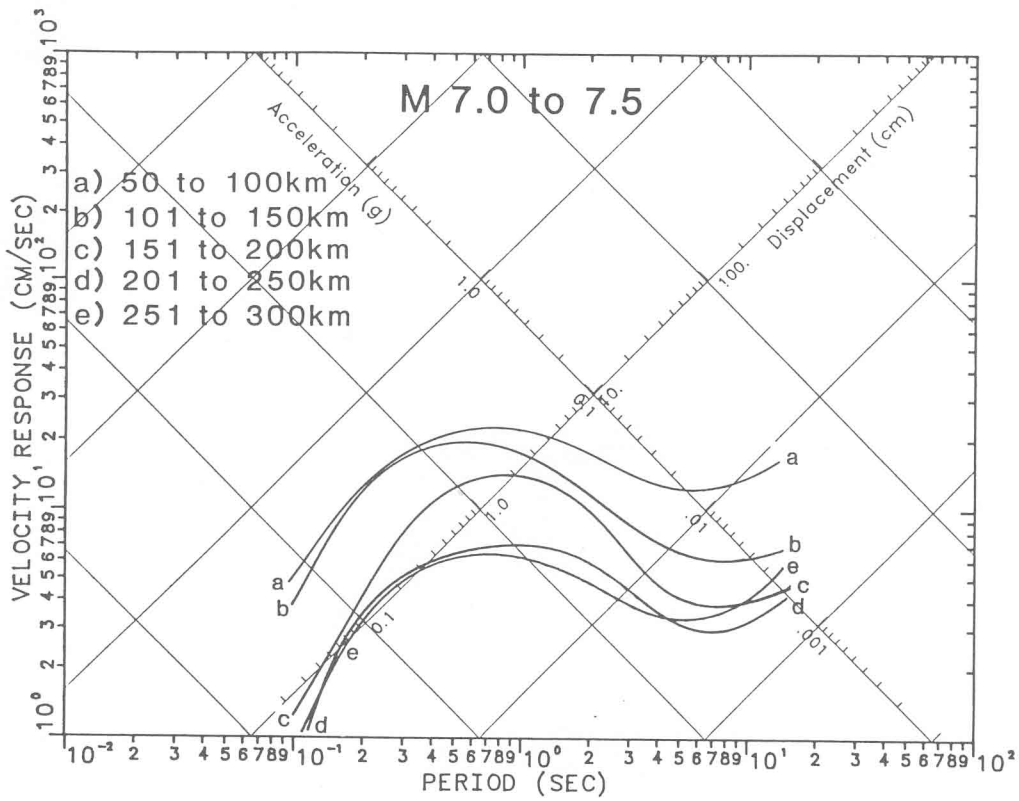
and western United States earthquakes (HEATON *et al.*, 1986). It may be that the distance attenuation is a function of earthquake size, with large subduction earthquakes having a relatively small distance attenuation.

Choosing a ground motion for design at a particular site is obviously a difficult and somewhat philosophical problem given the large scatter in the observed ground motions. However, once a design motion is chosen for a site, it may be very sobering to plot that design level against the actual data plotted in Figure 1.

Estimating Strong Ground Motions for Earthquakes of $M_w > 8\frac{1}{4}$

The Cascadia subduction zone has not experienced any large, shallow subduction earthquakes over its greater than 1000 km length for at least 150 years despite an apparent convergence rate of about 4 cm/yr. Although it is conceivable that convergence is occurring continuously through aseismic creep, the Cascadia subduction zone has many similarities to the subduction zones in southern Chile, southwestern Japan, Colombia, and Mexico (HEATON and HARTZELL, 1986). Each of these zones have experienced very large historic shallow subduction earthquake sequences and can be considered to be strongly coupled. If the Cascadia subduction zone is also strongly coupled, then earthquakes far larger than any of the events for which we presently have strong motion records can be postulated for this zone. In particular, the largest earthquakes experienced on these other subduction zones were: The 22 May 1960 Chilean earthquake (M_w 9.5), the 1707 Hoei earthquake of southwestern Japan ($M_w > 8\frac{1}{2}$), the 31 January 1906 Colombian earthquake (M_w 8.8), and the 3 June 1932 Jalisco earthquake of Mexico (M_s 8.2). HEATON and HARTZELL (1986) present circumstantial evidence that suggests (but does not prove) that large earthquakes along the Cascadia subduction zone may have an average repeat time of 400 to 500 years. Given the length of the apparent seismic gap and a suggested repeat time of more than 400 years, it seems difficult to eliminate the possibility of earthquakes comparable to the 22 May 1960 Chilean earthquake, the largest earthquake recorded this century (KANAMORI, 1977).

What might the ground motions look like from a giant earthquake such as the 1960 Chilean earthquake? This earthquake is in a different class from the earthquakes for which strong ground motions have been recorded; its seismic moment is at least one hundred times larger than that of the largest earthquake for which we have data. There are several approaches that could be utilized to estimate the nature

Figure 3

Smoothed (with period) logarithmic averages of pseudo velocity response spectra (5% damped) that are shown in Figure 1. Numerical values for these curves and standard deviations of the data about the average are found in Tables 1 and 2.
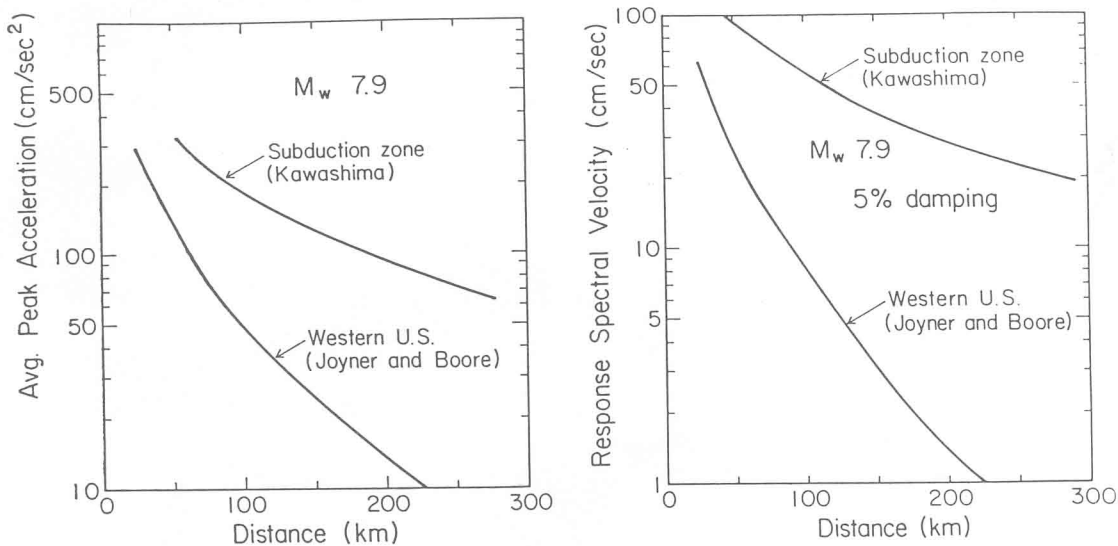
Figure 4

Comparison of predictions of average peak ground motions obtained by regression analysis of data from the southwestern United States and from Japan. Soil sites and 5% damping are assumed for the response spectra.

of motions from giant earthquakes. One approach would be to simply use the regression analyses of data from smaller earthquakes and extrapolate to very large magnitudes. However, there is little confidence that the functional form that was chosen to fit the data is appropriate to extrapolate outside the region for which there is data. A second approach would be a slight variation to the first. Once again data from smaller earthquakes could be extrapolated into the range of very large magnitudes, but the functional forms would be based on spectral scaling laws and similarity conditions. However, there is little reason to expect that an earthquake having a fault length of as much as 1000 km and rupture that may extend to the uppermost mantle will be similar to an earthquake with a fault length of 100 km and fault width that is confined to the offshore accretionary wedge.

Fortunately, teleseismic data are available from some of the most significant events of this century (HARTZELL and HEATON, 1985; HOUSTON and KANAMORI, 1986). In particular, teleseismic P-waveforms contain information about energy radiated by these earthquakes at periods as short as 1 second. Unfortunately, strong ground motions and teleseismic P-waveforms result from different complex combinations of source and wave propagation features. To infer strong ground motions directly from teleseismic P-waveforms would require a great leap of faith. In principal, we could use the teleseismic P-waveforms to deduce the detailed rupture history of a large event. We could then derive strong motion recordings from that rupture history. Of course, this presupposes that we accurately know the propagation effects of earth structure and that we have sufficient teleseismic data to infer the details of the rupture process at very short wavelengths. Although this approach can be dismissed as being impractical, it has fundamental similarities to the empirical Green's function technique that we employ in this study.

The Empirical Green's Function Technique

The basic idea behind the empirical Green's function technique is the notion that large earthquakes can be considered to be a linear combination of smaller ones. That is, to model a large earthquake, we merely superpose N smaller ones, where N is the integral ratio of the moment of the larger event to the smaller one. Since waves from the smaller and larger events travel through the same seismic velocity structure in the same manner, this technique allows us to remove this unknown from the modeling process. Furthermore, since the source of the smaller event has rupture properties that are probably similar to that of the larger event, this technique also allows us to model effects due to statistical irregularity of the rupture process. Descriptions and applications of the technique are given by HARTZELL (1978, 1985), KANAMORI (1979), IRIKURA (1983) HOUSTON and KANAMORI (1986), and others. A more quantitative discussion of this technique is also found in Appendix B of this paper.

Unfortunately, things are not quite as simple as they might appear at first glance. There are difficult questions involved in deciding how to sum these records together. For instance, if an earthquake rupture is a smooth, coherent process, then smaller ruptures must be summed in such a way that an irregular rupture process does not result. Just how to fit these records together is a very fundamental question that is explored further in Appendix B. The nature of the irregularity of the rupture process may be investigated by asserting that earthquake ruptures are self-similar with respect to size. However, this is an important issue and self-similarity should not be accepted as a matter of faith. Fortunately, this same empirical Green's function technique can be used to model teleseismic P-waveform data of historic giant earthquakes. This teleseismic data helps constrain the assumptions in the summation process. In this study, we are most concerned with estimating strong ground motions in the spectral band from 10 seconds to 10 hertz. We are not so concerned about ground motions in the spectral band comparable to the duration of giant earthquakes which may be more than 100 seconds. Thus we apply the empirical Green's function technique in such a way that we match the characteristics of short-period teleseismic waveforms. Because of effects introduced by the randomness that we assume in the timing of the Green's functions, summing enough records to match the moment ratio of the smaller and larger events may result in a significant overestimate of the short-period motions. This problem is discussed in Appendix B. To alleviate this problem, we sum just enough events to match the characteristics of the short-period teleseismic waveforms, even though this may not be consistent with the moment ratio of the two events.

In order to apply this technique, we must have an adequate set of records to use as empirical Green's functions. In this study we primarily use the records from two earthquakes for which we have the best combination of strong motion and teleseismic data; these are the 16 May 1968 Tokachi-Oki earthquake (M_w 8.2) and the 12 May 1978 Miyagi-Oki earthquake (M_w 7.5). The Miyagi-Oki event appears to be a rather simple single source, whereas the Tokachi-Oki event appears

Table 3

Empirical Green's Function.

Earthquake	Date	M_w	Green's Function Code	Station	Record Code	Distance (km)
Hyuganada	04/01/68	7.4	A	Hyaga	S–213	80
			B	Kochi	S–211	162
Tokachi-Oki	05/16/68	8.2	C	Muroran	S–234	201
			D	Aomori	S–235	175
			E	Hachinohe	S–252	130
			F	Miyako	S–236	180
Miyagi-Oki	06/12/78	7.5	H	Hachinohe	S–1202	262
			I	Akita	S–1200	240
			J	Ofunata	S–1210	101
			K	Shiogama	S–1201	95
			L	Onahama	S–1191	175
			M	Yamashita	M–217	370
St. Elias	02/28/79	7.8	Q	Icy Bay		77
			R	Yakutat		170

to be relatively complex. The actual strong motion records chosen to be Green's functions are given in Table 3. An inspection of these records (found in Appendix A) shows that there is a wide range in the character of the motions from station to station. As was discussed earlier, much of this character seems to be a site effect. In our summation procedure, we sum the records from several different sites and thus our synthetic records represent motions that are averaged in a poorly defined way over several sites. If ground motions are desired at a specific site, it may be better to sum records taken only from stations that appear to have simple site responses (hard rock sites?) and then apply a site correction that is appropriate. Of course, this is easier said than done and we have not attempted to eliminate Green's functions with complex site responses in this study.

Definition of the Source Geometry

The source characteristics of six of the largest earthquakes for which we have short-period teleseismic data are given in Table 4. Source parameters are also given for the four events in Table 3 chosen as empirical Green's functions. We will describe the details of the model geometry for only the largest of these, the 22 May 1960 Chilean earthquake (M_w 9.5). Unfortunately, there is still very little known about the spatial and temporal distribution of seismic energy release for this, or any other giant earthquake. There is little question that the rupture length was very long, on the order of 1000 km. For simplicity, we assume that the characteristics of the rupture do not change significantly along the fault length, although we present no real data to justify this assumption. The question of how the rupture varies down the dip is both problematic and of considerable concern since such variation can significantly affect

Table 4

Earthquake Parameters.

Earthquake	Date	M_w	$M_0 \times 10^{28}$ dyne-cm	Length (km)	Width (km)
Hyuganada	04/01/68	7.4	0.17	—	—
Miyagi-Oki	06/12/78	7.5	0.22	100	75
St. Elias	02/28/79	7.8	0.65	—	—
Tokachi-Oki	05/16/68	8.2	2.8	180	140
Kuriles	10/13/63	8.5	7.5	250	150
Rat Island	02/04/65	8.7	14.0	500	150
Aleutians	03/09/57	9.1	15.0	800	150
Kamchatka	11/04/52	9.0	35.	650	200
Alaska	03/28/64	9.2	75.	700	300
Chile	05/22/60	9.5	270.	950	200

the spatial distribution of the strong shaking. For example, we would like to know whether or not large amounts of seismic energy are radiated from directly beneath a site for which we simulate ground motions. Since it is likely that the rheology of fault zone materials changes with depth, it also seems likely that the rupture characteristics change with depth. It may be that significant slip occurs slowly at depth with little radiation of energy in the frequency band of interest. Because there is so little constraints on the assumption of fault width, we present the results both from models in which short-period radiation is confined mainly to the offshore regions and also from models in which seismic radiation is allowed to extend significant distances inland.

The geometries of several models of the Chilean earthquake are shown in Figures 5 and 6 and a summary of parameters for models presented in this study is found in Table 5. In Figure 5, we show several different ways to simulate a Chilean earthquake using the records from Miyagi-Oki-size earthquakes (4/1/68 Hyuganada *M* 7.4, 6/12/78 Miyagi-Oki *M* 7.5, and 2/28/79 St. Elias *M* 7.8). First consider the geometry of the model M–1140–200; the M stands for Miyagi-Oki, 1140 is the total number of records that are summed, and 200 is the fault width. The long-period moment ratio of the 1960 Chilean earthquake and the Miyagi-Oki earthquake is 1140. In this model, each subfault is assumed to be of dimensions 50 km long by 40 km wide. The letters in the subfaults tell which records were used as Green's functions for that subfault (see Table 3). The Green's functions were chosen such that the difference in distance between that required by the model geometry and that at which they were observed is a minimum. The Green's functions are also scaled for distance using the distance attenuation relationship of CROUSE *et al.* (1988). The subfaults with plus signs have Green's functions that are a simple average of their closest neighbors. In the synthesis of teleseismic *P*-wave records, the Green's function is assumed to be the same for each subfault. The rupture is assumed to propagate radially at a velocity of 3.2 km/sec from the hypocenter shown. In model M–1140–200, each subfault ruptures 12 times within a period of 60 seconds after the onset of rupture. The actual rupture times are random within 12, 5-second, evenly-spaced time windows.
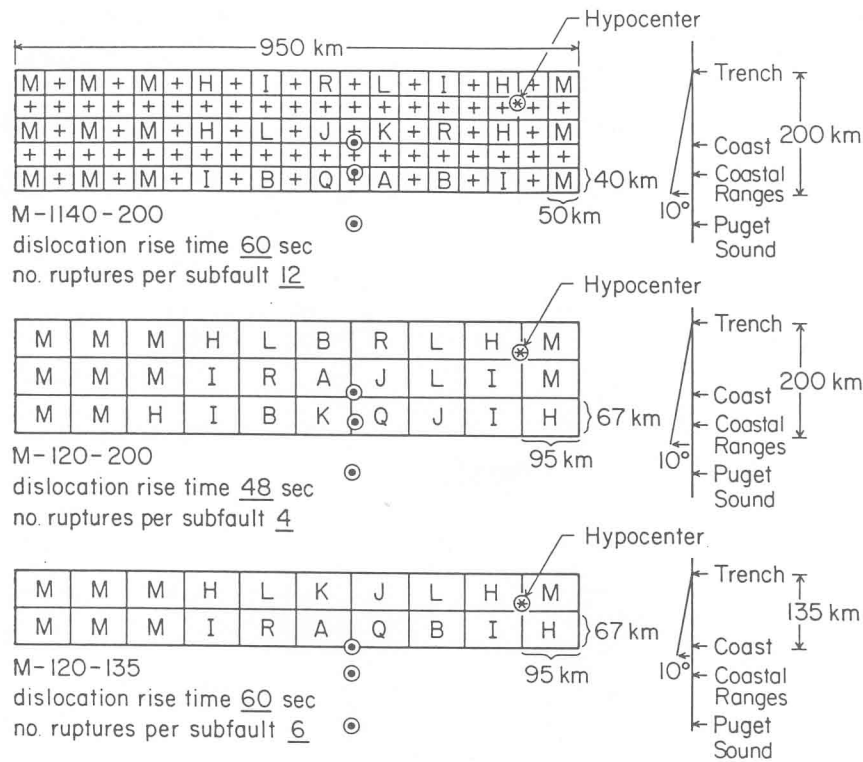
Figure 5

Geometry of fault models used to simulate an earthquake in the Pacific Northwest similar to the 22 May 1960 Chilean earthquake (M_w 9.5). Each box represents a subfault whose response is simulated by summing the ground motion from M_w 7.5 earthquakes. Letters in the boxes refer to Table 3 and they designate which records are used as Green's functions. Boxes with a + use a Green's function that is a linear interpolation of the Green's functions in adjacent boxes. Cross-sections, showing the relative position of the fault and the observation points are shown to the right.

The fault is assumed to dip 10 degree landward from a surface trace that is about 120 km offshore. The earthquake is observed at three different locations near the center of the rupture. One site is assumed to be on the coast, another is located within the coastal ranges about 50 km inland, and the final site is located in the Puget Sound region. When the rupture is assumed to have a width of 200 km, it extends beneath both the coastal and coastal ranges sites.

The second model, M–120–200, is very similar to the first except the total number of Green's functions that are summed is reduced to only 120. As discussed later, fewer Green's functions are required by the short-period teleseismic data than is required by the moment ratio. In this second model, each subfault is assumed to be 95 km long and 67 km wide. Each subfault ruptures 4 times within a period of 48 seconds after the onset of rupture. In the third model, M–120–135, the rupture surface is assumed to be significantly narrower (135 km) and is confined to mainly the offshore regions. Although it seems likely that the Chilean earthquake ruptured over a larger fault width than this, it may be that short-period waves emanated only from the shallower portions of the fault. The total number of Green's functions summed is

Table 5

Model Parameters.

Model Code	Length (km)	Width (km)	Dislocation Rise Time (sec)	*	m*	n*
1960 Chile M_w 9.5						
M–1140–200	950	200	60	19	5	12
M–120–200	950	200	48	10	3	4
M–120–135	950	135	60	6	2	6
T–96–200	900	200	64	6	2	8
T–24–200	900	200	50	6	2	2
T–6–100	900	100	50	6	1	2
1964 Alaska M_w 9.2						
M–364–300	700	300	32	13	7	4
M–88–300	700	300	34	11	4	2
1957 Aleutian M_w 9.1						
M–66–150	800	150	12	11	3	2
M–22–150	800	150	6	11	2	1
1952 Kamchatka M_w 9.0						
M–165–200	650	200	15	11	5	3
M–36–200	650	200	14	6	3	2
1965 Rat Island M_w 8.7						
M–55–150	500	150	5	11	5	1
M–18–150	500	150	4	6	3	1
1963 Kuriles M_w 8.5						
M–36–150	250	150	7	4	3	3
M–12–150	250	150	2	4	3	1
1968 Tokachi-Oki M_w 8.2						
M–9–140	180	120	4	3	3	1

* is the number of subfaults along the fault length; m is the number of subfaults along the fault width; n is the number of times each subfault ruptures.

120, the same as in the previous model. However, the number of times that each subfault ruptures is increased to 6 during a total dislocation rise time of 60 seconds.

In Figure 6, we show an alternate set of models for the Chilean earthquake in which records from the 1968 Tokachi-Oki earthquake (M_w 8.2) are used as empirical Green's functions. Most features of these models are very similar to those presented in Figure 5. However, since the Tokachi-Oki earthquake is a much larger event, only 96 of them are required to match the moment of the Chilean earthquake. Once again, the letters in each subfault refer to specific records listed in Table 3. Models T–96–200 and T–24–200 both have the same overall subfault geometries and are 900 km long by 200 km wide; the only difference being that each subfault ruptures 8 times over a total dislocation time of 64 seconds in T–96–200, whereas each subfault ruptures only twice over a dislocation time of 50 seconds in model T–24–200. In the last model, T–6–100, the Chilean earthquake is modeled as a single line of Tokachi-Oki earthquakes where short-period radiation is confined to
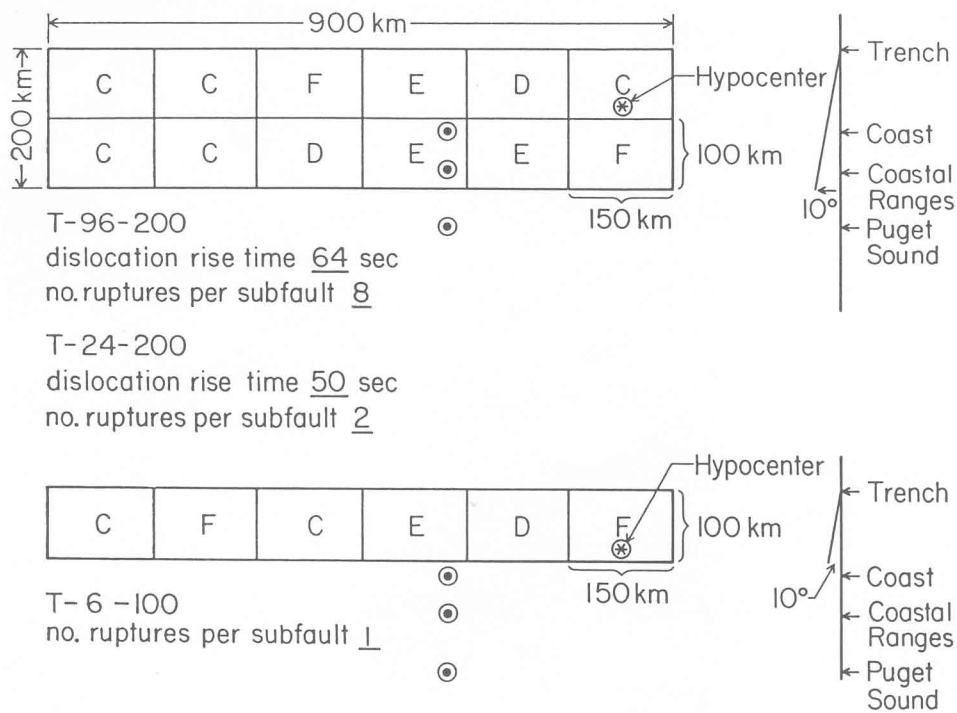
Figure 6
Same as Figure 5, except that 16 May 1968 Tokachi-Oki earthquake (M_w 8.2) records are used as Green's functions.

the offshore region. In this case only 6 Tokachi-Oki earthquakes are summed with each subfault experiencing only one rupture. Of the Tokachi-Oki Green's function simulations, this model fits the teleseismic P-wave amplitudes the best.

Results for Teleseismic P-waveforms

Before we discuss the strong ground motions that we obtained from our modeling procedure, we will present the salient features of our models of the teleseismic waveforms of giant earthquakes. These teleseismic models provide important constraints on the model parameters of our strong motion models. Simulations of teleseismic recordings of the 22 May 1960 Chilean earthquake are shown in Figure 7 using Miyagi-Oki earthquake records (M_w 7.5) as Green's functions and in Figure 8 using Tokachi-Oki (M_w 8.2) records as Green's functions. We model the Pasadena, California long-period Benioff seismograms (1–90) and the Tinemaha, California short-period Benioff seismograms (1–0.7) since both of the earthquakes that we use as Green's functions and also the giant earthquakes that we wish to model were well recorded on these seismometers. The peak amplitude of each record is given where the units are microns for the long-period Benioff records and the units are in centimeters (not corrected for magnification) for the short- period Benioff records. Since the Japanese earthquakes are observed at a range of about 75 degrees and the Chilean
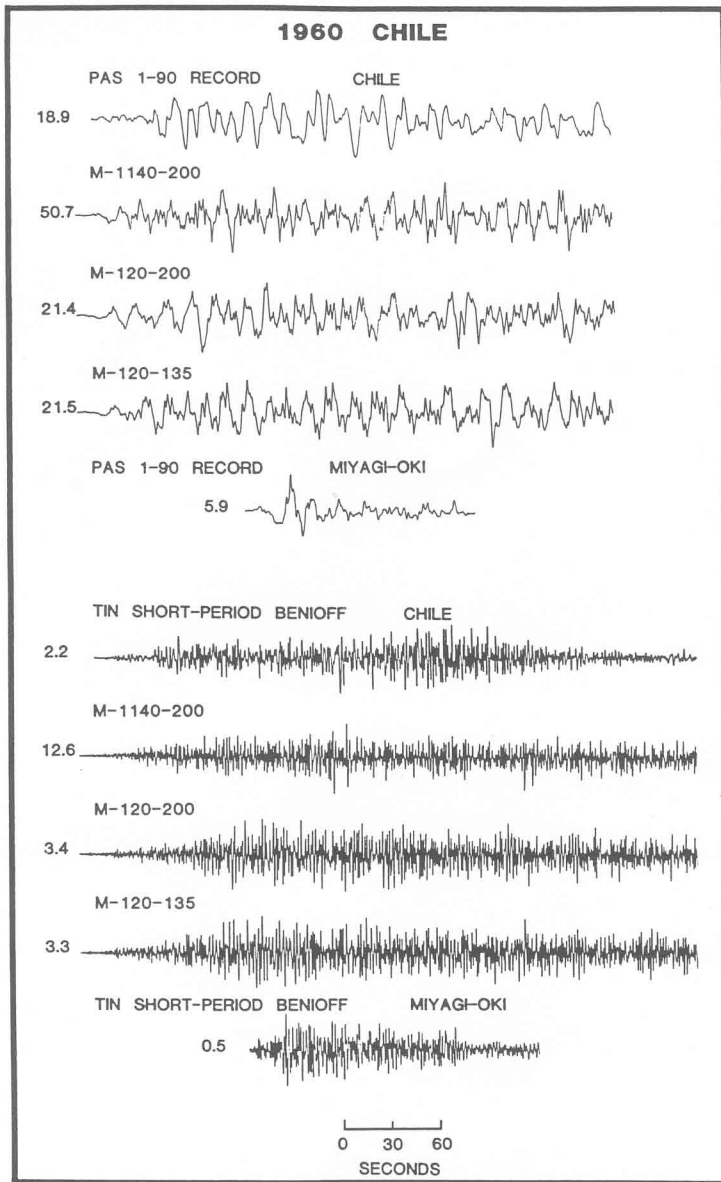
Figure 7

Comparison of observed long- and short-period vertical Benioff teleseismic *P*-wave seismograms with records synthesized using the 1978 Miyagi-Oki earthquake seismograms as Green's functions. Details of the model parameters are found in Figure 5 and the text. The Miyagi-Oki seismograms that were used as Green's functions are also shown. Peak amplitudes of the long-period Benioff records have been corrected for instrument magnification and are given in microns. Peak amplitudes for the short-period Benioff records are given in centimeters on the original seismograms.

earthquake is observed at about 85 degrees, the Japanese records were corrected for spherical spreading in the summation procedure, about a factor of 0.87 in this case.

Although the moment of the Chilean earthquake that is derived from long-period waves is about 1000 times that of an M_w 7.5 earthquake, it seems clear that summing the records from that many Miyagi-Oki earthquakes in a random way inevitably overestimates the observed waveforms (Figure 7). In a similar manner,
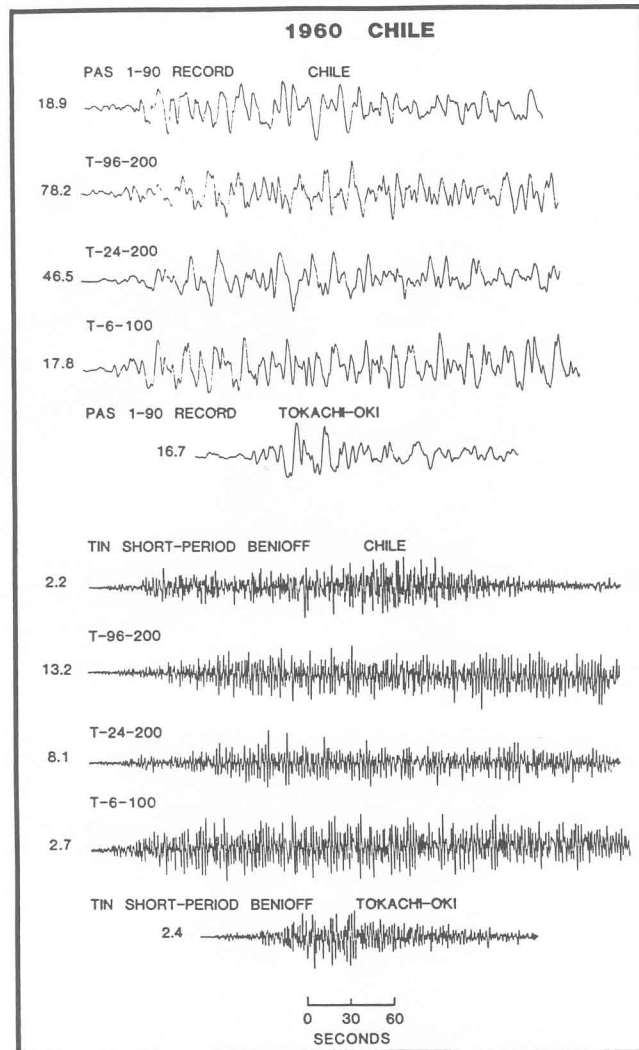
Figure 8
Same as Figure 7, except that seismograms from the 1968 Tokachi-Oki earthquake are used as Green's functions. Model parameters are found in Figure 6 and the text.

summation of the records from 96 Tokachi-Oki earthquakes results in synthetic records that are too large (Figure 8). In fact, the records from the Tokachi-Oki earthquake have peak amplitudes comparable to those observed for the Chilean earthquake. Thus it is important that our modeling procedure increase the duration of the signal without significantly increasing the peak amplitudes. In Figure 8 we see that it is necessary to sum only about 6 Tokachi-Oki earthquakes in order to match the overall amplitude and duration of the Chilean earthquake records. It should be noted that the deconvolutions of the Pasadena Benioff 1–90 records by HARTZELL and HEATON (1985) for both the Miyagi-Oki and Tokachi-Oki earthquakes yielded moments equal to the accepted long-period estimates. These results indicated that

the Pasadena Benioff records are representative records for these two events. Below we present teleseismic simulations of other great earthquakes using Miyagi-Oki as a Green's function which support the results obtained in the simulation of the Chilean earthquake, and argue against these results being due to nodal records.

A comparison of synthetic short-period Benioff records with that observed during the 1964 Alaskan earthquake (M_w 9.2) is shown in Figure 9. The teleseismic P-waves for this event are among the largest we observed for any earthquake; the Tinemaha short-period Benioff record is about twice the amplitude of the record for the Chilean earthquake and the Alaskan earthquake is the only event for which the
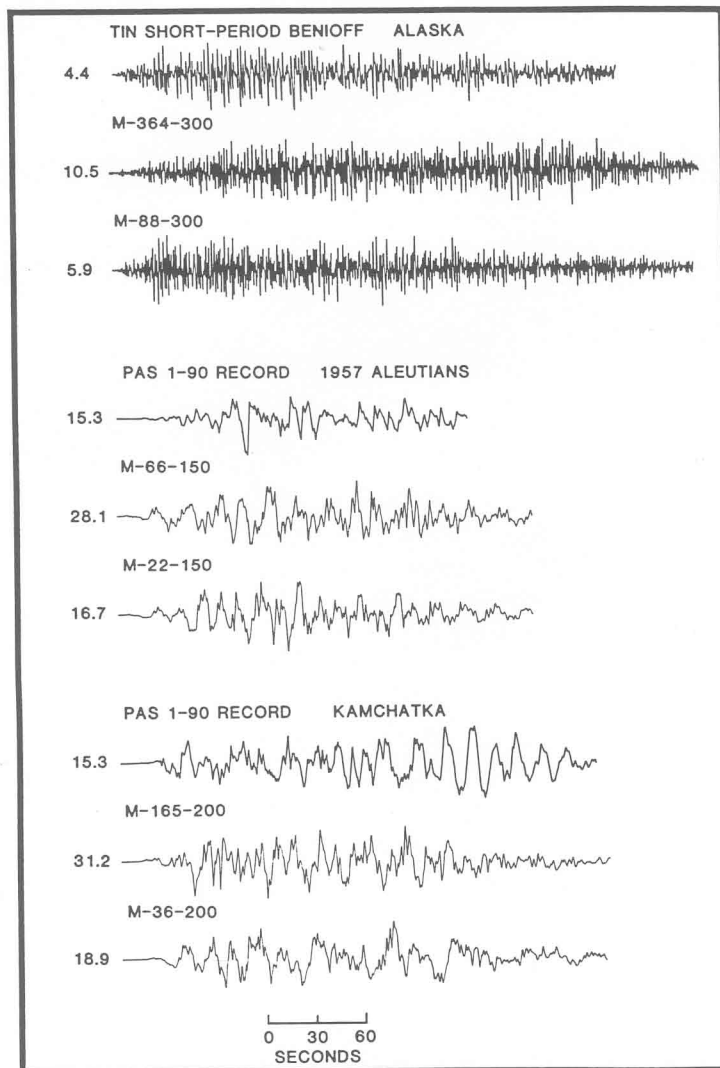
Figure 9

Comparison of observed teleseismic P-wave seismograms with records synthesized by summing Miyagi-Oki earthquakes records. In each case, the first model is the one for which enough Miyagi-Oki earthquakes were summed to match the long-period moment. In the second model, only enough records were summed to match the observed seismograms.

Pasadena long-period Benioff records were off scale. However, Alaska is relatively close to Pasadena, and when geometric spreading is considered, the Alaskan records are of comparable size to the Chilean records. The summation of 364 Miyagi-Oki records (the number indicated by the moment ratio) clearly overestimates the observed amplitude. Furthermore, the envelope of the waveform of model M–364–300 has a fairly uniform amplitude throughout the record, whereas the observed record seems to show a larger amplitude for the first 90 seconds than for the latter 90 seconds. This seems to provide corroborating evidence for the model of RUFF and KANAMORI (1983) in which they suggest that the earthquake initiated with the rupture of a large asperity with a diameter of about 200 km. In the model M–88–300, we have assumed that dislocations in the hypocentral area are about twice as large as those that occurred on the periphery of the rupture surface. In Figure 10, we show sketches of the spatial distributions of the dislocations that provided a reasonable match with the observed waveform envelopes for each of the earthquakes that we simulate. The model M–88–300, in which 88 Miyagi-Oki records are summed, gives a good overall fit to this data.

A comparison of synthetic long-period Benioff records for the 1957 Aleutian earthquake (M_w 9.1) with the observed is also shown in Figure 9. This earthquake has been assigned a very high energy magnitude because of its very long aftershock zone (SYKES, 1971; KANAMORI, 1977). However, direct measurements of the moment form very long-period surface waves are not currently available for this earthquake. The Pasadena long-period Benioff records are not particularly impressive and the summation of 66 Miyagi-Oki records (model M–66–150) results in significantly larger synthetics than the observed. The summation of only 22 Miyagi-Oki records (M–22–150) yields a more acceptable fit to the data. A fairly uniform dislocation distribution on a long, narrow fault (Figure 10) seems adequate to explain the Pasadena waveform.

Free oscillation recordings of the 1952 Kamchatka earthquake (M_w 9.0) provide fairly direct evidence that this event ranks among the giant historic earthquakes (KANAMORI, 1975). However, the summation of only 36 Miyagi-Oki records (M–36–200) provides an adequate fit to these records. The assumption of relatively uniform rupture along the fault plane seems adequate to explain the Pasadena records.

Comparisons of observed long- and short-period Benioff records from the 1965 Rat Island earthquake (M_w 8.7) are shown in Figure 11. The model M–18–150 has several asperities (Figure 10) that produce variations in the waveform envelope of the type that are seen in the observed long-period records.

In Figure 12, we show comparisons of the long- and short-period synthetics with the records observed for the 1968 Tokachi-Oki earthquake (M_w 8.2). A relatively detailed dislocation distribution has been deduced by KIKUCHI and FUKAO (1986) and this distribution (Figure 10) has been assumed in our model M–9–140. Summing the number of Miyagi-Oki records implied by the moment ratio of these two events results in a good match to the observed records.
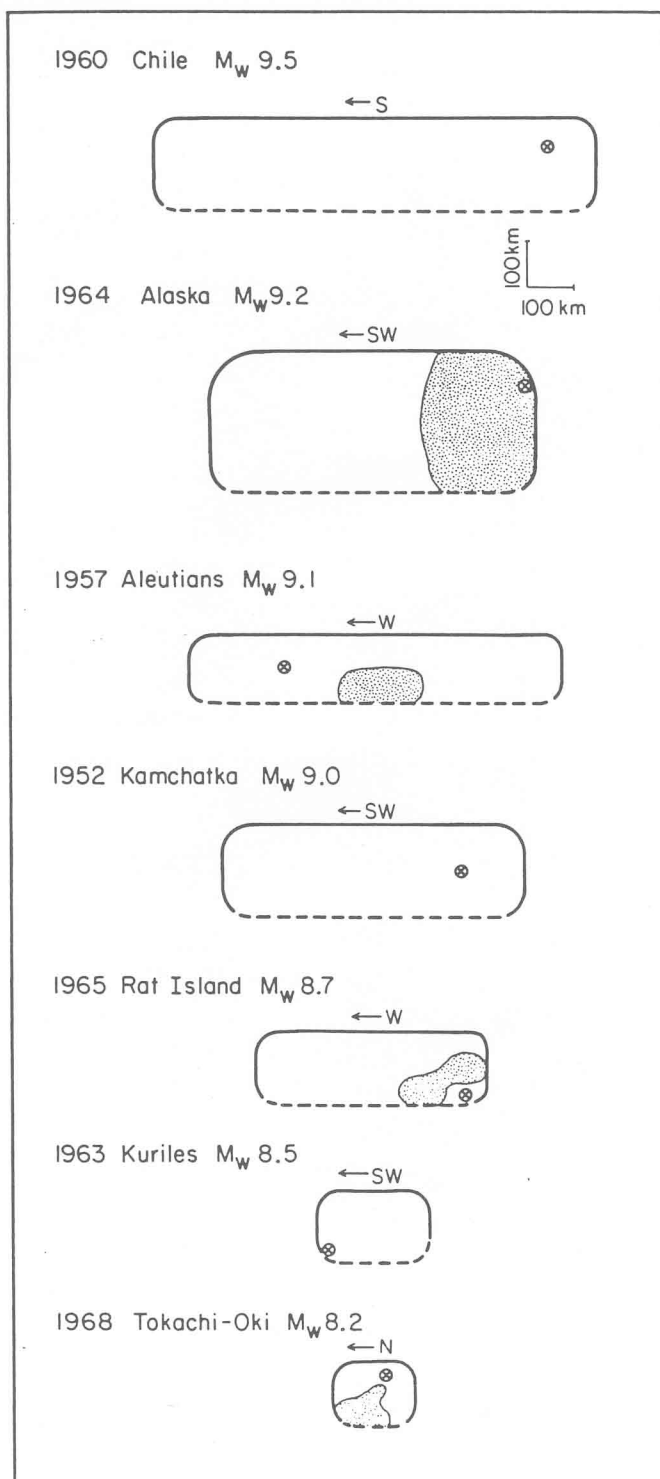
Figure 10

Schematic showing the assumed rupture characteristics of earthquakes modeled in this study. Although the bottom of the rupture surfaces are poorly determined, we considered the dashed line to define the bottom of the surface that radiated significant short-period energy. Hypocenters are shown by the $\otimes$ symbol and stippled regions designate areas that are thought to have relatively larger dislocations.
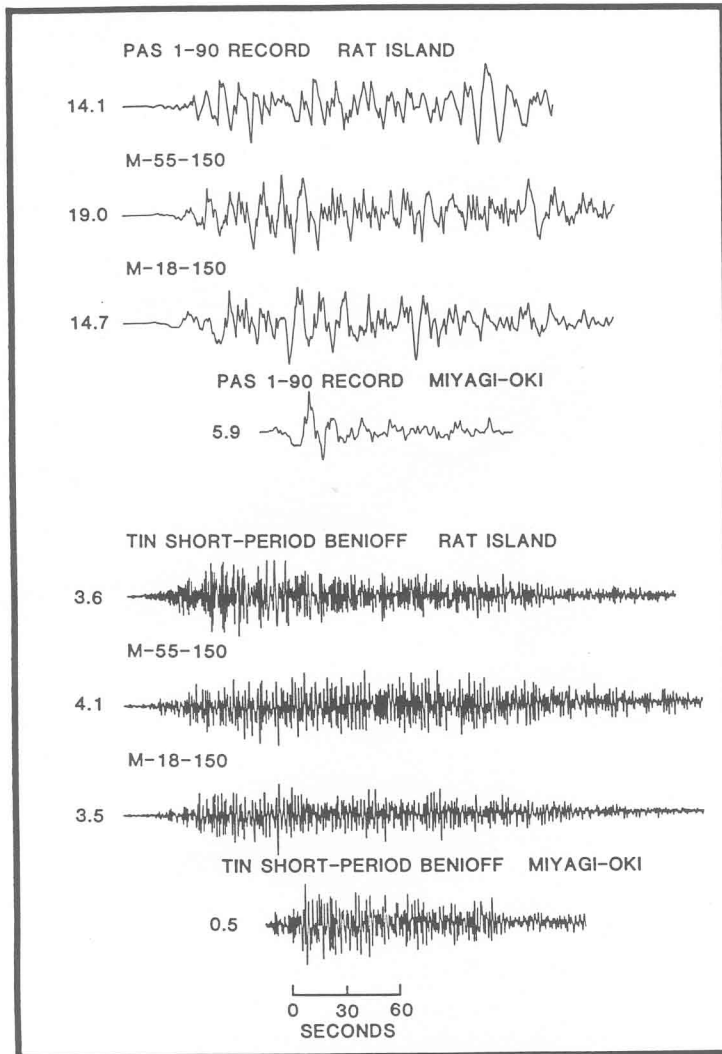
Figure 11

Comparison of observed teleseismic *P*-waveforms from the 1965 Rat Island earthquake with records synthesized by summing Miyagi-Oki earthquake records. Although the long-period moments of these earthquakes would indicate that 55 Miyagi-Oki records should be summed (M–55–150), a better match to the data is provided by the model in which only 18 records are summed (M–18–150).

The 1963 Kurile earthquake (M_w 8.5) is the last event that we consider. As can be seen in Figure 12, the observed records from this event are comparable in size to those observed from the Tokachi-Oki earthquake. The model M–12–150 assumes a relatively uniform dislocation distribution (Figure 10) and compares well with the observed records.

We have seen that the assumption that we can model giant earthquakes by randomly summing enough smaller ones to match the moments consistently overestimates the teleseismic *P*-waveforms. In several ways, this result is to be expected. As is pointed out by JOYNER and BOORE (1986) and also Appendix B, the random
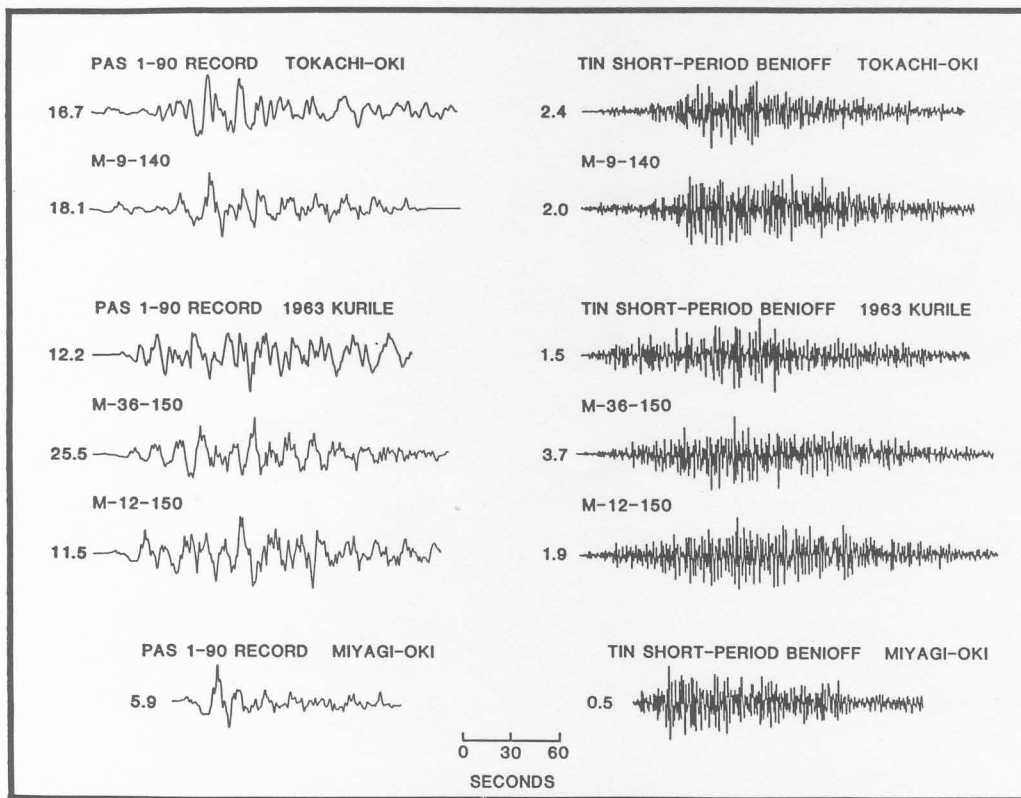
Figure 12

Comparison of observed teleseismic *P*-wave records from the 1968 Tokachi-Oki earthquake and the 1963 Kurile earthquake with records synthesized by summing Miyagi-Oki earthquake records. The summation of 9 Miyagi-Oki records (M–9–140), the number indicated from the moment ratio, provides a good match to the observed. However, for the 1963 Kurile earthquake, fewer records must be summed than is indicated by the moment ratios.

summation of N waveforms results in a $\sqrt{N}$ increase in high-frequency spectral levels; this is a larger increase than is produced by most spectral scaling laws that are based on the observed records of smaller earthquakes. Furthermore, HARTZELL and HEATON (1985) present clear evidence that teleseismic *P*-waves in the period range from 2 to 50 seconds saturate for earthquakes larger than about $8\frac{1}{4}$. This saturation effect can be seen both in the teleseismic time functions that they present and also in the Fourier amplitude spectra. In fact, the Fourier amplitude spectra presented by HARTZELL and HEATON (1985) seem to provide direct evidence that the rupture process of giant earthquakes is not self-similar to that of smaller ones. The increase in high-frequency spectral levels with moment appears to be less for earthquakes of $M_w > 8$ than for smaller earthquakes. This conclusion contrasts somewhat with the work of HOUSTON and KANAMORI (1986) who report that the amplitudes of high-frequency teleseismic *P*-waves grow at a constant rate for earthquakes varying from M_w 6 to M_w $9\frac{1}{2}$. The primary reason for this difference appears to be a difference in the giant earthquake data sample.

Results for Strong Ground Motions

Response spectra for the Chilean earthquake models described above and assuming the coastal ranges site located about 50 km from the coast are presented in Figure 13. The records that are used as Green's functions are found by cross-referencing Figures 4 and 5, Table 3, and Appendix A. Although the teleseismic motions for the models designated with an M were constructed by summing only Miyagi-Oki earthquake records, several of the Green's functions in the corresponding strong motion models were from the 1968 Hyuganada earthquake (M_w 7.4) and the 1979 St. Elias earthquake (M_w 7.8). These earthquakes have relatively simple far-field time functions and are similar in size to the Miyagi-Oki earthquake. We feel that including them in the Green's function set helps to provide synthesized ground motions that are less dependent on one particular set of records. The response spectra from the models designated T are obtained from summing records from the Tokachi-Oki earthquake only.

The response spectrum from each of these models is quite large. In particular, the spectra obtained by summing the number of records determined from the moment ratios (M–1140–200 and T–96–200) are alarmingly large. However, these models are inconsistent with the teleseismic data and thus we believe that they are not likely to be representative of the motions that may be encountered in giant earthquakes. It is not too surprising that our modeling procedure should produce large ground motions; the motions we use as Green's functions are already large. The sum of a number of these motions must result in a motion that is larger than the largest of the Green's functions.

In Figure 14, we show response spectra for the vertical ground motions produced by the models described above. These motions were synthesized using a procedure identical to the one used to sum the horizontal motions. In Figure 15, we show time histories for one horizontal component and the vertical component of ground motion for the model M–120–200 and for the coastal ranges site shown in Figure 5. We investigated many models in which we changed parameters (such as the hypocenter, the Green's function distribution, the number of Green's functions, the fault width) and the model M–120–200 represents a fair median to those models. Due to the assumption of random timing in our models, the hypocentral location

$\longrightarrow$

Figure 13

Synthesized pseudo-velocity response spectra (5% damping) for one component of horizontal ground motion from the models shown in Figures 5 and 6. The models in the top half are constructed by summing Miyagi-Oki-sized earthquake whereas the models in the bottom half are from summations of Tokachi-Oki earthquake records. Although the models M–1140–200 and T–96–200 are designed to match the long-period moment of the 1960 Chilean earthquake, they clearly overestimate the teleseismic P-waveforms and thus the spectra from these models are not considered to be plausible. The site is assumed to lie in the coastal ranges about 50 km from the coast.

SIMULATED MAGNITUDE 9.5 EARTHQUAKES

SIMULATED MAGNITUDE 9.5 EARTHQUAKE
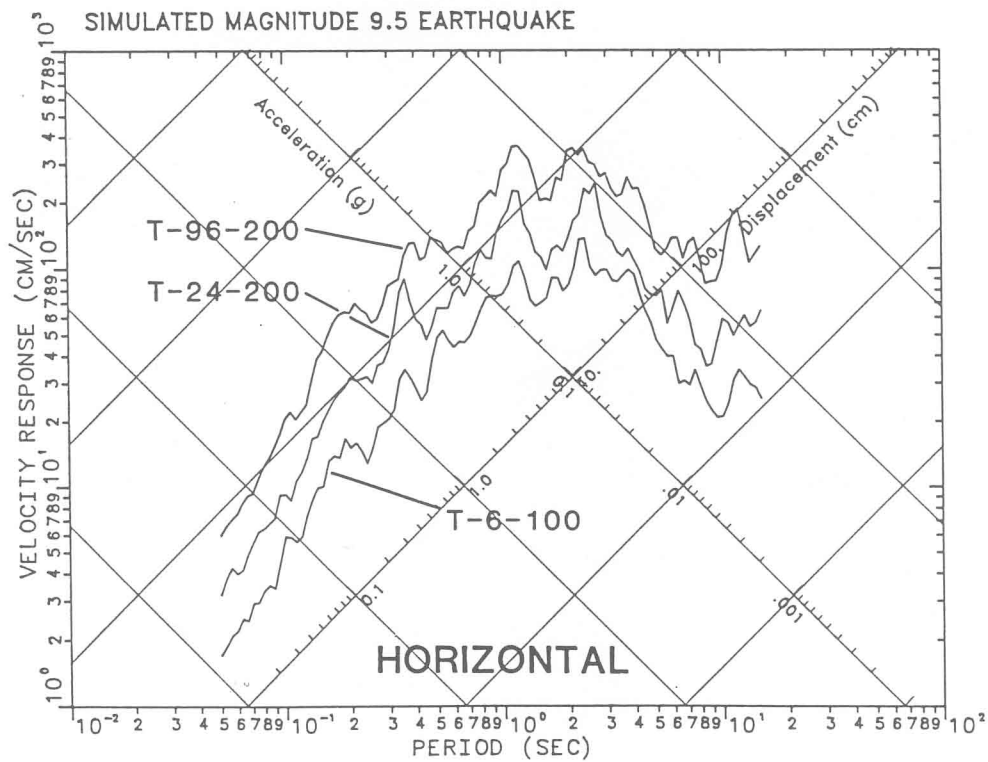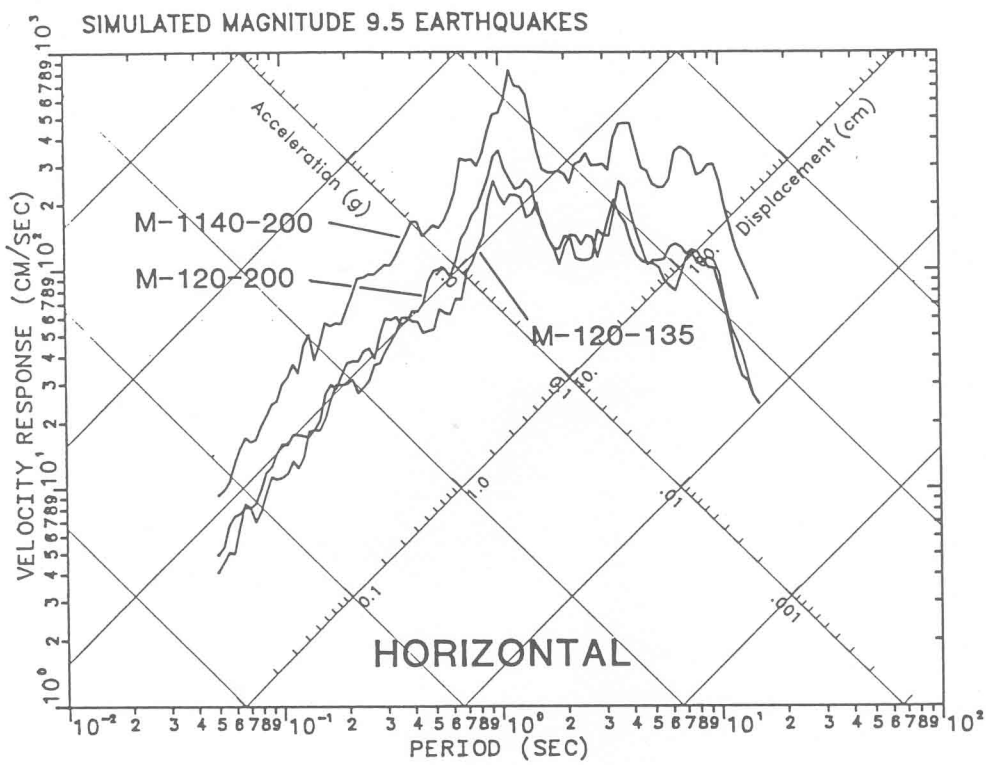
had little overall effect on either peak time domain or spectral amplitudes. Furthermore, the duration of strong shaking was fairly stable from model to model since it is mainly determined by the overall rupture length. The choice of individual records as Green's functions and the number of Green's functions to be summed appear to be the most important variables in our modeling procedure.

Since the individual records used as Green's functions have been filtered at periods longer than 10 seconds, their sum is also filtered in a similar manner. However in giant earthquakes, coastal regions may experience large static ground displacements; some coastal regions of Alaska were horizontally offset by 20 meters during the 1964 earthquake (PLAFKER, 1972). Obviously, the ground displacements given in Figure 15 do not account for static ground displacements. Recently, ANDERSON et al. (1986) presented stong motion recordings of the 19 September 1985 Mexico earthquake (M_s 8.1) in which there is convincing evidence for static offset of the recording sites. These offsets are on the order of 1 meter and occur in a linear ramp-like fashion over 10 to 20 seconds. In giant earthquakes, we anticipate that static offsets occur in a similar fashion, except that the displacements may exceed 10 meters and may occur over a duration of more than a minute. Ground motions of this nature can be modeled with acceptable accuracy using procedures similar to that described by HASKELL (1969). However, the accelerations associated with this very long-period motion are probably considerably smaller than the accelerations at higher frequencies that are presumably the result of irregularity of the rupture process. In some applications, such as the excitation of seiches, it may be important to consider the effects of the very long-period motions that give rise to static offsets.

In Figure 16, we show smoothed response spectra for the horizontal ground motions produced by the Chilean earthquake model M–120–200 as observed at sites located on the coast, in the coastal ranges 50 km inland, and in the Puget Sound region (see geometry in Figure 5). In this model, peak accelerations at the coast and in the Puget Sound are 0.89 g and 0.39 g, respectively. The time histories of ground motion are similar to those shown in Figure 15 for the coastal ranges site. The distance scaling relations of CROUSE et al. (1988) and KAWASHIMA et al. (1984) were used to scale the Green's functions in these calculations. The distance scaling relations of KAWASHIMA et al. (1984) indicate a somewhat stronger attenuation of motion with distance and their use results in motions that are about 10% higher and 10% lower at the coastal and Puget Sound sites, respectively. Although this model results in quite strong ground motions at Puget Sound, it should not be forgotten that Anchorage, Alaska lies at a similar point with respect to the Alaskan subduction zone. Although there are no strong motion recordings of the 1964 Alaskan earthquake, there was considerable damage in Anchorage and it seems clear that the ground motions were quite strong. If the zone of short-period seismic radiation is assumed to be narrower (model M–120–135), then the synthetic ground motions at the Puget Sound site drop by about 15%.
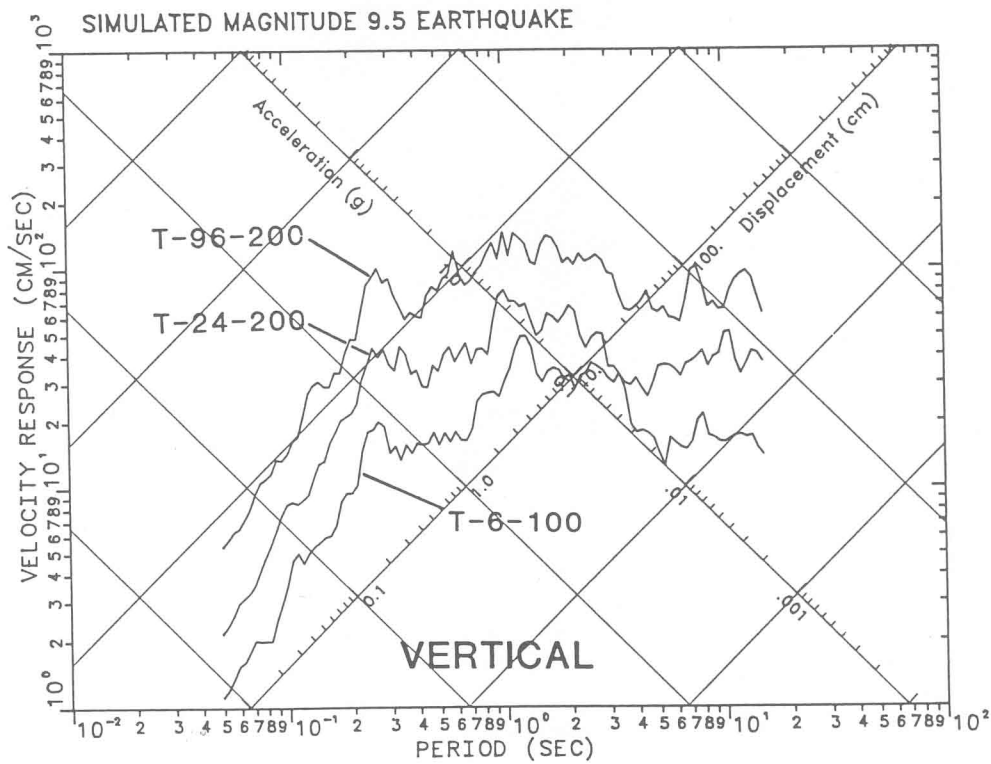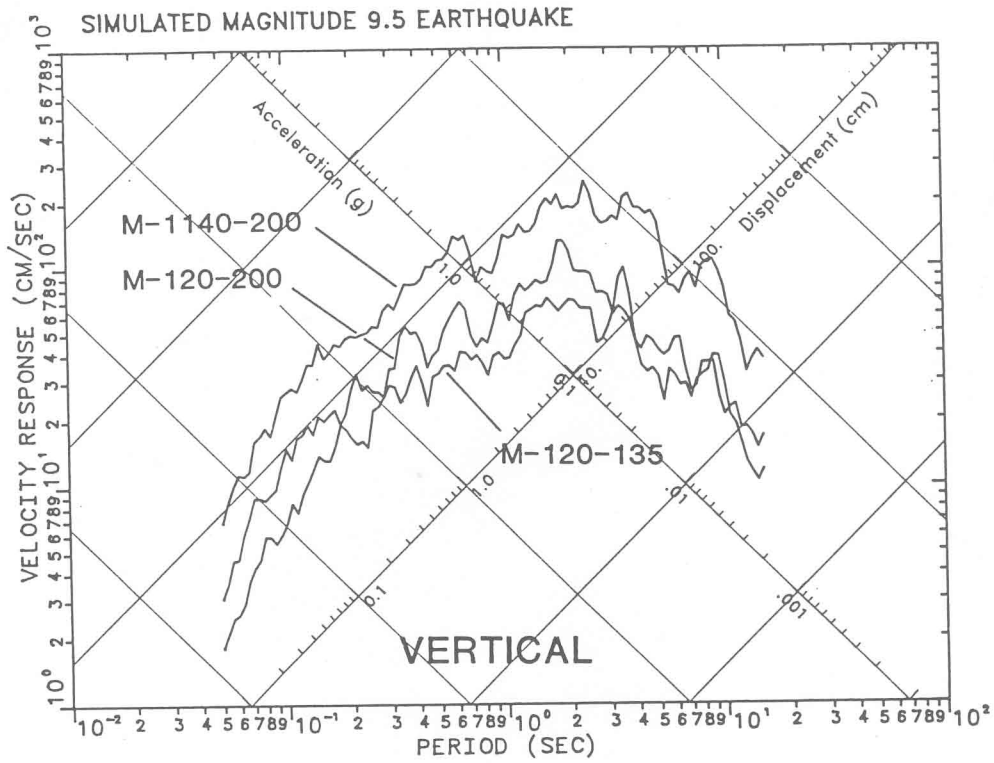
Figure 14
Same as Figure 13, except for the vertical component of synthesized ground motion.
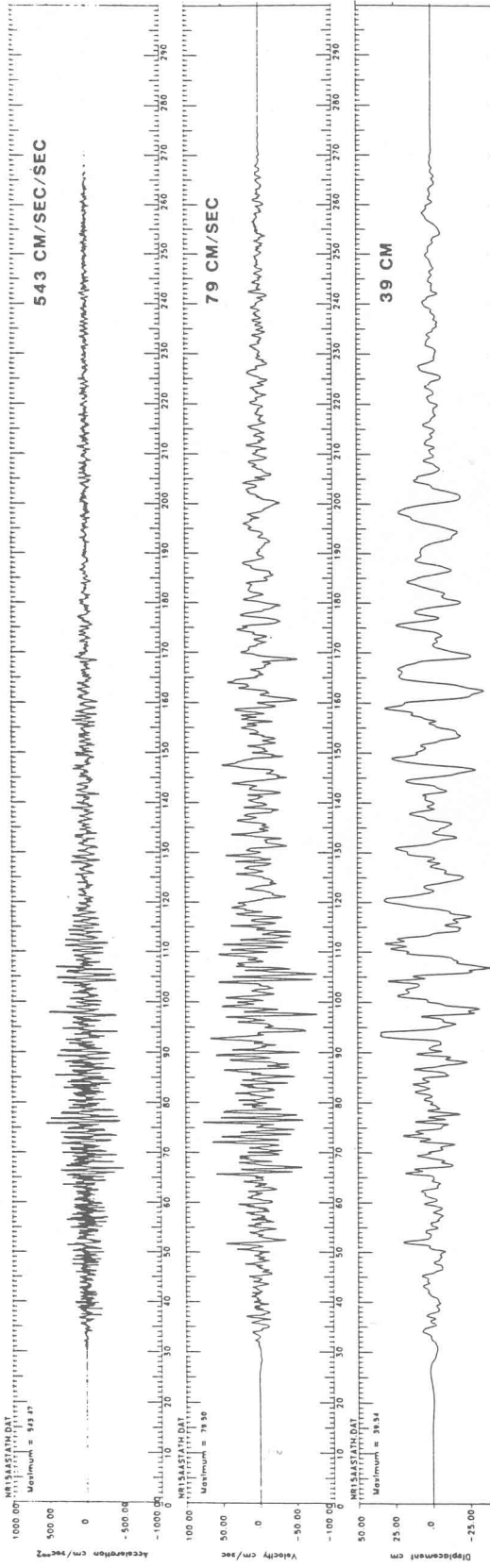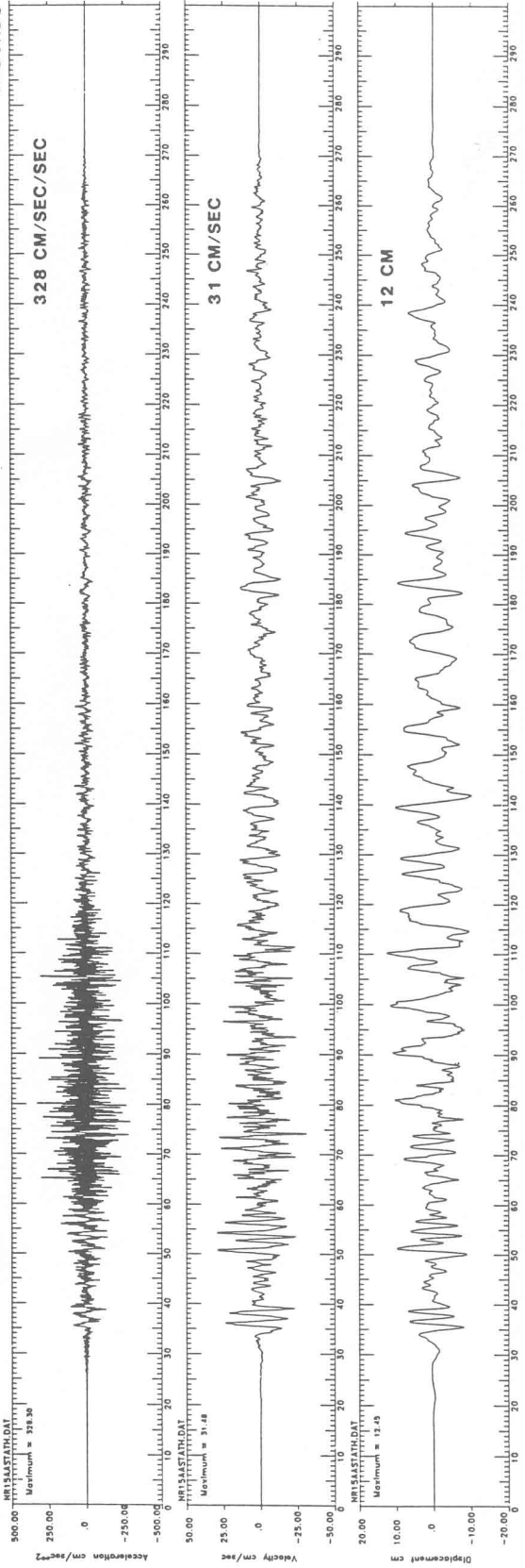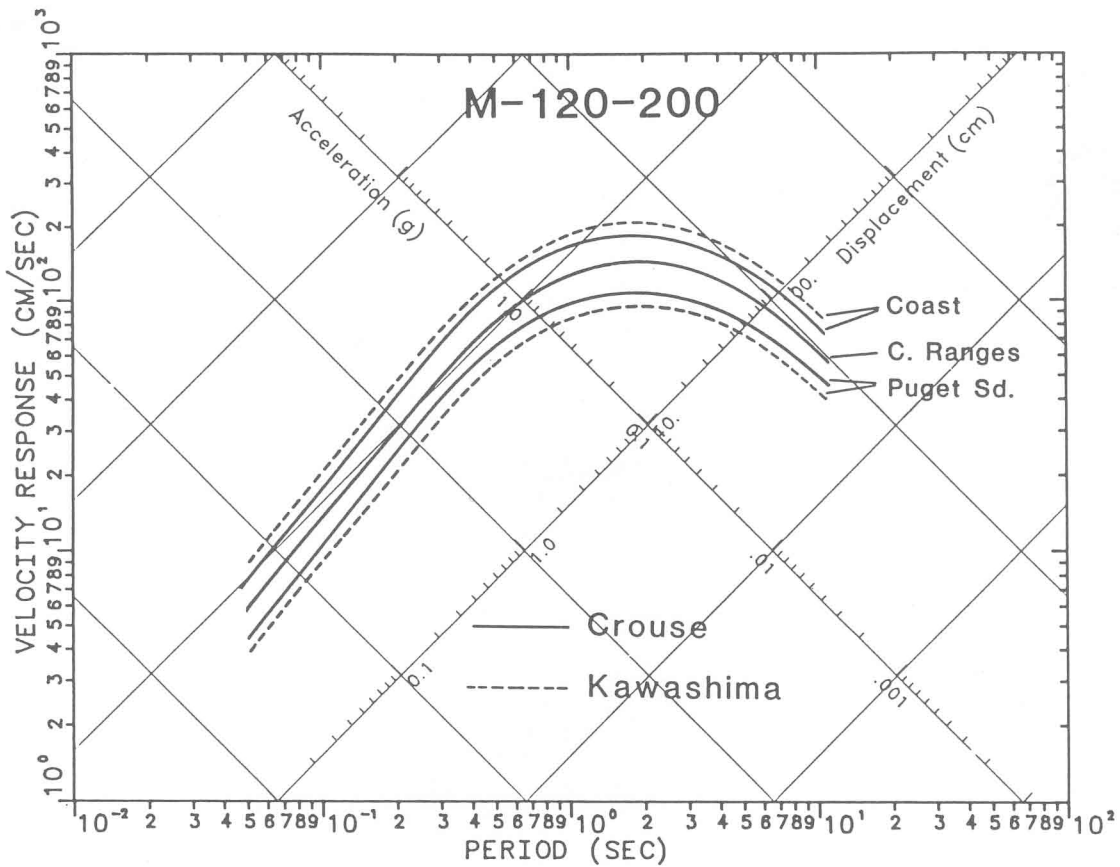
Figure 16

Comparison of synthetic response spectra as a function of site distance from the coast. Most of the models in this study are constructed using the CROUSE et al. (1988) distance attenuation law (solid curves). Use of the distance attenuation law of KAWASHIMA et al. (1984) results in motions that are nearly identical at the coastal ranges site and about 10% larger and 10% smaller at the coast and Puget Sound sites, respectively (dotted lines).

In addition to constructing models of the 1960 Chilean earthquake, we also constructed models of the 1964 Alaskan earthquake, the 1952 Kamchatka earthquake, and the 1957 Aleutian earthquake. Response spectra of horizontal and vertical components of synthetic ground motions are shown in Figure 17. The rupture parameters are those used to produce synthetic teleseismic P-waveforms that give a good overall match to the observed data (Figure 9). The synthetic

Figure 15

Synthetic ground motion for a giant earthquake in the Pacific Northwest that is similar to the 1960 Chilean earthquake. The site is assumed to be in the coastal ranges. This record was formed by summing records from Miyagi-Oki-sized earthquakes and is considered to be one of the larger motions that can be considered as reasonable for this site. Average ground motions for similar conditions may be somewhat smaller.
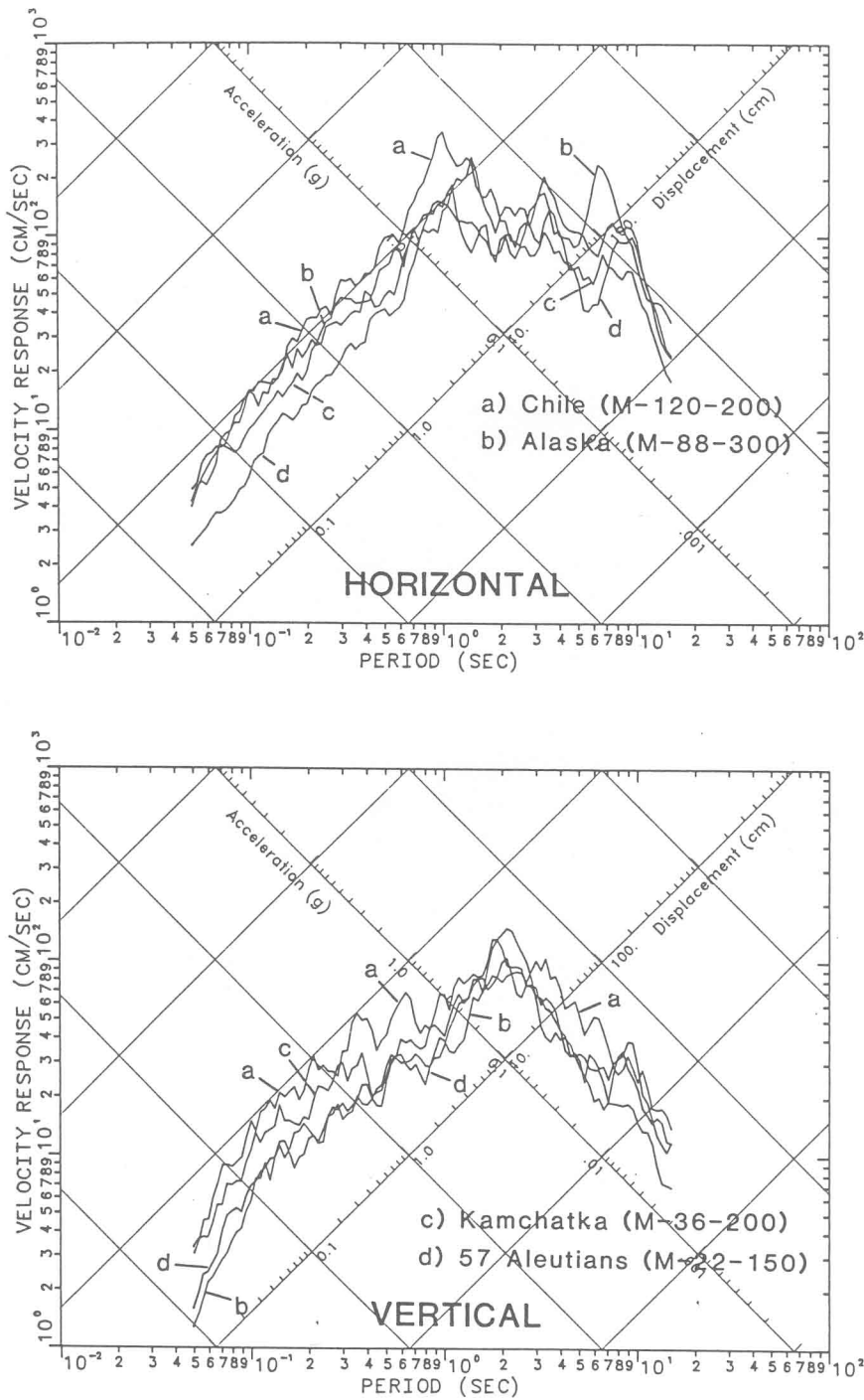
Figure 17

Comparison of synthetic response spectra (5% damping) for models of the four giant earthquakes $(M_w > = 9.0)$ for which we have teleseismic P-wave data. Records from Miyagi-Oki-sized earthquakes are used as Green's functions and the motions are for a coastal ranges site. Schematics of the assumed fault geometries are shown in Figure 10. These motions are considered to be somewhat larger than the average motions that could be expected for sites at this distance.

motions are for the coastal ranges site and records from the Miyagi-Oki earthquake, the Hyuganada earthquake, and the St. Elias earthquake were used as Green's functions. All of the response spectra have similar shapes since the same set of records were used as Green's functions in each model. The number of records that are summed is the most important variable in determining the overall difference in the response spectral amplitudes for these different earthquakes.

Discussion and Conclusions

What is the overall significance of the synthetic ground motions that we have presented? Which, if any, of the motions represents the average motion and what is the scatter about the mean likely to be? In the case of actual data from smaller earthquakes, we noted the very large scatter for a given magnitude and distance range. There is little reason to expect that similar scatter does not exist for giant earthquakes as well. This scatter also helps to confuse the interpretation of our synthetic motions. Clearly the summation procedure assures that the final synthetics are at least as large as the largest of the motions that are summed. Thus Green's function records that fall within the large end of the scatter will dictate the size of the synthetic motion. To avoid this, it might be best to use only median records as Green's functions. However, the data set is very limited and too few (if any) records are available that could be confidently classified as median records. This situation is further complicated by some confusion about averaging procedures. That is, when we considered the spectra of earthquakes of $M_w < 8\frac{1}{4}$, we computed logarithmic averages (Figure 3). Logarithmic averages were used to de-emphasize the contribution of a few large records, if present. These logarithmic averages are about 80% as large as arithmetic averages for the same data. However, our synthetic ground motions result from the arithmetic sum of records within the data set. From these remarks, it does seem clear that most of our synthetic motions are likely to fall above the average motion for a giant earthquake.

In Figure 18, we present a schematic summary of the variation of idealized response spectra with energy magnitude for a coastal ranges site. The spectra for earthquakes of M_w $7\frac{1}{4}$ and 7.9 are smoothed interpretations of the averaged data presented in the first part of this paper. The spectrum shown for a M_w $9\frac{1}{2}$ earthquake is a compromise between the two models that produced the largest (M–120–200) and the smallest (T–6–100) ground motions and that were also compatible with the teleseismic waveforms of the 1960 Chilean earthquake. The response spectra for M_w 9 and $8\frac{1}{2}$ earthquakes were obtained by interpolation. The spectra presented in Figure 18 are only about two-thirds as large as the spectra that we obtained from most of our modeling using the records from Miyagi-Oki sized earthquakes as Green's functions. Because of the problems introduced by using a record set with very large scatter as Green's functions, we believe that our
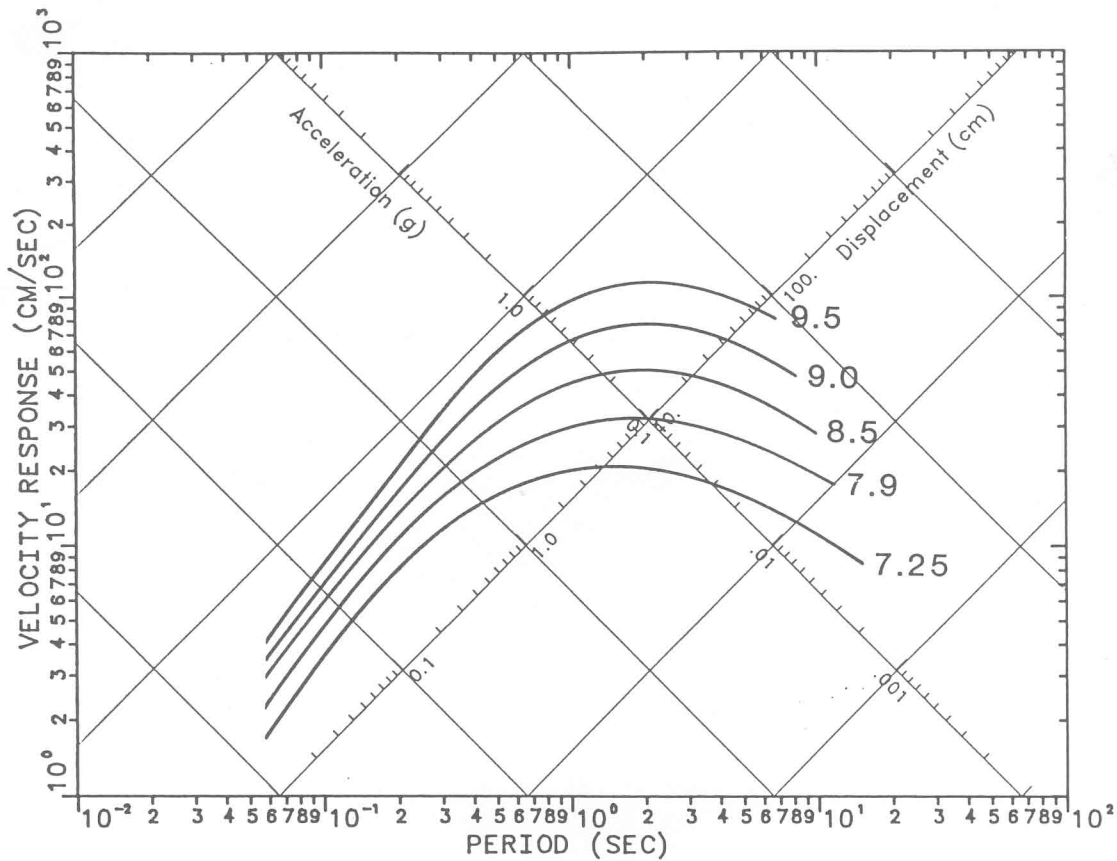
Figure 18

Estimates of the variation in average horizontal ground motion response spectra (5% damping) as a function of energy magnitude for a coastal range site. Scatter of actual data about mean values may be similar to that observed in the data displayed in Figure 1.

M-designated models are systematically larger than the mean. We believe that the spectra presented in Figure 18 are probably more representative of what average ground motions may be for giant earthquakes. However, it is important to recognize that we have not developed a rigorous methodology to produce average ground motions.

In Figure 19, we compare several of the response spectra that we produced for the coastal ranges site with the response spectrum of the S14°W component of motion at Pacoima Dam during the 9 February 1971 San Fernando, California earthquake (M_w 6.7), which is one of the largest motions recorded for any earthquake. The models M–120–200 and T–6–100 are shown since they produced the largest and smallest ground motions that were compatible with our teleseismic modeling. The model designated as "average" in Figure 19 is approximately equal to our "preferred" response spectrum for a M_w $9\frac{1}{2}$ that is shown in Figure 18. At high frequencies, all of our synthetic ground motions are clearly smaller than the Pacoima motion. However, at periods greater than 1 second, our synthetic motions are nearly comparable in strength to the Pacoima record.
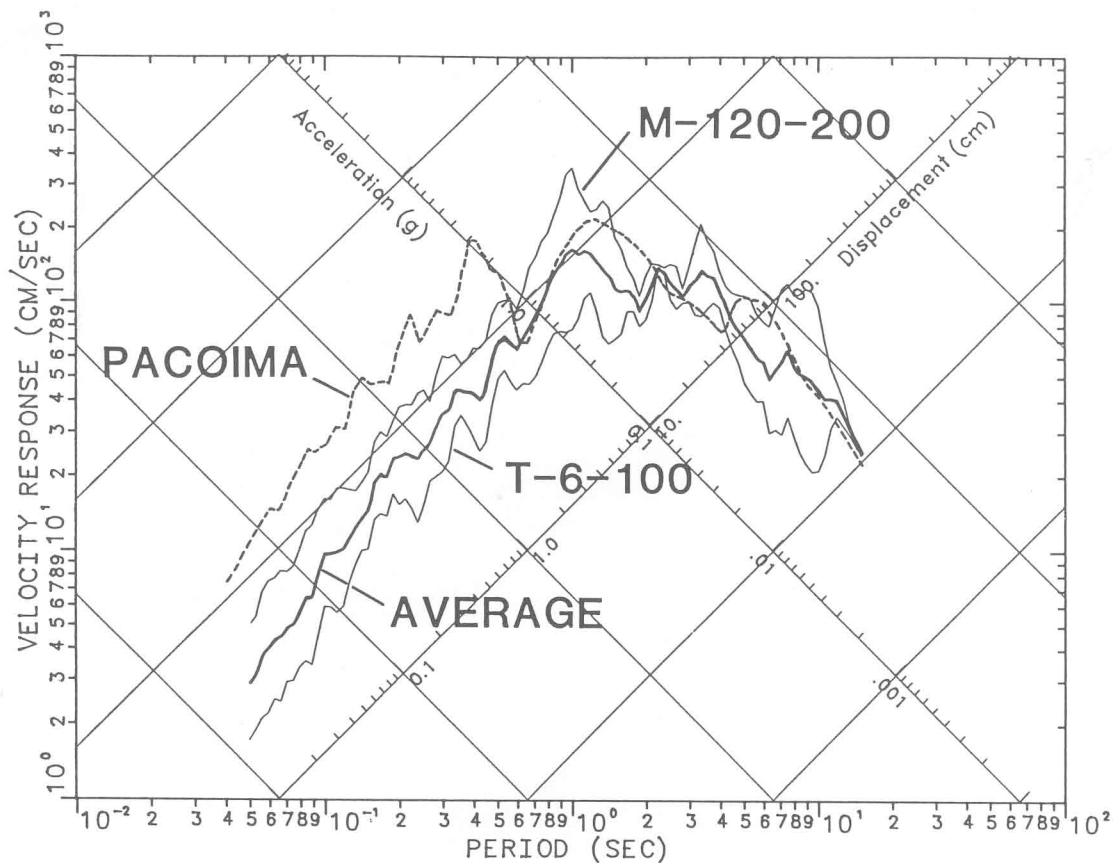
Figure 19

Comparison of the response spectrum of the S14W component of ground motion at Pacoima Dam from the 9 February 1971 San Fernando earthquake (M_w 6.7) with synthetic response spectra assuming a coastal ranges site and an earthquake similar to the 1960 Chilean earthquake. M–120–200 is one of the largest motions that is thought to be feasible and T–6–100 is one of the smallest motions produced in this study. The spectrum designated as average is similar to the one used in Figure 18.

Given that there are presently no strong motion recordings of giant earthquakes and that there are many uncertainties in our modeling procedure, there are still many uncertainties in estimating just how large and damaging the motions would be from a giant earthquake in the Pacific Northwest. We have seen that there is evidence that a large portion of the moment history of giant earthquakes is a very long period and cannot be seen in short- and intermediate-period teleseismic body-wave records. Nevertheless, this is small solace since the short-period records from such earthquakes are still among the largest ever recorded. Furthermore, data we do have suggests that relatively strong shaking occurs at surprisingly large distances from M_w 8 earthquakes. At this point, it is only natural to assume that M_w $9\frac{1}{2}$ earthquakes can produce even larger ground motions. In any event, it is clear that the 1960 Chilean and 1964 Alaskan earthquakes caused great damage over very large regions. The suggestion of a similar earthquake in an area as developed as the Pacific Northwest is a very disturbing notion.

Appendix A

Appendix A consists of figures that summarize the strong ground motion data set used in this study. The figures show the locations of strong motion recording sites, ISC mainshock and aftershock locations, the time histories of one horizontal component of ground acceleration and velocity for each site, and, in some cases, the teleseismic time function derived by HARTZELL and HEATON (1985). Common scales are used so that teleseismic time functions can be compared directly with strong ground motion time histories. The Japanese records were taken directly from the MORI and CROUSE (1981) catalogue (designated as Exxon) and also from a collection assembled by the Japanese Port and Harbor Research Institute (designated as PHRI). The Alaskan records are taken from BEAVAN and JACOB (1984), the Peruvian records are from BRADY and PEREZ (1977), and the Solomon Islands records are from DENHAM and SMALL (1971). All of these records, except for the ones from the Port and Harbor Research Institute, are available from the NOAA World Data Center in Boulder, Colorado. Additional information concerning the conditions under which these and other data were recorded have been tabulated by CROUSE *et al.* (1980).

Figures A1 to A20

Summary of strong ground motions from large ($M_w \geq = 7.0$) shallow subduction earthquakes considered in this study. Mainshock epicenters are designated with a star, aftershocks are shown as dots, and recording sites are shown as solid triangles. One horizontal component of ground acceleration and velocity are shown for each recording. Teleseismic far-field time functions reported by HARTZELL and HEATON (1985) are shown when available. All distances used in this study are epicentral distances, except in the case of the 16 May 1968 Tokachi-Oki earthquake (M_w 8.2) where distances are measured relative to the $\times$ symbol which is more central to the rupture surface.
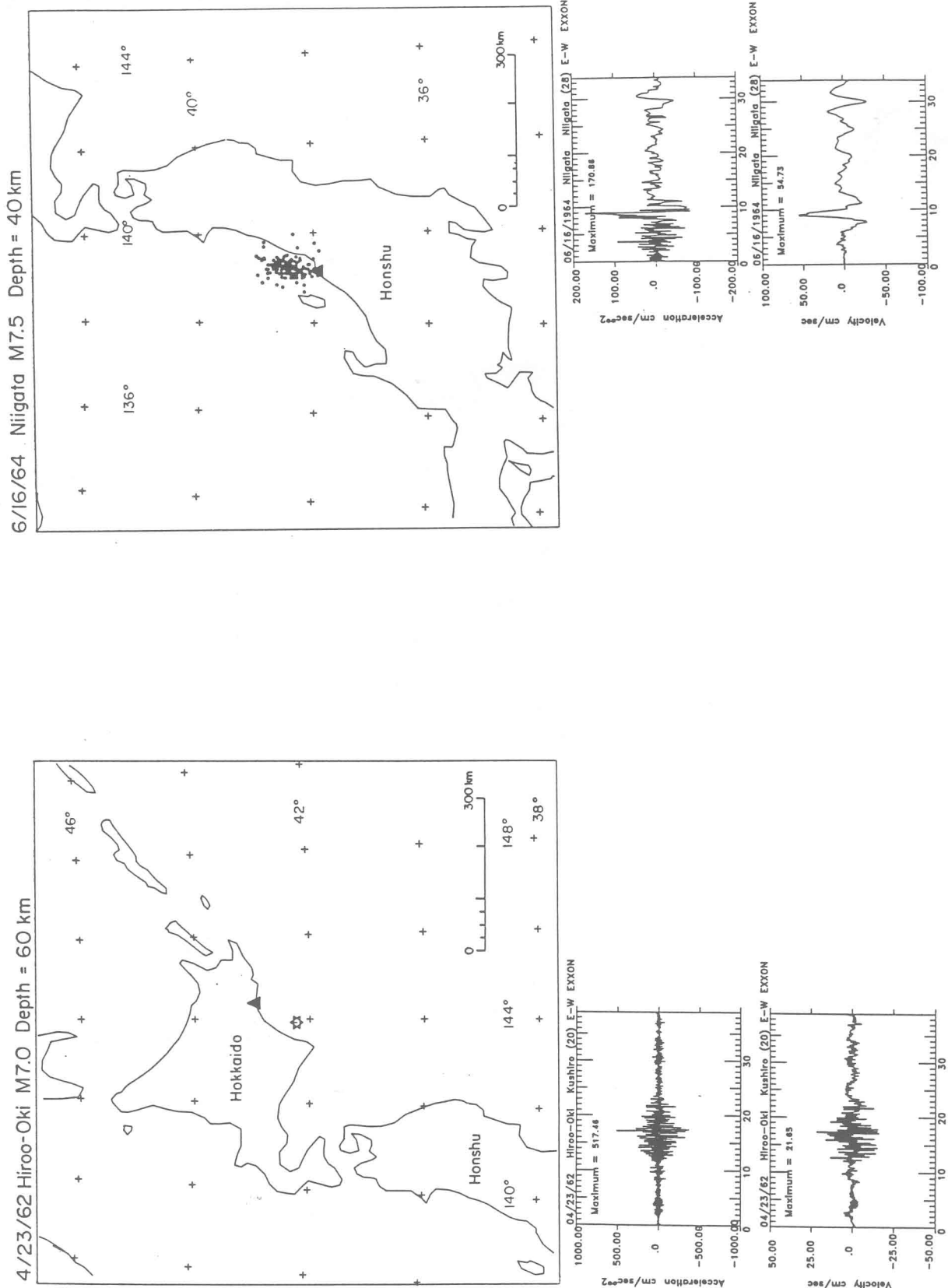
Fig. A1.
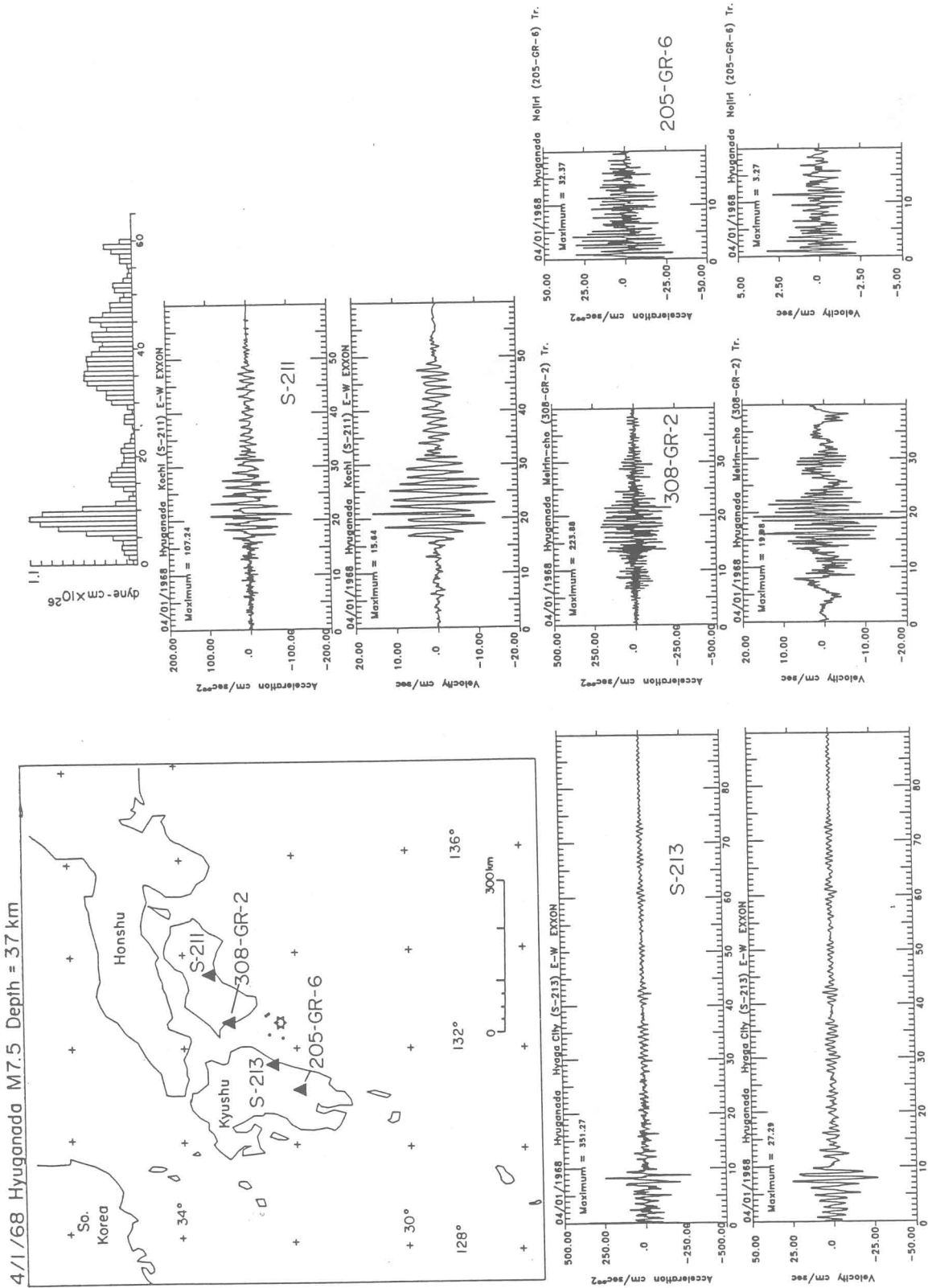
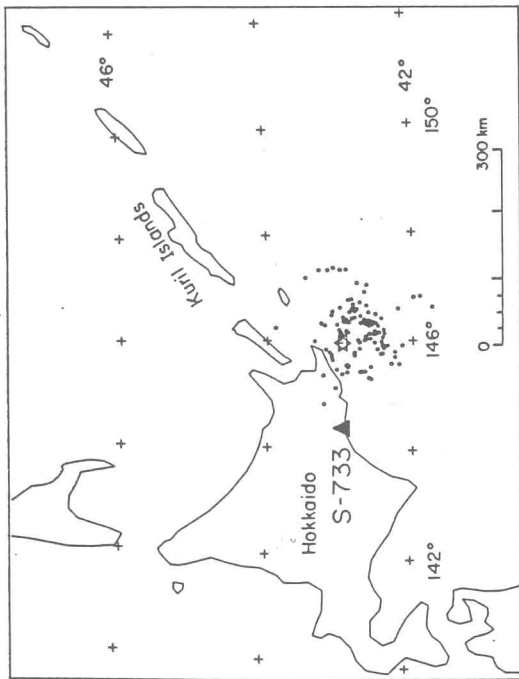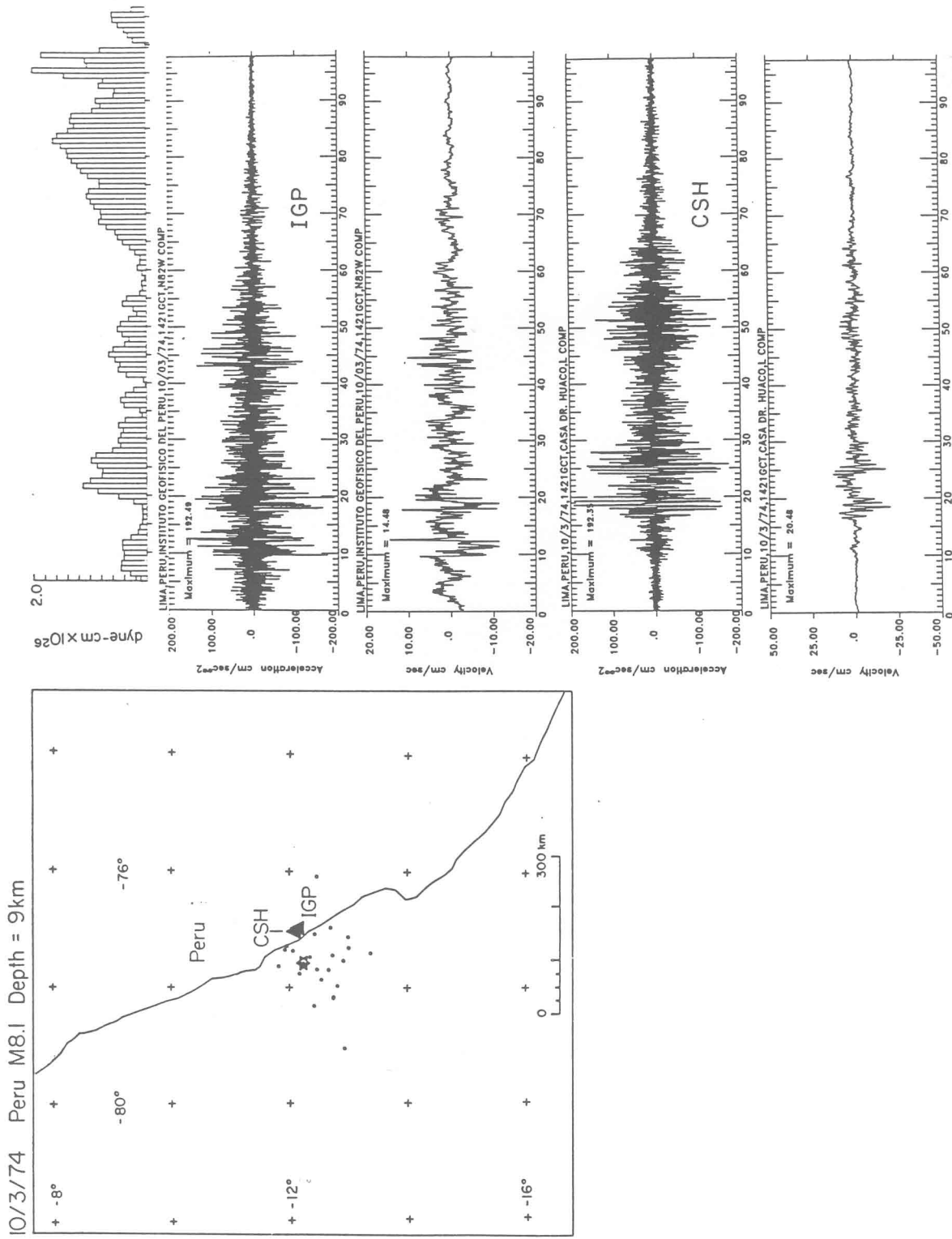Fig. A2.
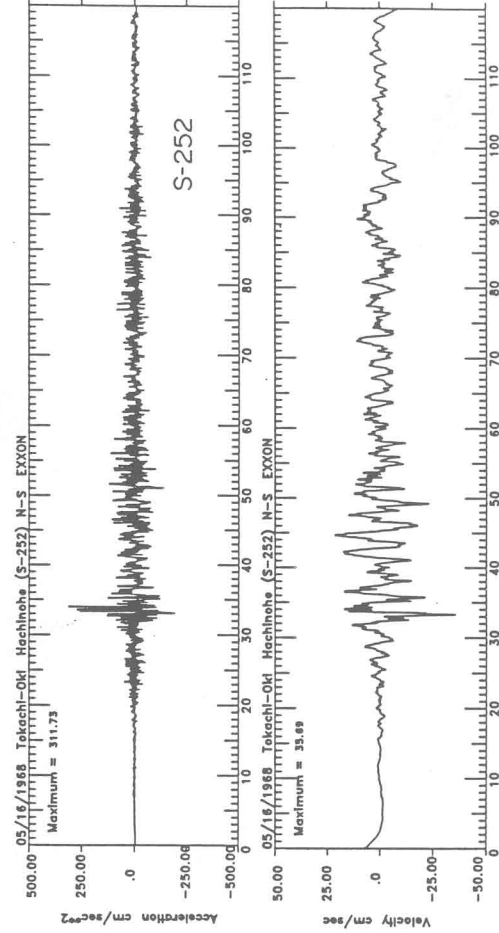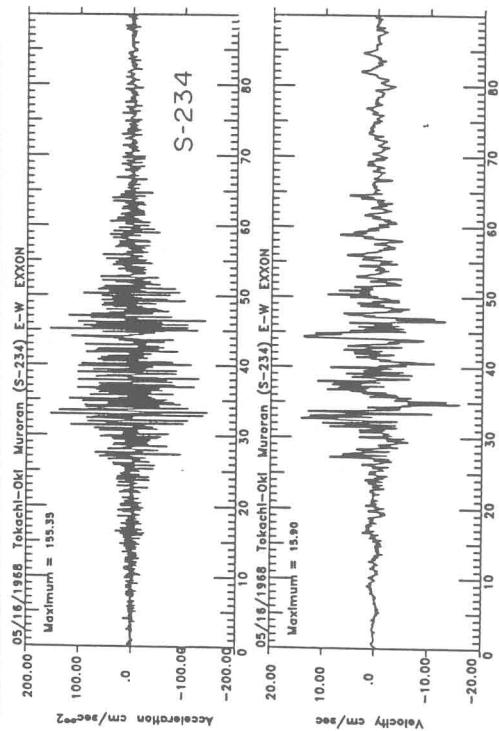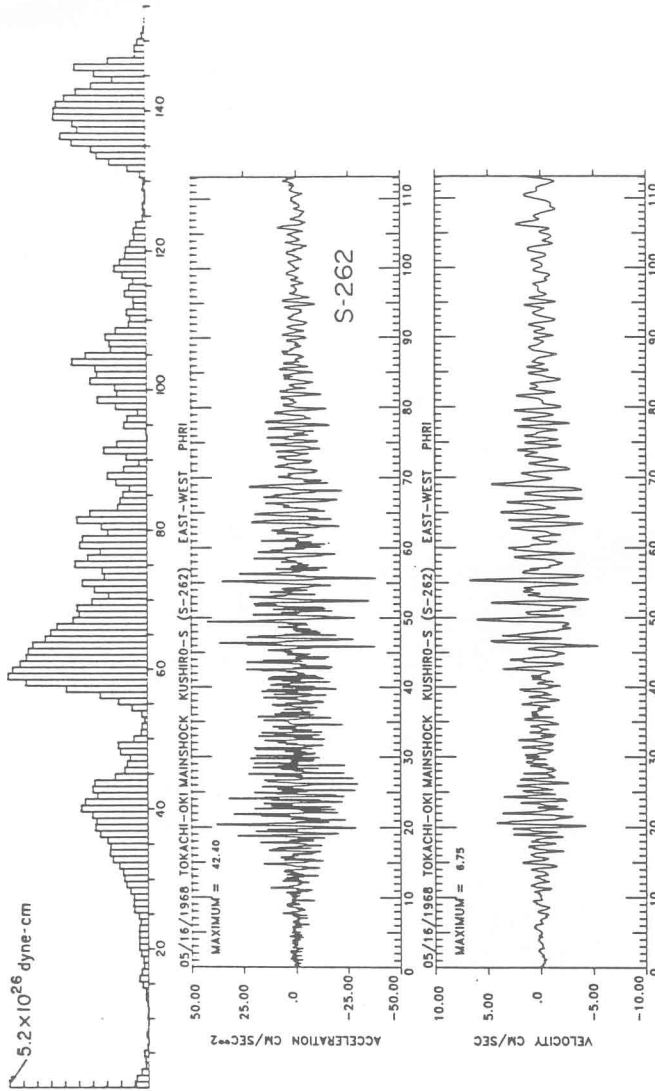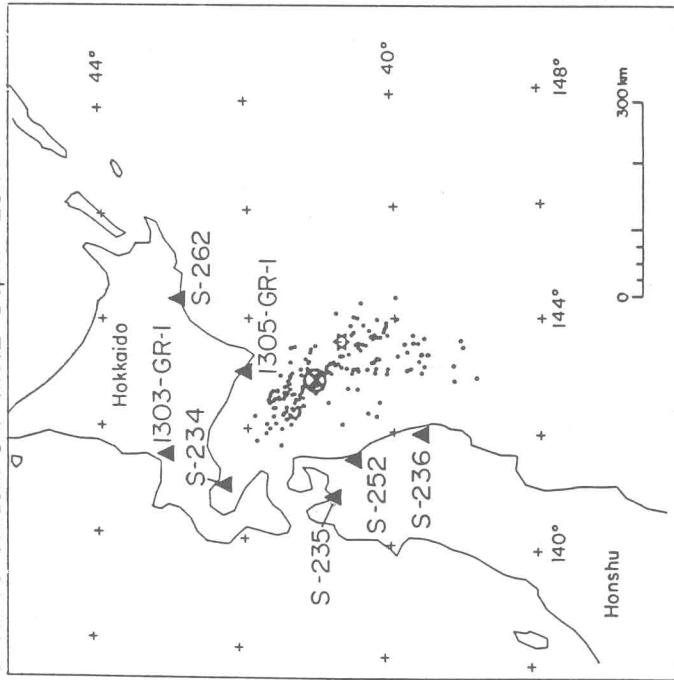
Fig. A3.
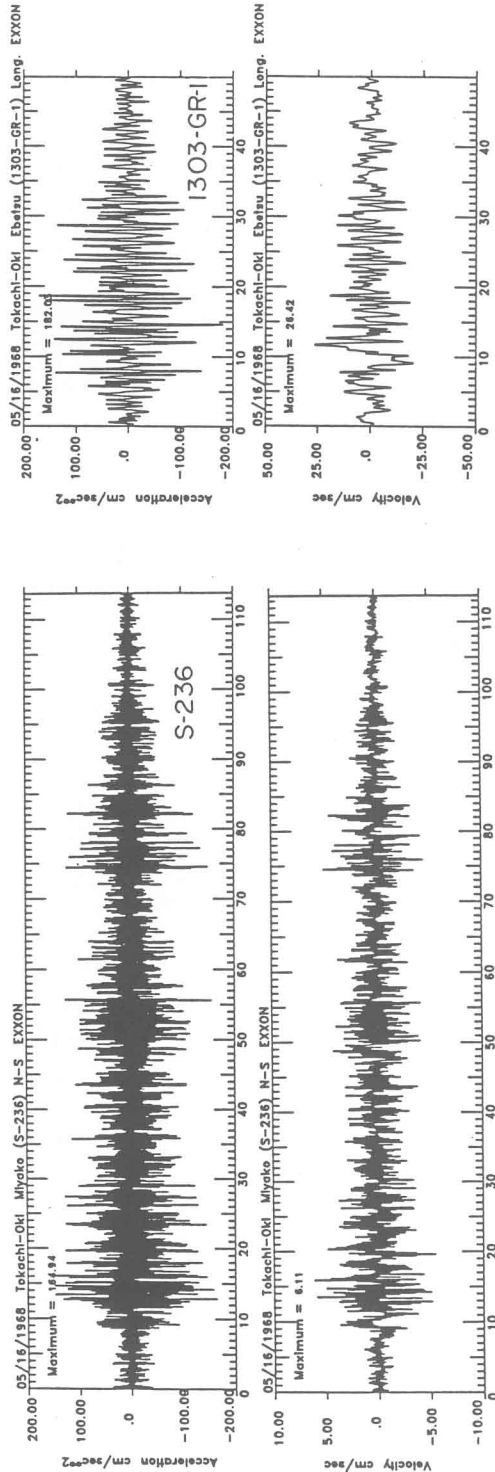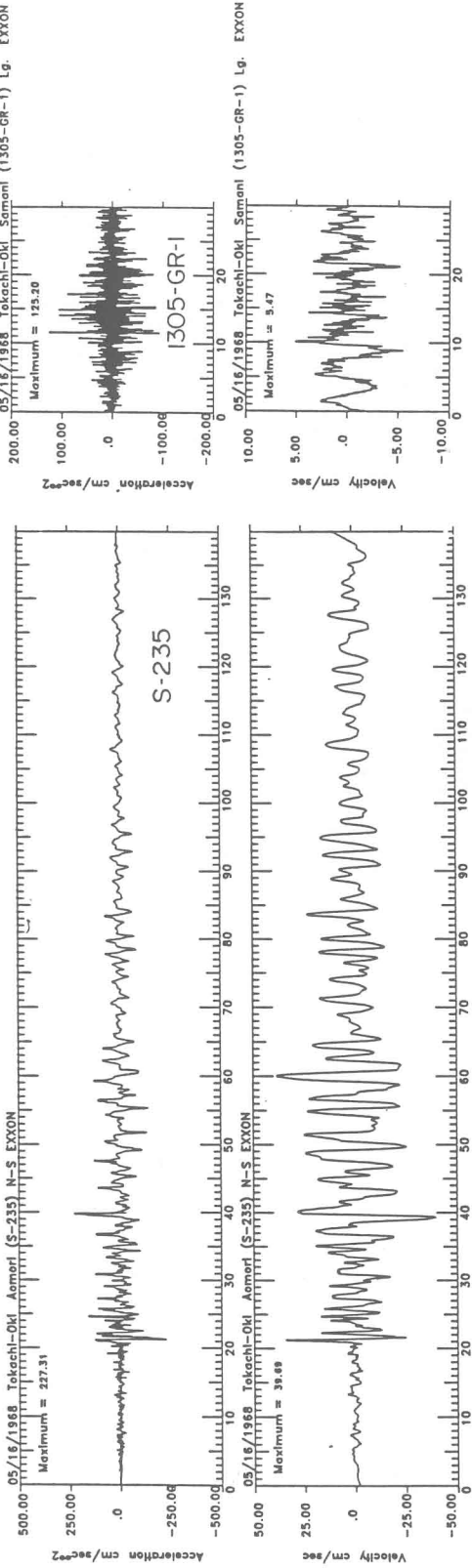
Fig. A4.
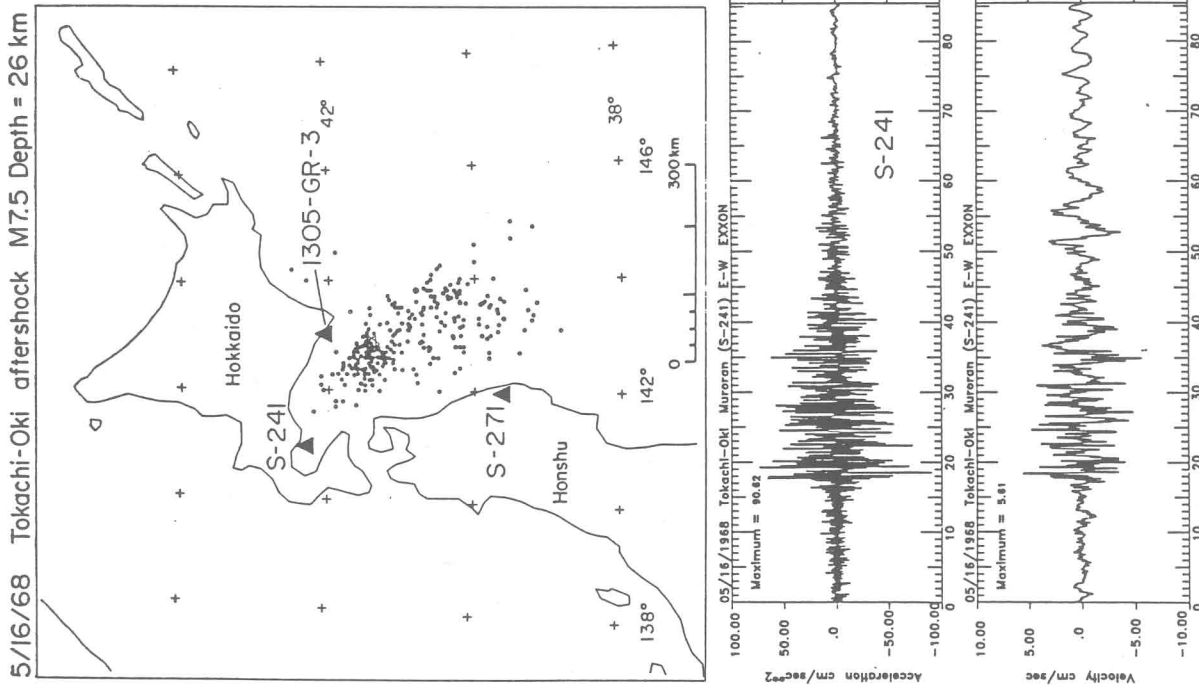
Fig. A5.
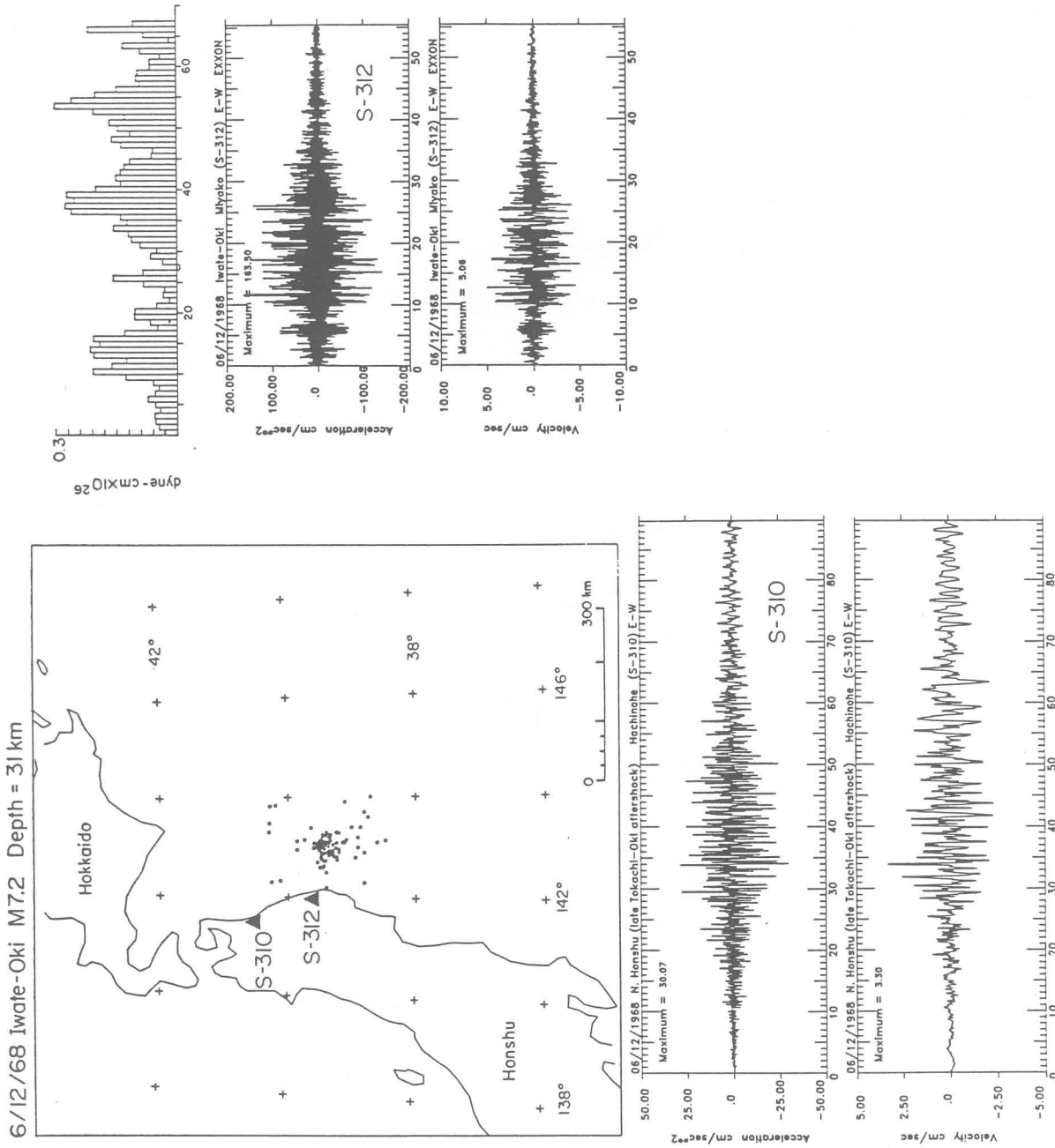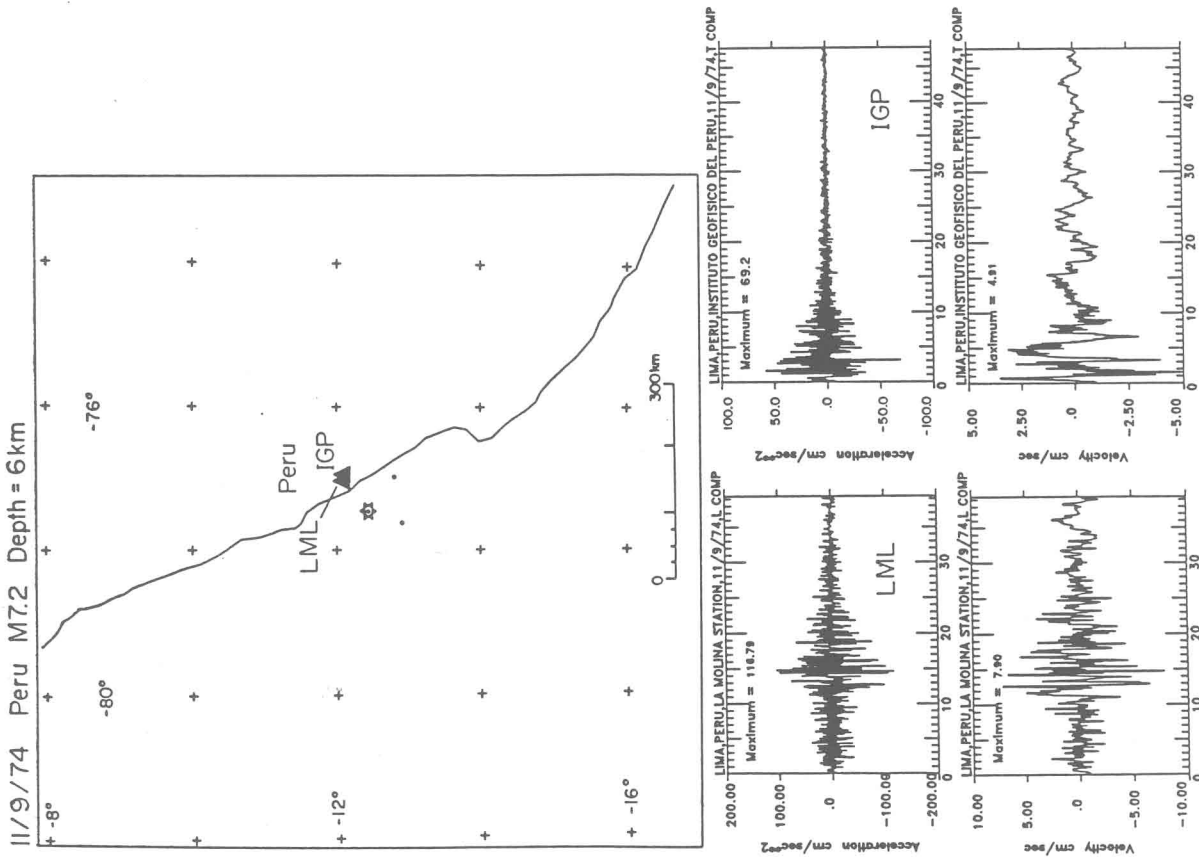
Fig. A6.
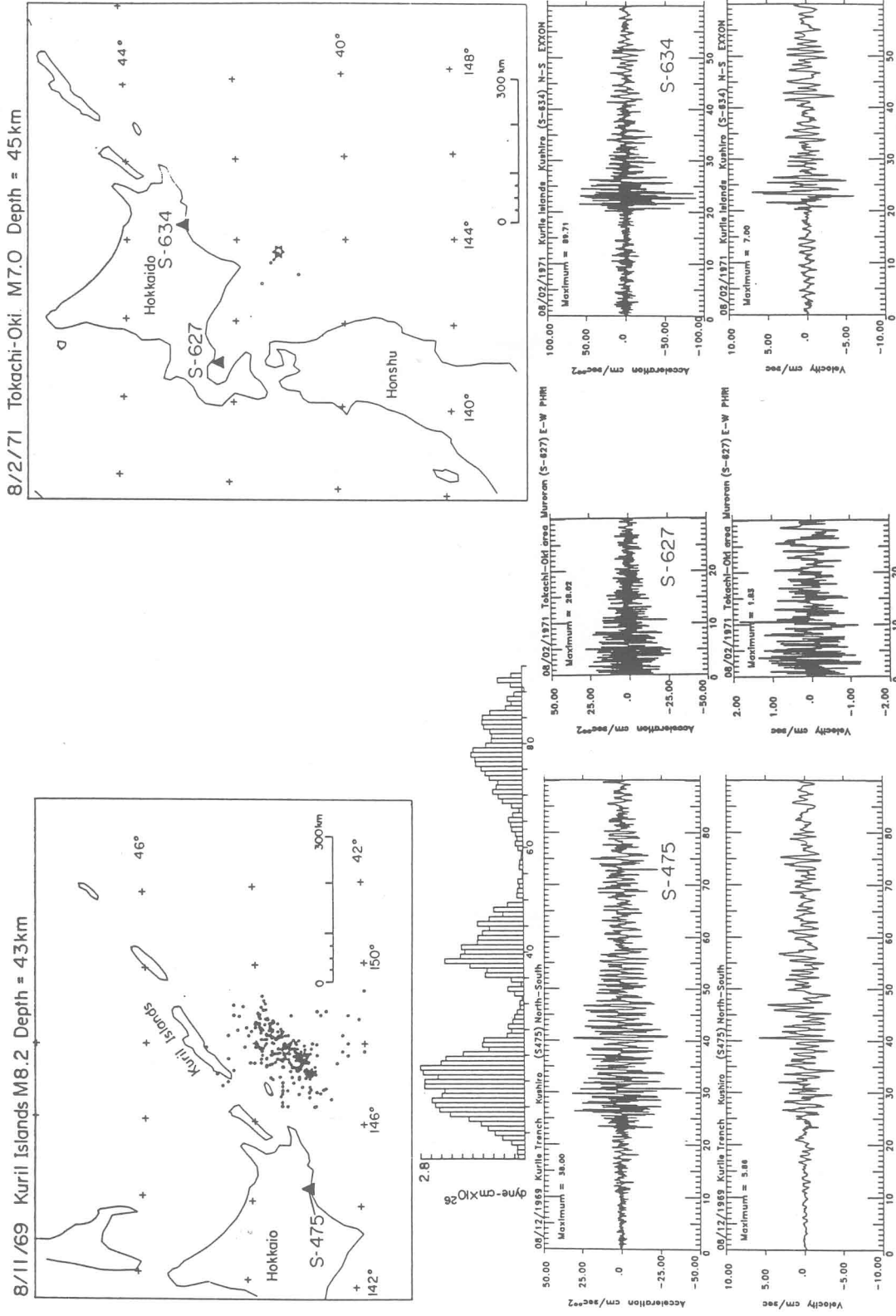
Fig. A7.
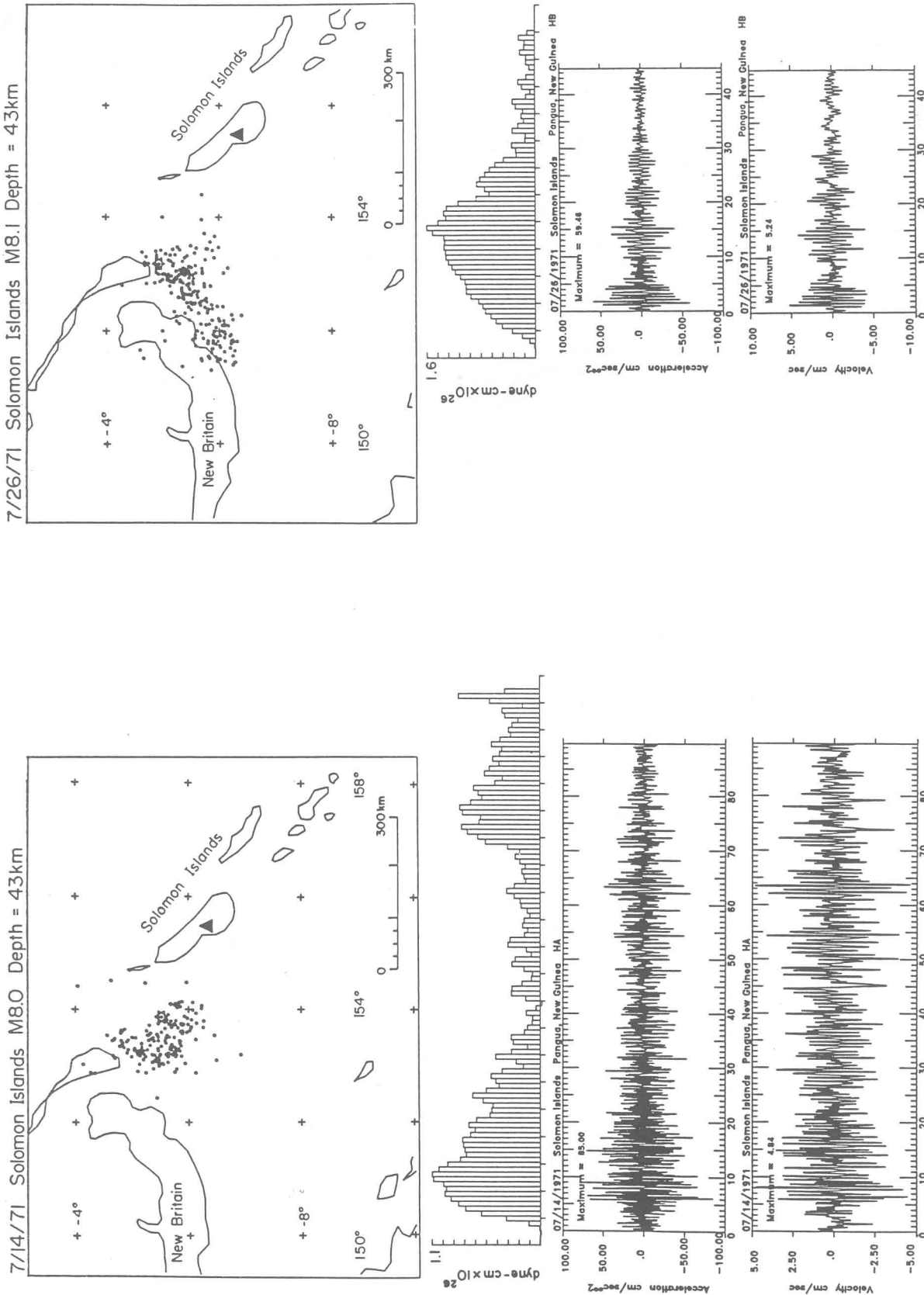
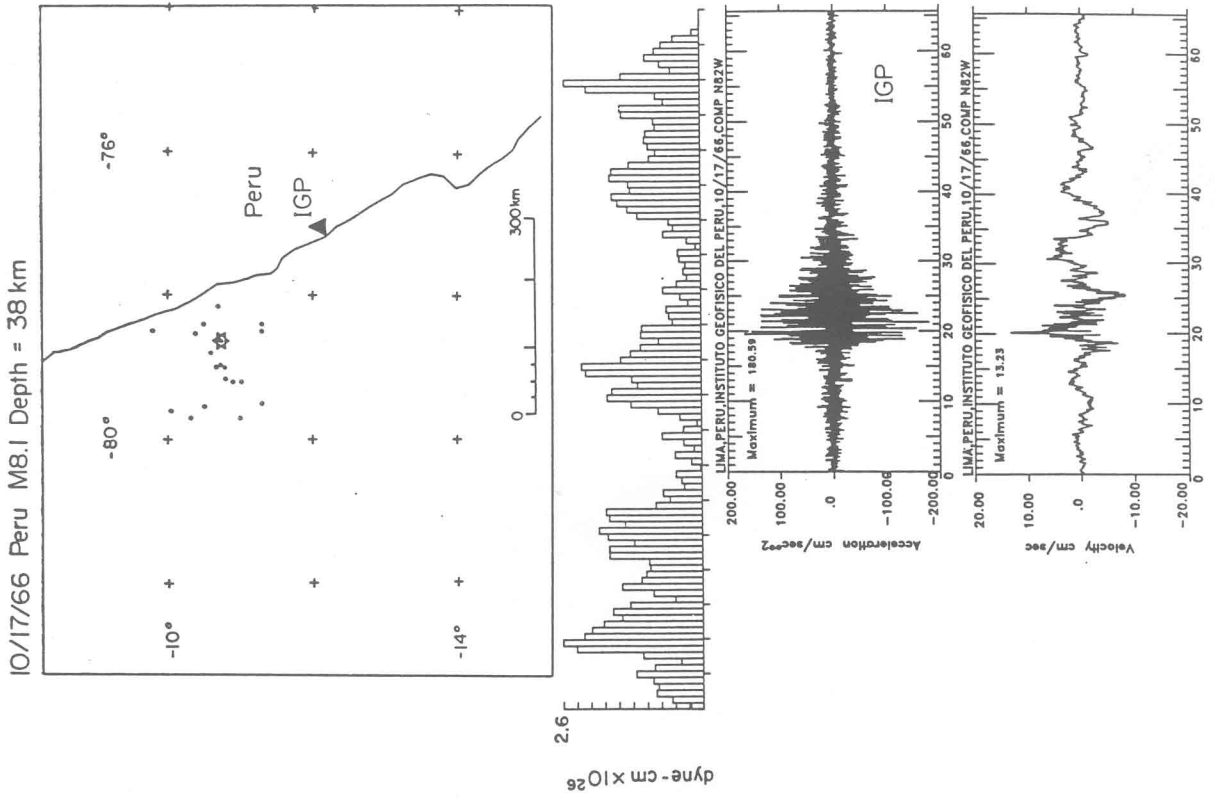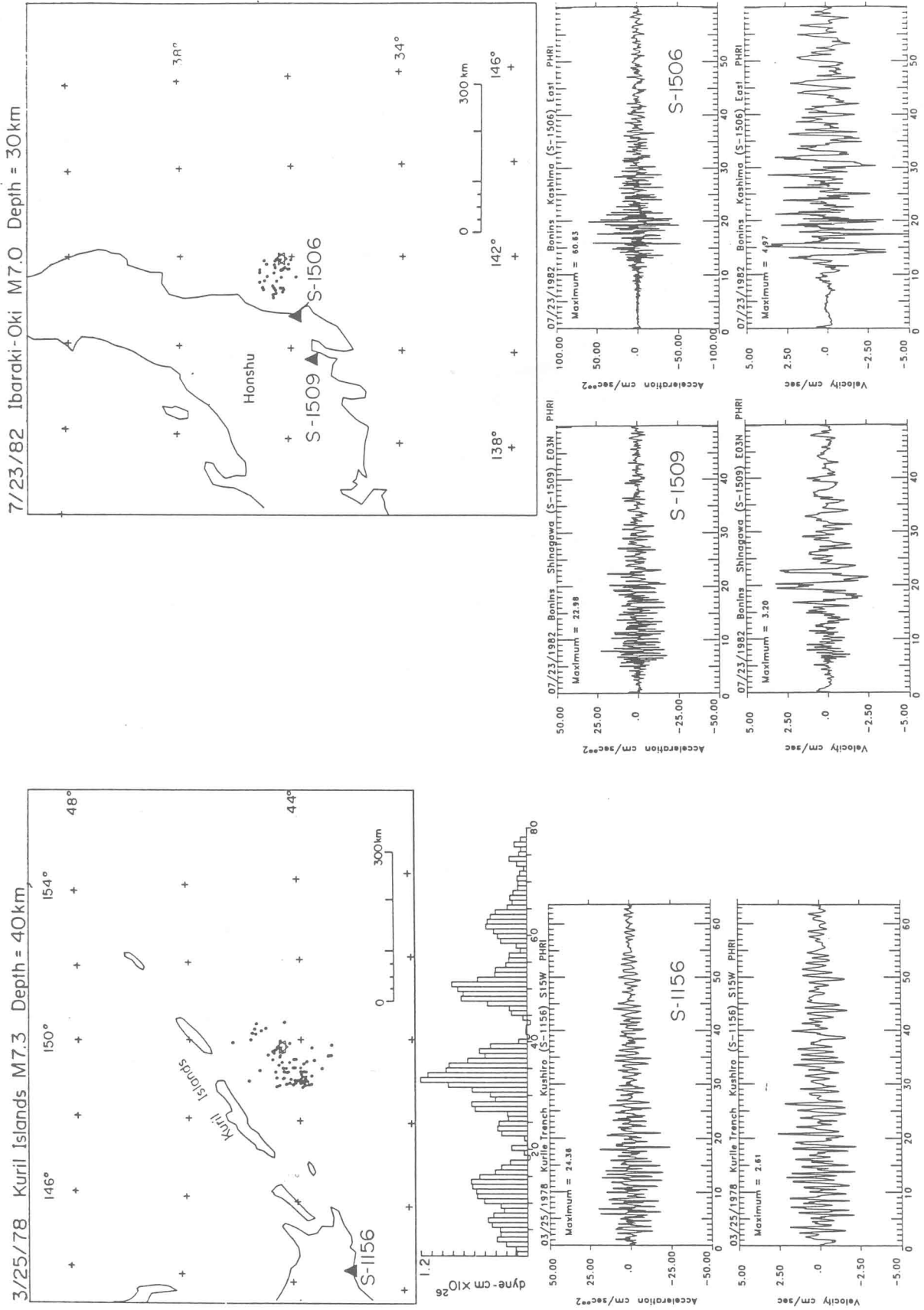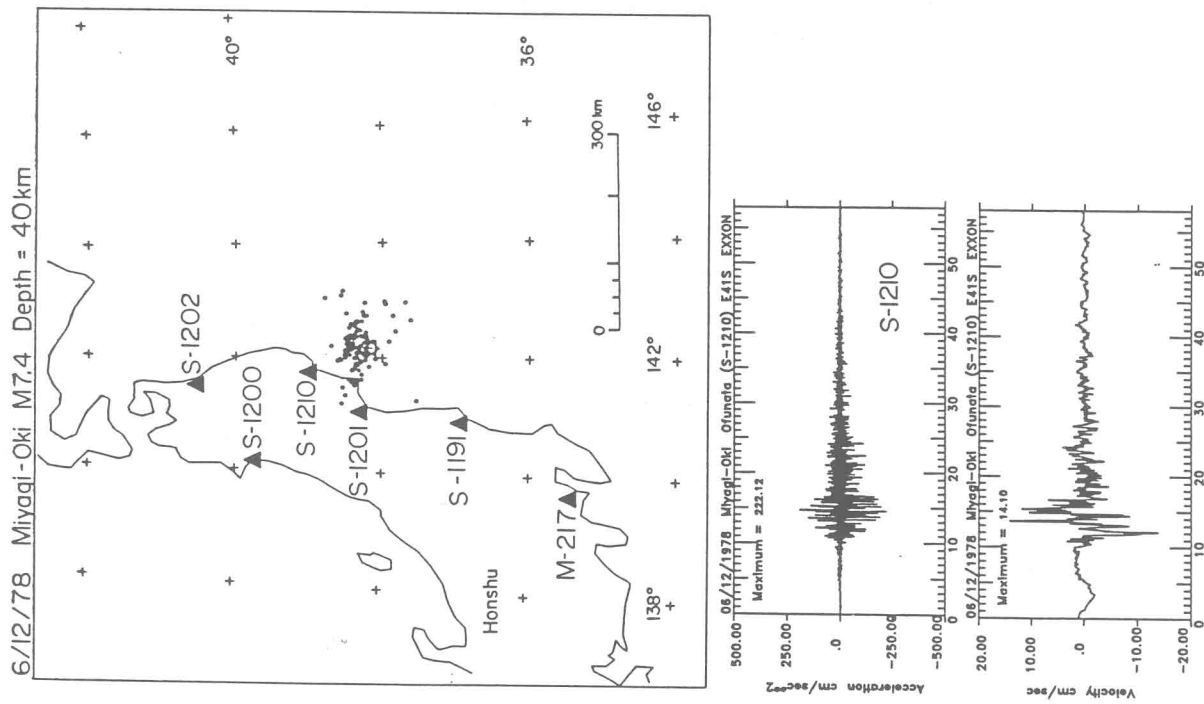Fig. A8.
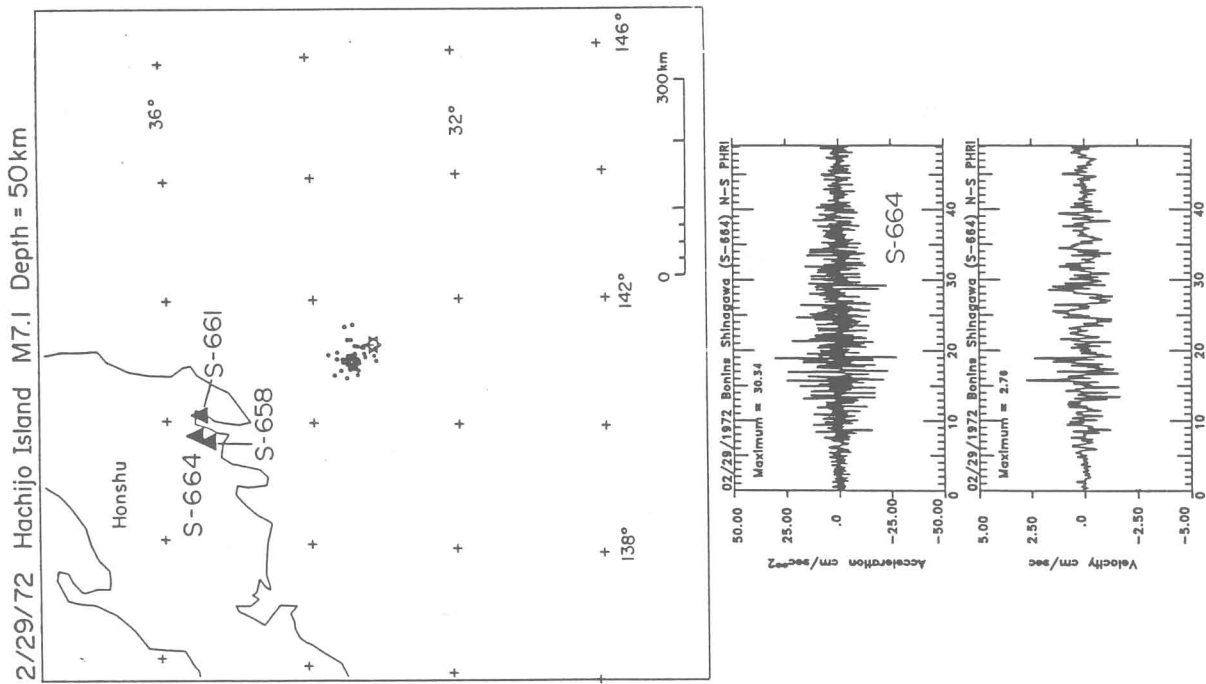
Fig. A9.
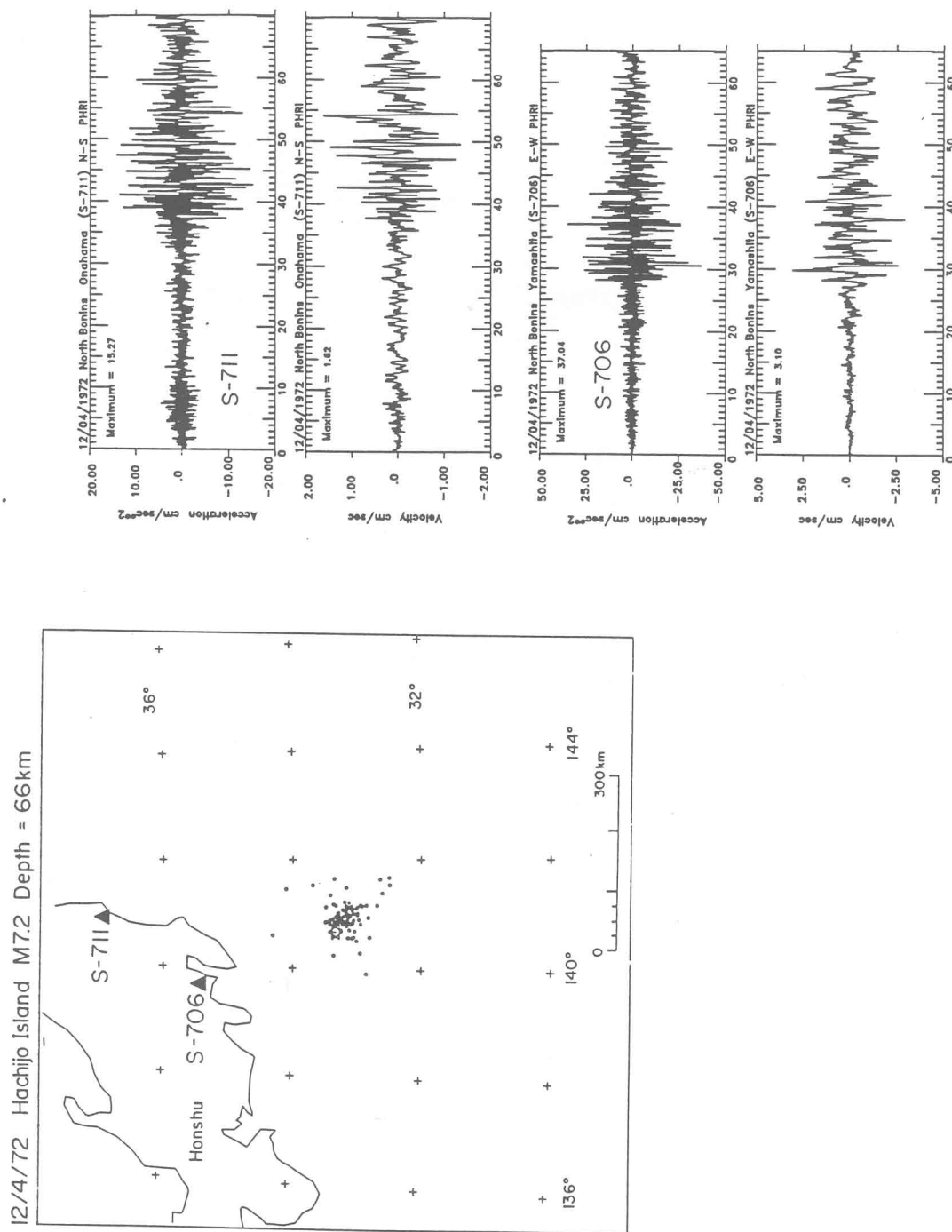
Fig. A10.
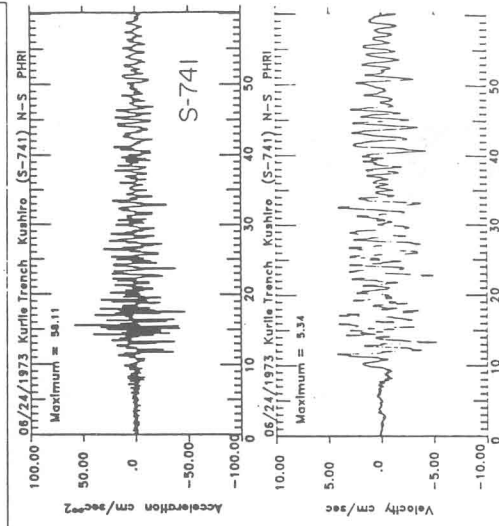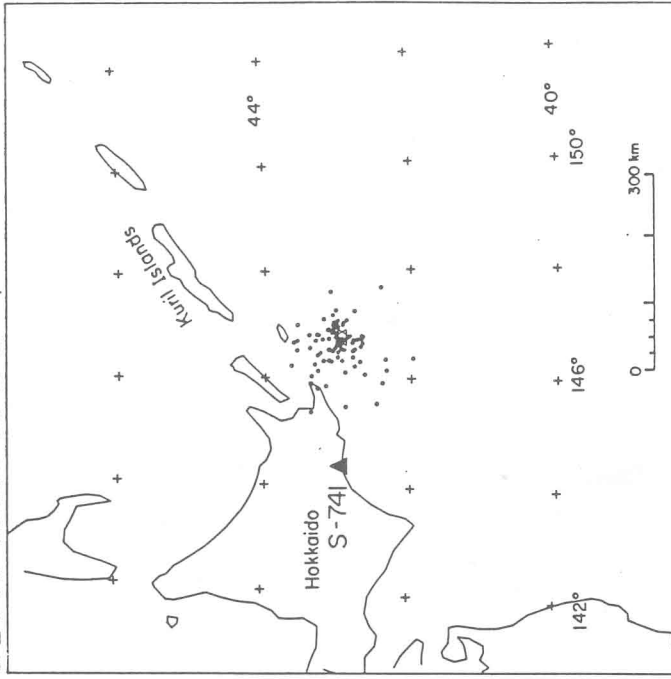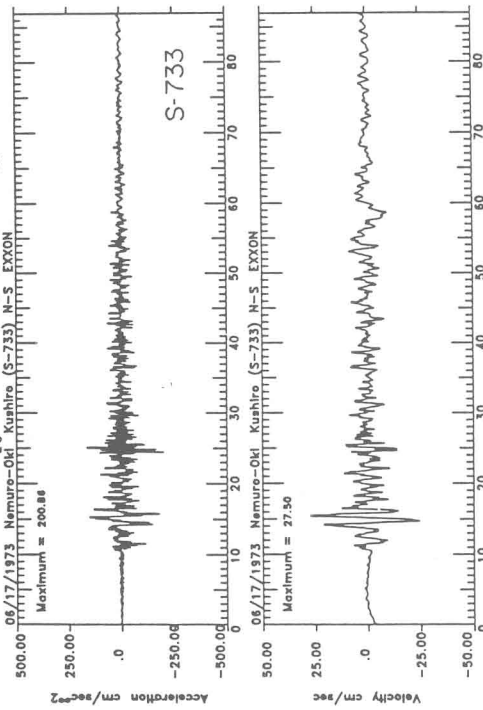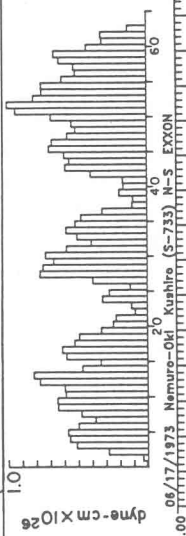
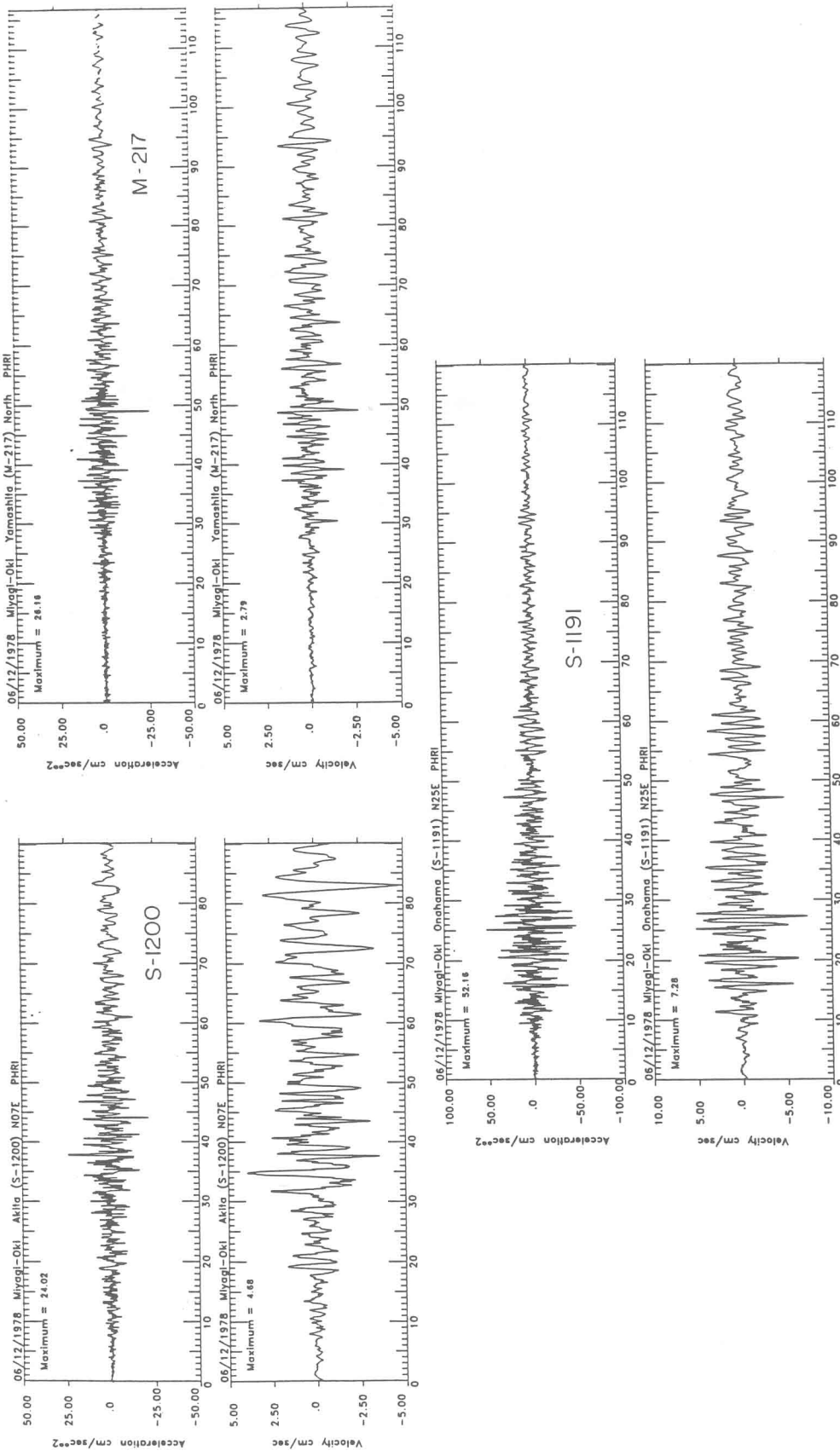Fig. A11.

Fig. A12.

Fig. A13.

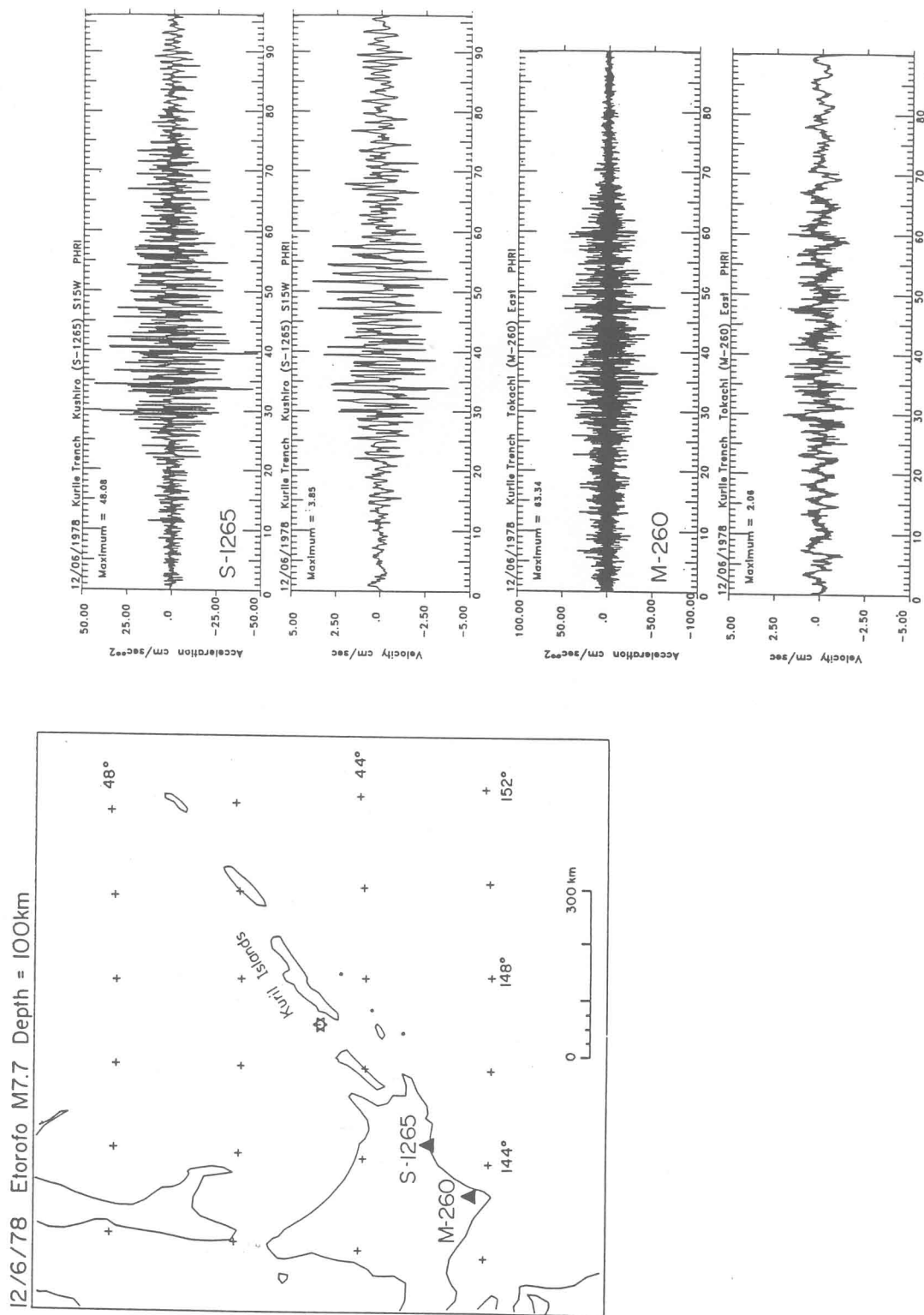Fig. A14.

Fig. A15.

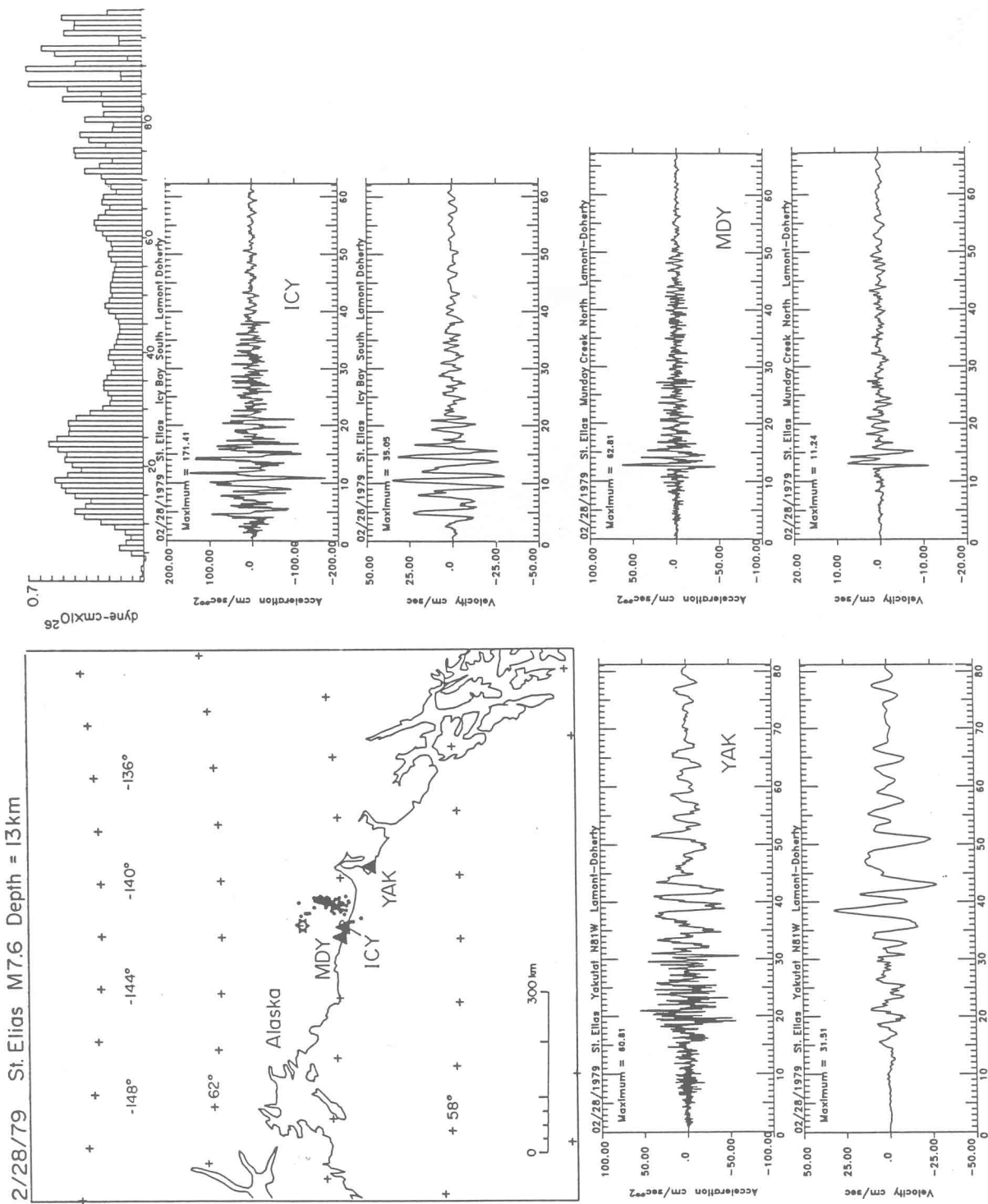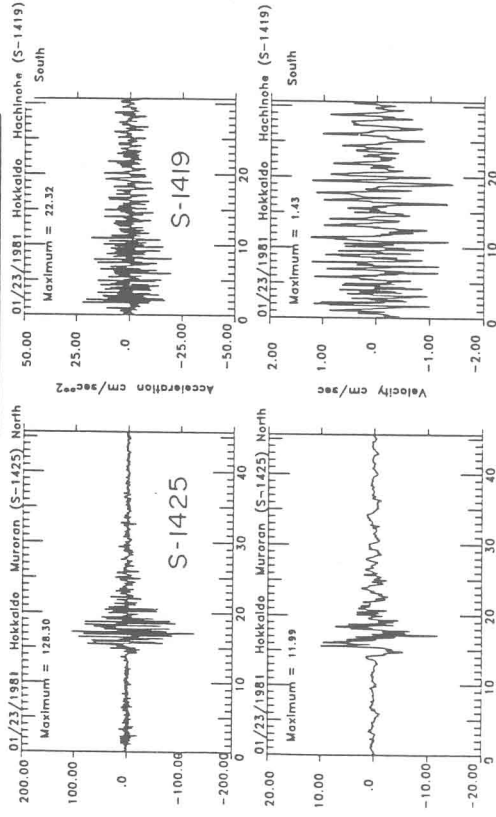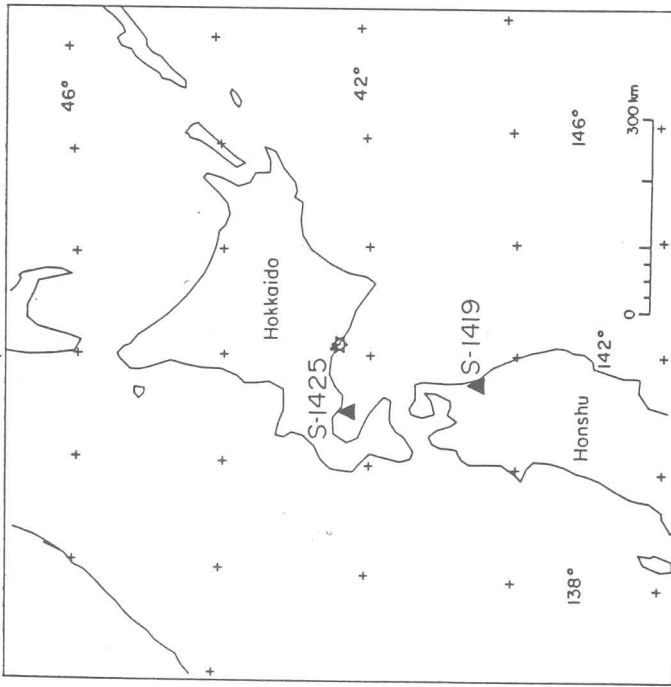6/12/78   Miyagi-Oki M 7.4

Fig. A16.

Fig. A17.

Fig. A18.

1/23/81 Urakawa M7.1 Depth = 130km

3/21/82 Urakawa M7.1 Depth = 40km
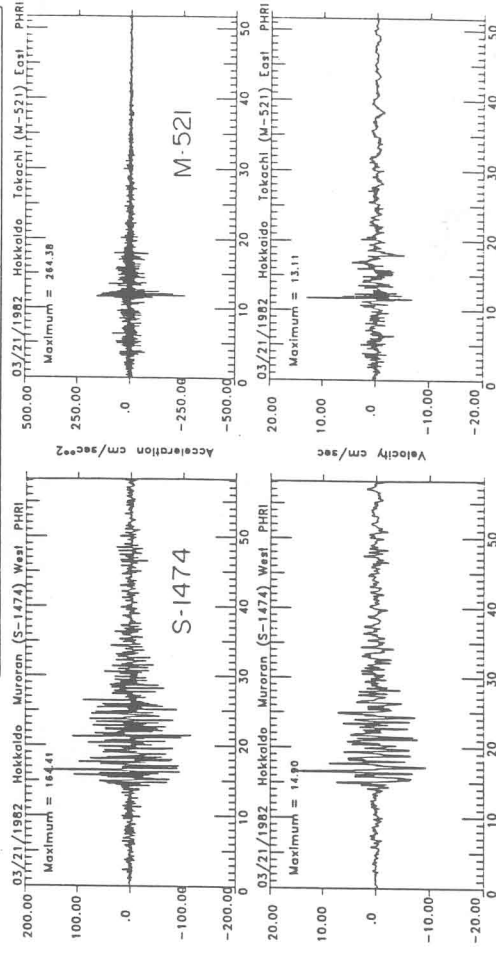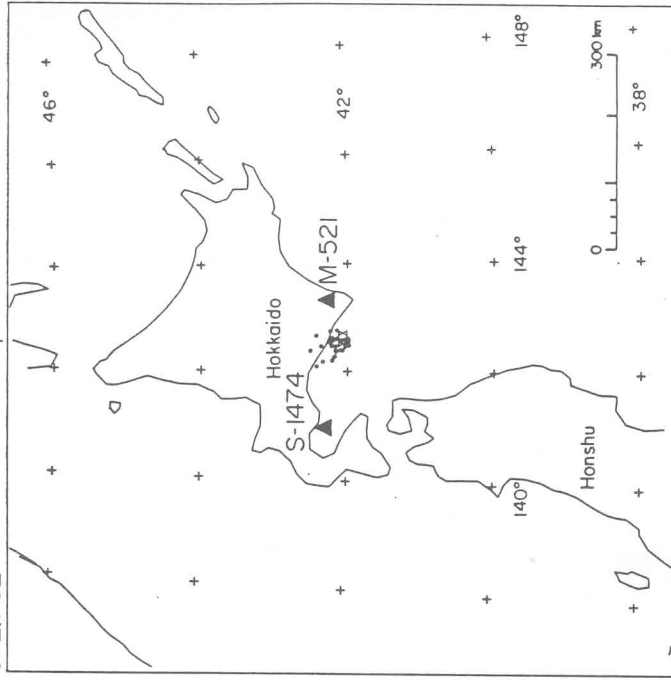
Fig. A19.

Fig. A20.

Appendix B

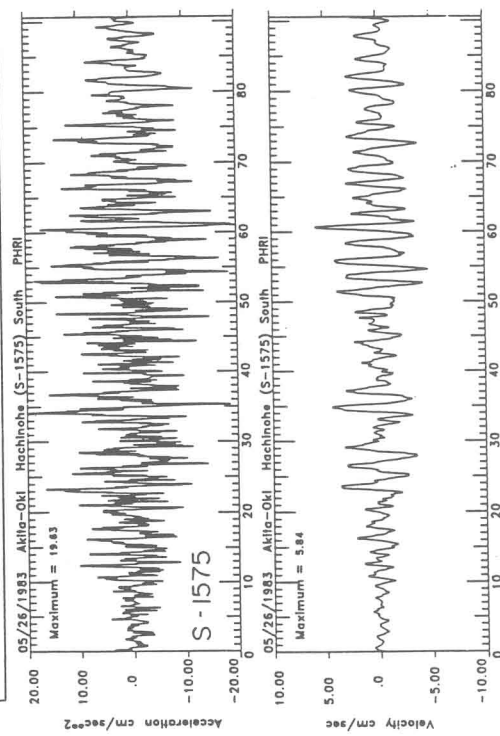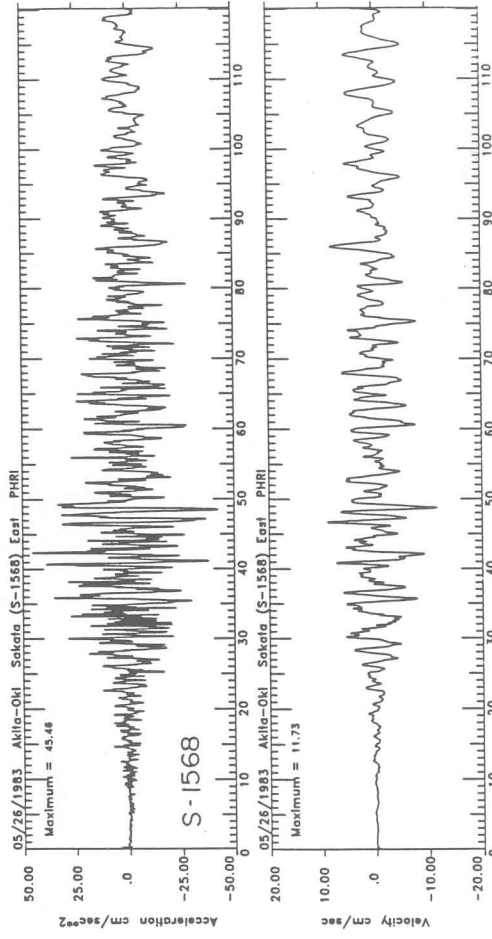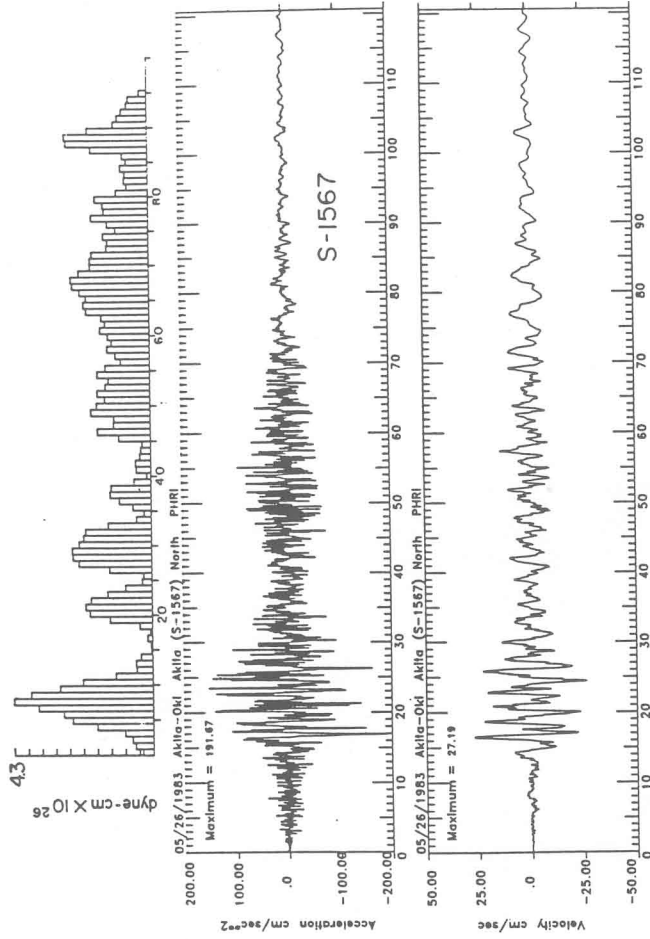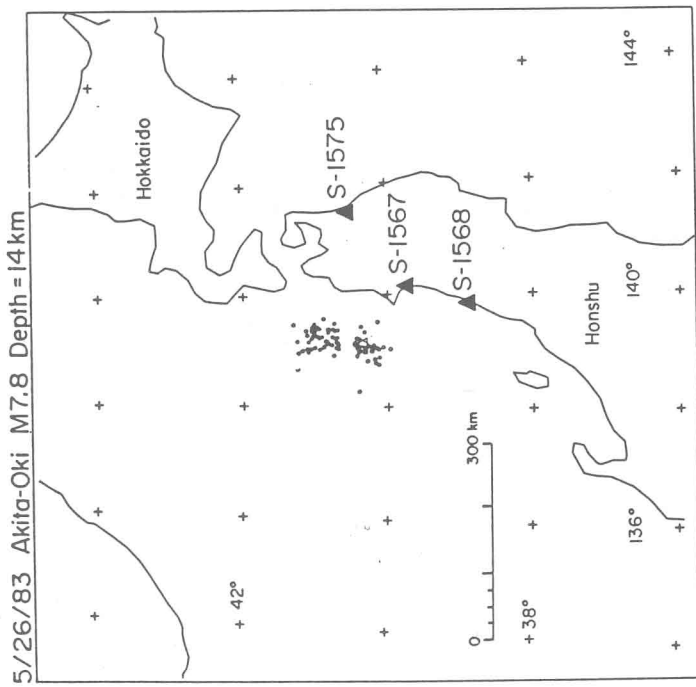In this Appendix, we present a more quantitative discussion of the empirical Green's function technique. The ground motion $\mathbf{U}(t)$ that results from a complex distribution of dislocation time histories, $D(x, y, t)$, that are distributed on a planar fault of length L and width W can be written as

$$\mathbf{U}(t) = \int_0^L \int_0^W \dot{D}(x, y, t) * \mathbf{G}(x, y, t) \, dy \, dx, \tag{B1}$$

where x and y are cartesian coordinates along the fault strike and plunge, respectively, $\mathbf{G}(x, y, t)$ is the double-couple impulse response of the medium, and $\cdot$ and $*$ denote differentiation and convolution operators with respect to time. This expression is quite general and is valid in both the near- and far-fields provided that the earth is a linear system. Because the system is linear, we can always divide the solution into a sum over subfaults, or

$$\mathbf{U}(t) = \sum_{i=1}^{\ell} \sum_{j=1}^{m} \mathbf{U}_{ij}(t), \tag{B2}$$

where

$$\mathbf{U}_{ij}(t) = \int_{(i-1)\Delta L}^{i\Delta L} \int_{(j-1)\Delta W}^{j\Delta W} \dot{D}(x, y, t) * \mathbf{G}(x, y, t) \, dy \, dx, \tag{B3}$$

and where

$$\Delta L = \frac{L}{\ell}$$

$$\Delta W = \frac{W}{m}. \tag{B4}$$

Now suppose that we already possess ground motions $\mathbf{u}_{ij}(t)$ that resulted from a smaller earthquake that ruptured the i, j-th subfault. Its motion would be given by

$$\mathbf{u}_{ij}(t) = \int_{(i-1)\Delta L}^{i\Delta L} \int_{(j-1)\Delta W}^{j\Delta W} \dot{d}_{ij}(x, y, t) * \mathbf{G}(x, y, t) \, dy \, dx, \tag{B5}$$

where $d_{ij}(x, y, t)$ is the dislocation time history distribution for the smaller earthquake. If a function $F_{ij}(t)$ exists such that

$$D(x, y, t) = F_{ij}(t) * d_{ij}(x, y, t) \tag{B6}$$

for $(i-1)\Delta L \leq x < i\Delta L$ and $(j-1)\Delta W \leq y < j\Delta W$, then

$$\mathbf{U}_{ij}(t) = F_{ij}(t) * \mathbf{u}_{ij}(t), \tag{B7}$$

and then

$$\mathbf{U}(t) = \sum_{i=1}^{\ell} \sum_{j=1}^{m} F_{ij}(t) * \mathbf{u}_{ij}(t). \tag{B8}$$

So in principle, if we have good data from smaller events and if we know what the functions $F_{ij}(t)$ are, then we can obtain the ground motions of a large earthquake from smaller ones. Of course, this assumes that the slip history of the larger event can be obtained from a linear combination of slip histories of the smaller events.

Unfortunately, determination of $F_{ij}(t)$ is somewhat problematic. It is customary to assume that $F_{ij}(t)$ exists and that it consists of a sequence of n Dirac-delta functions distributed over the dislocation rise time of the larger event, where n is the integral ratio of the dislocations for the larger and smaller events. This is actually an important assumption and we will discuss alternative assumptions later. For now, however, assume that $F_{ij}(t)$ has the form

$$F_{ij}(t) = \sum_{k=1}^{n} \delta(t - T_{ij} - \tau_k), \tag{B9}$$

where T_{ij} is the delay time for the rupture front to travel from the hypocenter to the ij-th subfault and the τ_k's are a yet undefined distribution of times between zero and the dislocation rise time. Combining (B8) and (B9), we obtain

$$U(t) = \sum_{i=1}^{\ell} \sum_{j=1}^{m} \sum_{k=1}^{n} u_{ij}(t - T_{ij} - \tau_k), \tag{B10}$$

where the ratio of the seismic moments of the larger event M_0 to the smaller event M_0' is

$$\frac{M_0}{M_0'} = \frac{LWD}{\Delta L \Delta W D'} = \ell m n = N. \tag{B11}$$

One simple distribution of the τ_k's is to assume that

$$\tau_k = (k-1)\frac{t_d}{n}, \quad k = 1, 2, 3, \ldots n \tag{B12}$$

where t_d is the duration of the dislocation of the large event. Unfortunately, this has the effect of convolving the empirical Green's functions with a picket fence function of periodicity t_d/n and the resulting synthetics ring at this period. In order to avoid this, a random time shift can be added to τ_k, or

$$\tau_k = (k - \chi_k)\frac{t_d}{n}, \tag{B13}$$

where χ_k's are uniform random numbers between 0 and 1. Combining (B13) and (B10), we obtain

$$U(t) = \sum_{i=1}^{\ell} \sum_{j=1}^{m} \sum_{k=1}^{n} u_{ij}\left[t - T_{ij} - (k - \chi_k)\frac{t_d}{n}\right]. \tag{B14}$$

Although the empirical Green's functions $u_{ij}(t)$ must, in general, change from one subfault to another, in many respects they may be statistically quite similar to

each other. This is particularly true in teleseismic cases since the observer-subfault geometry changes little from subfault to subfault. In order to study the general properties of the empirical Green's function technique, we approximate $\mathbf{u}_{ij}(t)$ by

$$\mathbf{u}_{ij}(t) \approx A_{ij}\mathbf{u}(t - \xi_{ij}), \tag{B15}$$

where $\mathbf{u}(t)$ is an observed record having general characteristics similar to other records, A_{ij} is a distance attenuation scaling factor, and ξ_{ij} is the source to receiver travel-time correction. Combining (B15) and (B14), we obtain

$$\mathbf{U}(t) \approx \mathbf{u}(t) * P(t), \tag{B16}$$

where

$$P(t) = \sum_{i=1}^{\ell} \sum_{j=1}^{m} \sum_{k=1}^{n} A_{ij}\delta\left[t - T_{ij} - \xi_{ij} - (k - \chi_k)\frac{t_d}{n}\right]. \tag{B17}$$

We can refer to $P(t)$ as a transfer function since it specifies how the record from a small earthquake can be transformed into the record of a larger earthquake. In Figure B1, we show $P(t)$ for the models M–1140–200 and M–120–135 (see Figure 5) and for both a coastal ranges strong motion site and also a teleseismic site. In the teleseismic case, the envelope of $P(t)$ is approximately constant in time since A_{ij} is
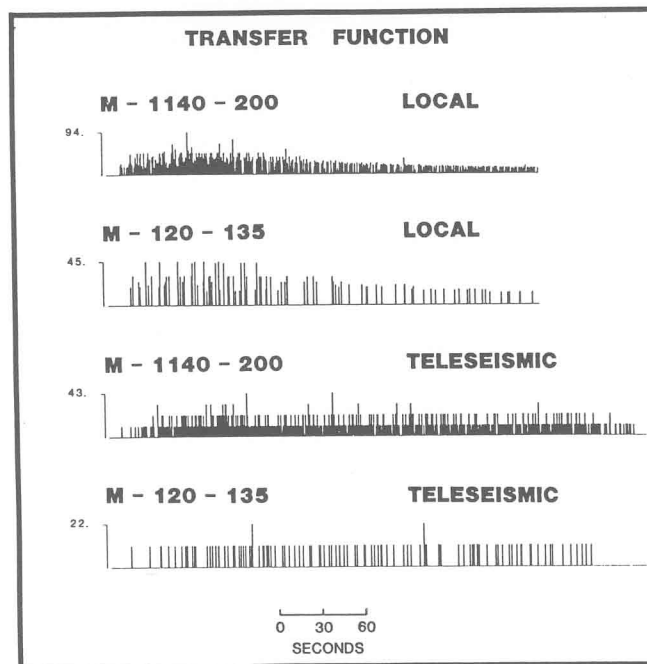

Figure B1

Examples of the form of the transfer function $P(t)$ defined by equation (B17) and assuming a coastal ranges site and two of the models of the 1960 Chilean earthquake shown in Figure 5. In the case of the teleseismic records, synthetic motions are determined by convolving the empirical Green's function with these transfer functions. Each spike represents an impulse function.

assumed to be 1.0 everywhere. In the strong motion case, the envelope has more character since the A_{ij} are determined from the CROUSE *et al.* (1988) distance attenuation relationship and also since the effects of directivity are more complex in the local field.

We can discover the spectral scaling implications of the empirical Green's function technique by studying the spectral characteristics of $P(t)$. In Figure B2, we show the Fourier amplitude spectra $\hat{P}(\omega)$ of the transfer functions shown in Figure B1. We studied many transfer functions and although the detailed shapes of their Fourier amplitude spectra are generally quite complex, we found that we could approximate their envelopes by

$$
\hat{P}(\omega) \approx \begin{cases} N; & \omega < 2/T_f \\ \dfrac{2N}{T_f \omega^\alpha}; & \dfrac{2}{T_f} < \omega < \left(\dfrac{2}{T_f}\sqrt{N}\right)^{1/\alpha} \\ \sqrt{N}; & \left(\dfrac{2}{T_f}\sqrt{N}\right)^{1/\alpha} < \omega, \end{cases} \tag{B18}
$$

where T_f is the total duration of $P(t)$, N is the total number of Green's functions that are summed, and α is a spectral fall-off parameter having a value between 1.0 and 3.0, depending on the nature of the fault geometry and rupture characteristics.
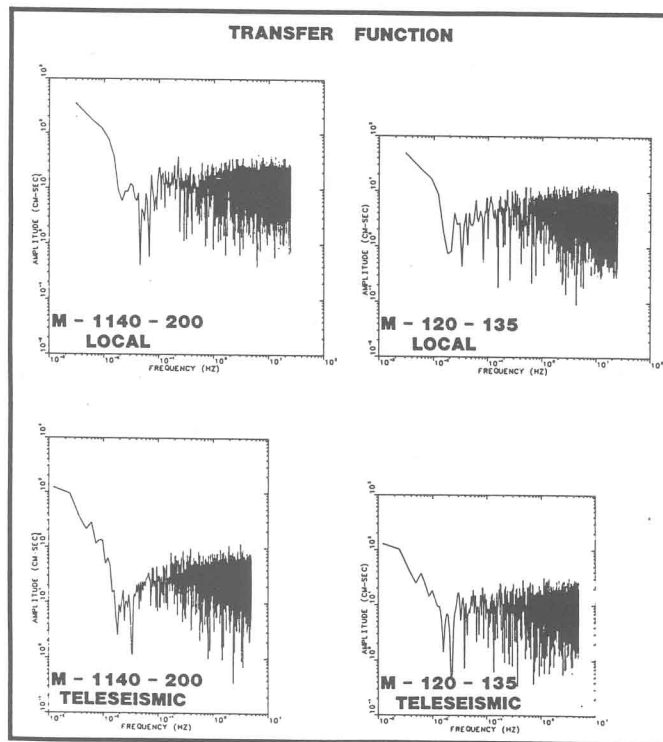

Figure B2
Fourier amplitude spectra of the transfer functions shown in Figure B1.

The fact that the high-frequency level of $\hat{P}(\omega)$ is $\sqrt{N}$ arises naturally (and inevitably) from the assumption that the individual Dirac-delta functions comprising $P(t)$ are shifted by random time delays.

If we assume that earthquake spectra obey certain simple similarity laws (and there is no good reason that they must), we can gain insight to the physical meaning of $\hat{P}(\omega)$. Suppose that we assume that $\hat{U}(\omega)$ and $\hat{u}(\omega)$ are self-similar and have a simple shape described by

$$\hat{U}(\omega) = \begin{cases} CM_0; & \omega < \omega_c \\ CM_0\left(\dfrac{\omega_c}{\omega}\right)^v; & \omega > \omega_c, \end{cases} \tag{B19}$$

where C is a scaling constant, v is a spectral fall off parameter, and ω_c is a corner frequency given by

$$\omega_c = DM_0^\beta, \tag{B20}$$

where D and β are also scaling constants. The spectral shape of $\hat{u}(\omega)$ is described in a similar fashion as

$$\hat{u}(\omega) = \begin{cases} CM_0'; & \omega < \omega_c' \\ CM_0'\left(\dfrac{\omega_c'}{\omega}\right)^v; & \omega > \omega_c', \end{cases} \tag{B21}$$

where

$$\omega_c' = DM_0'^\beta. \tag{B22}$$

We can now find $\hat{P}(\omega)$ such that it is compatible with our general similarity laws. From (B16) and (B19) through (B22) we have

$$\hat{P}(\omega) = \frac{\hat{U}}{\hat{u}} = \begin{cases} N; & \omega < \omega_c \\ N\left(\dfrac{\omega_c}{\omega}\right)^v; & \omega_c < \omega < \omega_c', \\ N^{1+\beta v}; & \omega_c' < \omega \end{cases} \tag{B23}$$

where $N = M_0/M_0'$. Comparing (B23) with (B18), we conclude that the empirical Green's function technique that we have described will produce self-similar spectra if those spectra are characterized by

$$1 + \beta v = \tfrac{1}{2}. \tag{B24}$$

In many spectral scaling laws, it is assumed that the corner frequency scales with moment as

$$\omega_c = DM_0^{-1/3}, \quad \text{or} \quad \beta = -1/3. \tag{B25}$$

If (B25) is assumed, then from (B24),

$$v = 3/2. \tag{B26}$$

In other words, if we assume that the corner frequency scales inversely with the cube root of the seismic moment, then the empirical Green's function technique that we have described will produce self-similar spectra only if the records have spectral falloffs of $\omega^{-3/2}$. Unfortunately, such spectra are physically unreasonable since they result in infinite radiated energy at high frequencies.

A frequently used spectral scaling law is one that was introduced by BRUNE (1970), in which it is assumed that $\beta = -1/3$ and $v = 2$. If this is the case, then $\hat{P}(\omega)$ would have to have the following form

$$\hat{P}(\omega) = \begin{cases} N; & \omega < \omega_c \\ N\left(\dfrac{\omega_c}{\omega}\right)^2; & \omega_c < \omega < \omega_c'. \\ N^{1/3}; & \omega_c' < \omega \end{cases} \qquad (B27)$$

Unfortunately, the summation of N records with a random phase lag inevitably leads to a synthetic having a high-frequency level that is larger than the original by a factor of $\sqrt{N}$. In order to obtain an empirical Green's function technique that is consistent with BRUNE's (1970) spectral scaling law, JOYNER and BOORE (1986) propose that $N^{4/3}$ records should be randomly summed and that the final motion should be multiplied by $N^{-1/3}$. If $\alpha = 2$, $\beta = -1/3$, and if we replace N by $N^{4/3}$ in (B18) and then multiply the result by $N^{-1/3}$, then it is easy to see that we obtain a $\hat{P}(\omega)$ that is identical to the one that is required by the Brune spectral scaling law given by (B27).

The apparent inconsistencies that we have noted can be traced directly to the assumption given by (B9). It is this assumption that forces the high-frequency levels to scale as $\sqrt{N}$. If we assume that the stress drops and rupture aspect ratios of small and large earthquakes are identical (i.e., $\ell = m = n$), then we can reproduce the JOYNER and BOORE (1986) model by assuming that

$$F_{ij}(t) = \frac{1}{n} \sum_{k=1}^{n^2} \delta(t - T_{ij} - \tau_k). \qquad (B28)$$

This is equivalent to saying that the dislocation of a large earthquake looks like the filtered sum of dislocations of smaller ones. In both assumptions (B9) and (B28), it is assumed that high-frequency energy is radiated from a patch throughout the duration of the dislocation on that patch. However, one could easily postulate that high-frequencies are only radiated during the initial phases of the rupture and that the dislocation is very smooth once the rupture front has broken through all adjacent areas. In this case, we might assume that $F_{ij}(t)$ may be approximated by

$$F_{ij}(t) = \delta(t - T_{ij}) + h(t), \qquad (B29)$$

where $h(t)$ is a relatively smooth, positive function having a total area of $(n-1)$ and a duration of t_d. If we assume that $\ell = m = n$ and (B29), then it is not difficult to see that this assumption will lead to a $\hat{P}(\omega)$ in which the long-period levels grow as N, but the high-frequency levels grow as $N^{1/3}$ (provided that $h(t)$ is sufficiently smooth). Both assumptions (B28) and (B29) lead to the conclusion that the high-frequency energy radiated from a subfault is the same for both small and large earthquakes. This is undoubtedly an oversimplification of the real case, but aspects of this generality may well be true.

Self-similarity is a very useful concept since it provides rules for the way in which large earthquakes can be produced from smaller ones. However, it is difficult to argue that giant subduction earthquakes such as the 1960 Chilean earthquake must have rupture processes that are self-similar to those of smaller earthquakes. The aspect ratio of these giant earthquakes may be different from that of smaller ones. Furthermore, the rheology of the fault and surrounding rock is undoubtedly a function of depth and there is little reason to expect that the nature of the rupture process is the same for earthquakes that are confined to the shallow part of the interface and giant earthquakes which may rupture into the uppermost mantle. In their study of teleseismic P-waveforms from 60 of the largest subduction earthquakes, HARTZELL and HEATON (1985) find that the average spectra of giant earthquakes do not appear to be self-similar to the average of smaller earthquakes (see their Figure 11a).

Given these complications, we have chosen to apply the empirical Green's function technique in a simple way such that it matches the teleseismic P-waveforms in the frequency range that is relevant to strong ground motions. We simply sum enough records to match the teleseismic short-period amplitudes. As might be expected, this number is less than that given by the ratio of the moments of the larger and smaller earthquakes. Clearly, this procedure would seriously underestimate long-period (greater than 20 sec.) motions. However, since our strong motion empirical Green's functions have already been filtered so that they have no information at these periods, we believe that little is lost in our application of the procedure.

References

ANDERSON, J. G., P. BODIN, J. N. BRUNE, J. PRINCE, S. K. SINGH, R. QUAAS, and M. ONATE (1986), *Strong ground motion from the Michoacan, Mexico, earthquake*, Science *233*, 1043–1049.

BEAVAN, J. and K. H. JACOB (1984), *Processed strong motion data from subduction zones: Alaska*, in *Lamont-Processed Strong Motion Data, Report 1* (Lamont-Doherty Geological Observatory, Palisades, NY) 249 p.

BRADY, A. G. and V. PEREZ (1977), *Strong-motion earthquake accelerograms, digitization and analysis, records from Lima, Peru: 1951 to 1974*, U.S. Geol. Surv. Open-File Report, 77–587.

BRUNE, J. N. (1970), *Tectonic stress and the spectra of seismic shear waves from earthquakes*, J. Geophys. Res. *75*, 4997–5009.

CROUSE, C. B., J. A. HILEMAN, B. E. TURNER, and G. R. MARTIN (1980), *Compilation assessment and expansion of the strong earthquake ground motion data base*, U.S. Nuclear Regulatory Commission, NUREG/CR–1660.

CROUSE, C. B., Y. K. VYAS, and B. A. SCHELL (1988), *Ground motions from subduction zone earthquakes*, Bull. Seism. Soc. Am. *78*, 1–25.

DENHAM, D. and R. G. SMALL (1971), *Strong motion data centre: Bureau of Mineral Resources, Canberra*, Bull. New Zealand Soc. for Earthq. Eng. *4*, March.

GUZMAN, R. A. and P. C. JENNINGS (1976), *Design spectra for nuclear power plants*, Journal of the Power Division, ASCE *102*, Po2, Proc. paper 12521, 165–178.

HARTZELL, S. H. (1978), *Earthquake aftershocks as Green's functions*, Geophys. Res. Letters *5*, 1–4.

HARTZELL, S. H. (1985), *The use of small earthquakes as Green's functions*, in Proceedings: *Strong-Ground-Motion Simulation and Earthquake Engineering Applications* (eds. R. E. Scholl and J. L. King) Electric Power Research Institute, NP–4299, Project 2556–1, pp. 22–1 to 22–8.

HARTZELL, S. H. and T. H. HEATON (1985), *Teleseismic time functions for large shallow subduction zone earthquakes*, Bull. Seism. Soc. Am. *75*, 965–1004.

HASKELL, N. A. (1969), *Elastic displacements in the near-field of a propagating fault*, Bull. Seism. Soc. Am. *59*, 865–908.

HEATON, T. H. and S. H. HARTZELL (1986), *Source characteristics of hypothetical subduction earthquakes in the northwestern United States*, Bull. Seism. Soc. Am. *76*, 675–708.

HEATON, T. H. and H. KANAMORI (1984), *Seismic potential associated with subduction in the northwestern United States*, Bull. Seism. Soc. Am. *74*, 933–941.

HEATON, T. H., F. TAJIMA, and A. W. MORI (1986), *Estimating ground motions using recorded accelerograms*, Surveys in Geophysics *8*, 25–83.

HOUSTON, H. and H. KANAMORI (1986), *Source spectra of great earthquakes: Teleseismic constraints on rupture process and strong motion*, Bull. Seism. Soc. Am. *76*, 19–42.

IRIKURA, K. (1983), *Semi-empirical estimation of strong ground motions during large earthquakes*, Bull. Disas. Prev. Res. Inst., Kyoto Univ. *33*, 63–104.

JOYNER, W. B. and D. M. BOORE (1981), *Peak horizontal acceleration and velocity from strong-motion records including records from the 1979 Imperial Valley, California, earthquake*, Bull. Seism. Soc. Am. *71*, 2011–2038.

JOYNER, W. B. and D. M. BOORE (1982), *Prediction of earthquake response spectra*, U.S. Geol. Survey, Open-File Report, 82–977.

JOYNER, W. B. and D. M. BOORE (1986), *On simulating large earthquakes by Green's function addition of smaller earthquakes*, Proceedings of the 5th Maurice Ewing Symposium on Earthquake Source Mechanics (eds. S. Das, J. Boatwright and C. Scholz), AGU, 269–274.

KANAMORI, H. (1970), *Synthesis of long-period surface waves and its application to earthquake source studies—Kurile Islands earthquake of October 13, 1963*, J. Geophys. Res. *75*, 5011–5027.

KANAMORI, H. (1975), *Re-examination of the Earth's free oscillations excited by the Kamchatka earthquake of November 4, 1952*, Phys. Earth Plane. Int. *11*, 216–216.

KANAMORI, H. (1977), *The energy release in great earthquakes*, J. Geophys. Res. *82*, 2981–2987.

KANAMORI, H. (1979), *A semi-empirical approach to prediction of long-period ground motions from great earthquakes*, Bull. Seism. Soc. Am. *69*, 1654–1670.

KAWASHIMA, K., K. AIZAWA, and K. TAKAHASHI (1984), *Attenuation of peak ground motion and absolute acceleration response spectra*, in Proceedings of the Eighth World Conference on Earthquake Engineering Vol. II, San Francisco, 257–264.

KELLEHER, J., J. SAVINO, H. ROWLETT, and W. McCANN (1974), *Why and where great thrust earthquakes occur along island arcs*, J. Geophys. Res. *79*, 4889–4899.

KIKUCHI, M. and Y. FUKAO (1987), *Inversion of long-period P-waves from great earthquakes along subduction zones*, Tectonophysics *144*, 231–247.

LIU, H. L. and T. H. HEATON (1984), *Array analysis of the ground velocities and accelerations from the 1971 San Fernando, California, earthquake*, Bull. Seism. Soc. Am. *74*, 1951–1968.

MORI, A. W. and C. B. CROUSE (1981), *Strong motion data from Japanese earthquakes*, World Data Center A, Report SE-29, National Oceanic and Atmospheric Administration, Boulder, CO.

OHTA, Y., H. KAGAMI, N. GOTO, and K. KUDO (1978), *Observation of 1- to 5- second micrometers and their application to earthquake engineering. Part I: Comparison with long-period accelerations at the Tokachi-Oki earthquake of 1968*, Bull, Seism. Soc. Am. *68*, 767–779.

PLAFKER, G. (1972), *Tectonics*, in *The Great Alaskan Earthquake of 1965, Seismology and Geodesy* (National Academy of Sciences, Washington, D.C.).

RUFF, L. and H. KANAMORI (1983), *The rupture process and asperity distribution of three great earthquakes from long-period diffracted P-waves*, Phys. Earth Planet. Inter. *31*, 202–230.

SYKES, L. (1971), *Aftershock zones of great earthquakes, seismicity gaps, and earthquake prediction for Alaska and the Aleutians*, J. Geophys. Res. *76*, 8021–8041.

TRIFUNAC, M. D. (1976), *Preliminary analysis of the peaks of strong ground motion—dependence of peaks on earthquake magnitude, epicentral distance, and recording site conditions*, Bull. Seism. Soc. Am. *66*, 189–219.

WU, F. T. and H. KANAMORI (1973), *Source mechanism of February 4, 1965, Rat Island earthquake*, J. Geophys. Res. *78*, 6082–6092.